Methane Emissions Project

Borough of Versailles, Pennsylvania

Attachment II

SEISMIC REFLECTION STUDY

October 31, 2007

Prepared for

National Energy Technology Laboratory

By

Vladislav Kaminski and William Harbert
University of Pittsburgh
Geology and Planetary Sciences

DISCLAIMER

ACKNOWLEDGEMENTS

An endeavor of this complexity is only possible by the united effort of many individuals and organizations. The reflection seismic surveys were completed as a small portion of a larger project directed by Mr. Terry Ackman of the Pittsburgh National Energy Technology Laboratory of the United States Department of Energy. Additional help in this work came from Mr. Wayne Mathis of HL Technologies, Mr. Jim Swearingen of WesternGECO, Mr. Brian Toelle of Schlumberger, Mr. Elmo Christensen of Industrial Vehicles International, Inc., Mr. Scott Williams of I/O Corporation, Mr. Chuck Harding and Mr. Rob Morris of EdgeTech Corporation, Mr. Mat Ralston of Parallel Geoscience Corporation, and Mr. Mark Thomas and Mr. William Schuller of RDS. A thorough review of this report and helpful comments was completed by Dr. Doug Wyatt, Senior Fellow, Washington Group International. The authors are deeply grateful for his insightful and careful review. Reflection seismic surveys using a portable Stratavisor system were made possible by Mr. Jim Fowler of IRIS (Incorporated Research Institutions for Seismology) - PASSCAL (Program for Array Seismic Studies of the Continental Lithosphere). The patience and kindness of the people of Versailles, their congressional representatives, police, municipal and city workers, are gratefully acknowledged.

Cover Photo: Versailles, PA, circa 1920 (Photo courtesy of Mrs. Josephine Cindric).

This study is respectively dedicated to the people of Versailles.

TABLE OF CONTENTS

LIST OF FIGURES

LIST OF EQUATIONS

LIST OF TABLES

1.0 Abstract

Reflection seismic surveys were completed in the Versailles area to identify possible zones of natural gas accumulation and/or migration routes for gas from deeper to shallow regions. Because of the urban nature of the survey region, it was very challenging to collect and process these data. While some areas of data were degraded by "wipe out" zones probably related to fill, interpretable results were obtained. The data from the I/O System II based 3D reflection survey, when processed using Amplitude versus Angle techniques (referred to as either AVA or Amplitude variation with offset, AVO processing) to derive the seismic attributes of shear wave reflectivity and Poisson reflectivity, showed some regions of anomalous behavior, which we interpret as possible subsurface regions of gas accumulation. Seismic imaging was successful in identifying possible shallow, intermediate, and deep regions of gas accumulation in this area.
Associated with most of the shallow level regions are layers that appear to be stopping vertical gas migration. Where these layers are punctured by abandoned, uncased well holes or fractures, vertical migration of methane would be expected to occur. Deeper anomalous regions of possible gas accumulation were possibly revealed using the shear wave reflectivity AVO seismic attribute. Such gas accumulation could be related to trapping of vertically migrating gas from coal units or from the original producing unit of the McKeesport Gas Field, the Speechley sandstone. The possible source of the gas is not considered in this report.

Marine profiles 02 and 05 may show gas-filled fractures and voids, as interpreted by enhanced reflectivity. Together, these data suggest multiple levels of possible gas accumulation (variation in pore-filling phases) at shallow, intermediate, and deep depths. Because of a lack of well-derived velocities, it is challenging to convert these two-way travel times to depths; however, some estimates are included in this report.

(This page intentionally left blank)

2.0 Introduction

Three reflection seismic surveys were completed at Versailles, Pennsylvania in support of a multidisciplinary effort to mitigate gas migration related to abandoned wells of the McKeesport Gas field. The goals of the reflection seismic surveys were to determine the location of natural gas accumulations and possible migration paths to the surface. The McKeesport Gas field, a short lived, but intensely explored field, was abandoned and a residential neighborhood built over the top of abandoned wells (Figure 1). In addition, several subsurface coal beds are a possible source of coal bed methane gas and limited data suggests that natural gas may have been stored in underground formations some time around the late 1950's.

Methane (CH_4) is a colorless, odorless gas that occurs as the principal component in natural gas reservoirs, and is also associated with coal (as coal bed methane or CBM). It can be formed by bacterial processes and the decomposition of vegetation in the absence of oxygen. It is less dense than air and can form explosive mixtures with air when present between explosive limits of 5 to 15% (Lide, 1991). The explosive limits are defined as the lower explosive limit (LEL) and upper explosive limit (UEL) for a gas to ignite and explode.

Gas leakage has been observed at other sites, such as the Playa Vista region of Los Angeles. At Playa Vista, over 100 abandoned wells have been postulated to exist and may be allowing gas to leak to the surface (Snepp and Moyer, 2006), although broad zones of elevated soil gas concentration related to faults and aquifer river gravels have also been reported (Exploration Technologies, Inc., 2000). At Playa Vista, gas leakage is thought to move to the surface and into gravel and aquifer units, though the source of the methane gas is controversial (Figure 2). However, in response to the gas leakage at Playa Vista, the Building and Safety Code was modified for new construction to include vents, alarms, and a membrane placed between the ground and foundation (for details refer to Ordinance No. 175790 passed by the Council of the City of Los Angeles, February 12, 2004). In 2002, structures that were built after 1986 in the Fairfax District were required to be retrofitted with gas mitigation systems (Stark, 2007).

A major underground storage gas leak (Figure 3) caused explosion and fires in Hutchinson, Kansas, as described in Allison (2001), Nissen et al. (2002) and Xia (2002). Geyser-like fountains of natural gas and brine were observed during this event (Figure 3). Mitigation of the hazard was aided by geophysical investigation of this site.

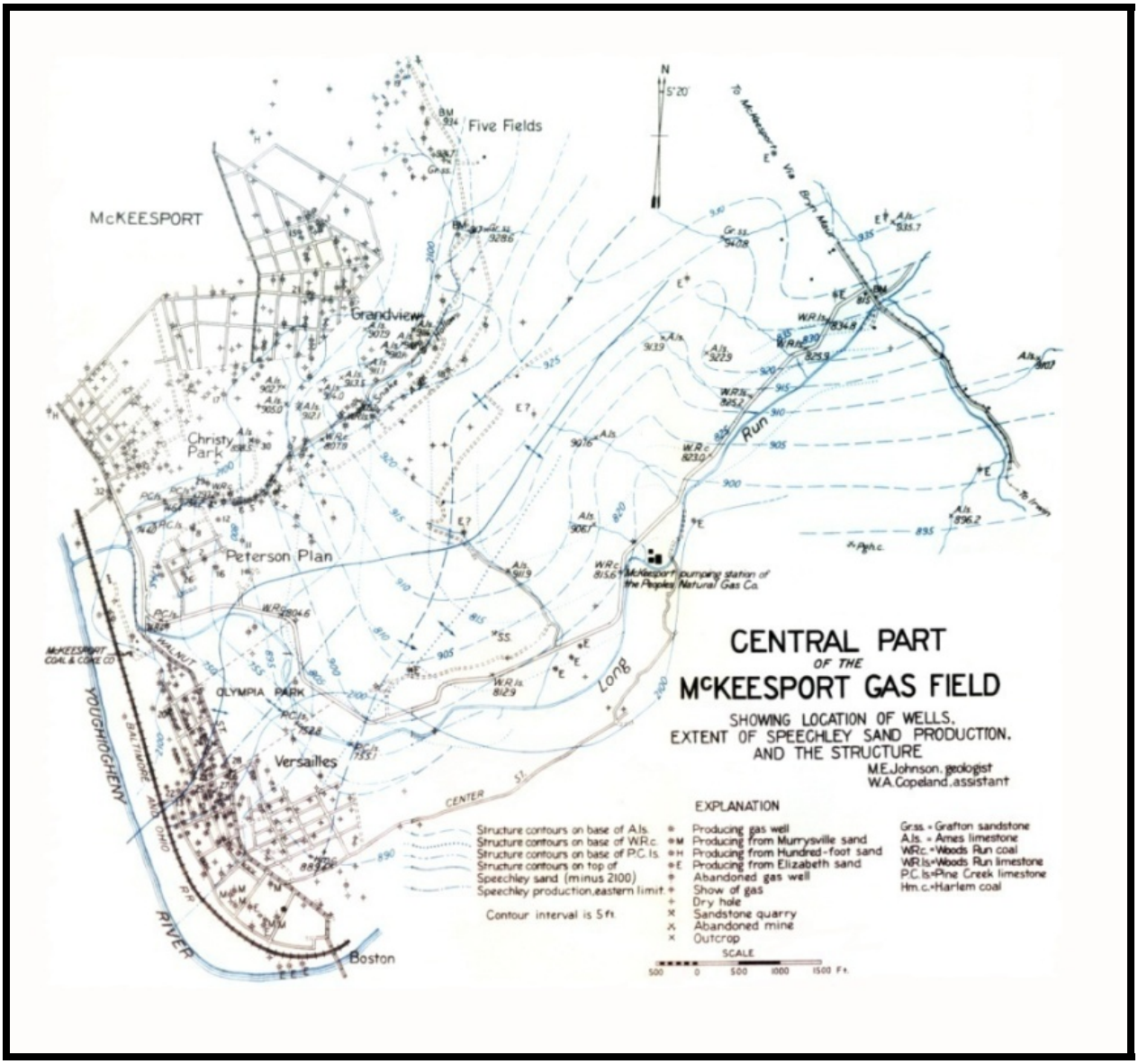

Figure 1. Geometry of McKeesport Gas Field. The region of study was the Versailles portion of the field in the lower left of this figure (from M. E. Johnson 1929).

Figure 2. Surface topography in Playa Vista area. (photo from Siegel, 2006).

Figure 3. Thirty foot high geyser of natural gas, dirt, water and debris near Hutchinson, Kansas. Photo from The Hutchinson News and Allison (2001).

Extensive geotechnical and geophysical studies were completed immediately after this tragic explosion. Both magnetic (Xia, 2002) and reflection seismic (Nissen et al., 2002) studies were completed to determine the source of gas and migration routes to the surface. It was proposed by Nissen et al. (2002) that a thin fracture-prone unit of dolomites appeared to be a conduit for leaking gas between the storage site and Hutchinson.

In the present study, three seismic methods were used. In the first, a sledge hammer source and 60 station reflection seismic lines were used to estimate depth to bedrock and rock velocities for shallow geological units. Marine reflection seismic profiles were then collected to look for gas anomalies in river sediment. These observations led to the determination of porosity and permeability for some surface samples from immediately across the river from Versailles. There was variation in these measurements; all data is included in this report.

A three dimensional reflection seismic survey was completed using an EnviroVib™ energy source. Although building land fill has to some extent obscured some portions of the lines, when processed using innovative crooked line processing techniques, seismic attributes reflections caused by subsurface geology were observed. These data were additionally processed, using reflection amplitude variation with offset in the pre-stack dataset, to derive apparent anomalous reflection zones.

3.0 Approach

Initially, reflection seismic surveys were collected at a Geophysical Test Site developed at the Pittsburgh campus of the National Energy Technology Laboratory of the United States Department of Energy to test our approach. Following this initial work, three 60 energy point seismic reflection lines were collected at the Versailles site. The hardware used to collect the reflection seismic data consisted of a sixty-channel Geometrics Stratavisor, multichannel recorders, and vertical sensors, and a Mark Products L40 with a 40 Hz natural frequency response, which was borrowed from IRIS-PASSCAL for this survey.

A sludge hammer energy source was used along with the 40 Hz vertical component geophones for the Stratavisor reflection surveys, Geophone spacing was 1 meter with hammer strikes, or energy points, located at each geophone (Figure 4). No off end energy points were used in these surveys. Field geometries were similar to those shown in Figure 4, where geophones are visible along with the Stratavisor system. Shot and geophone locations were determined using GPS and plotted in UTM Zone 17N NAD83 northing/easting coordinates. Processing of the reflection seismic processing of the Stratavisor reflection seismic lines was completed using the Parallel Geosciences package. Processing was considerably aided by the help of Mr. Mat Ralston of PGC, whose expertise and help are gratefully acknowledged.

Figure 4. One of several reflection seismic lines collected at the Geophysical Test Site at the Pittsburgh campus NETL/DOE facility. Geophones are visible along this 2D line. Data was processed using the PGC (Parallel Geosciences Corporation) and University of Kansas SurfSeis™ software. This allowed the determination of 2D profiles and 1D velocity inversion for both P and S wave velocities.

Because of the limited energy produced with each hammer strike, the depth of imaging was relatively limited in these lines. The typical processing sequence for these lines is shown below (Figure 5). Processing of the Stratavisor lines was useful in determining the shallow structure; however, the energy of the source limited its utility in this study.

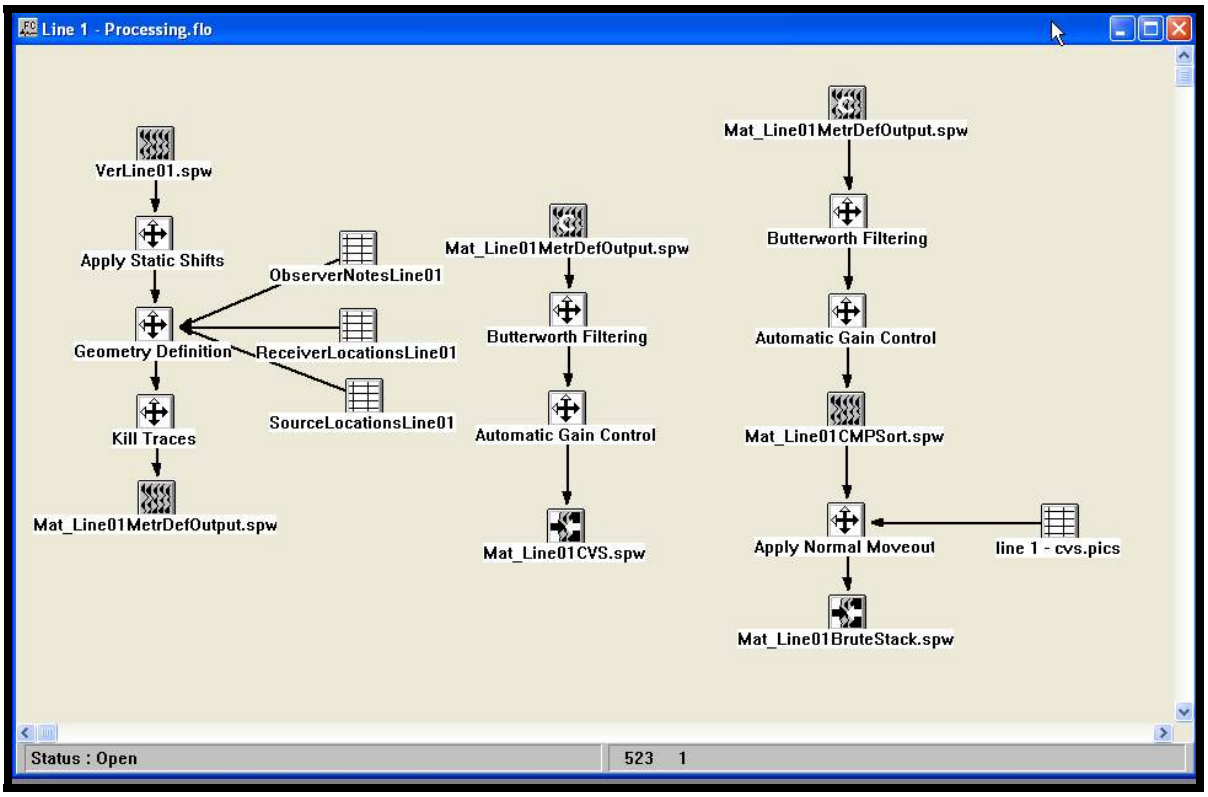

Figure 5. Processing sequence for Stratavisor lines using the PGC Flow software package. The help of Mr. Mat Ralston in this processing is gratefully acknowledged.

Surface waves were clearly observed in the shot gathers of the Statavisor collected data and it was determined to invert these for one dimensional (1D) P and S wave velocity profiles. 1D profiles of P and S wave velocity structure were calculated (Figure 6) and (Figure 7) using SurfSeis™ software to analyze surface waves recorded during the Stratavisor surveys, available from the Kansas Geological Survey.

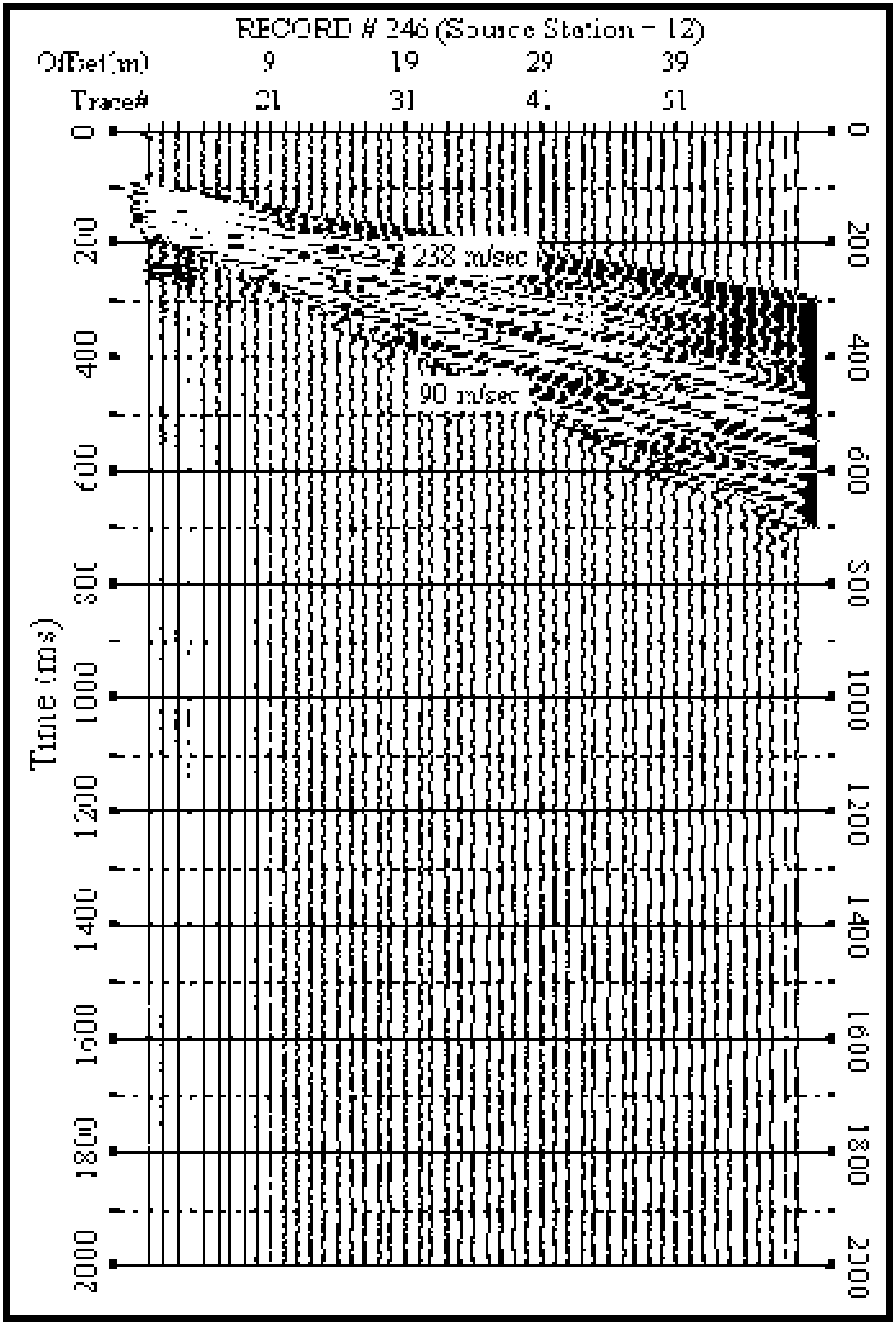

Figure 6. Record 246 from Stratavisor survey completed in Versailles. Note the highlighted surface waves with velocities between 238 m/sec (781 ft/sec) and 90 m/sec (295 ft/sec) surface these waves can be used to determine subsurface velocity structure. The derived 1D inversion for velocity is shown in the next figure.

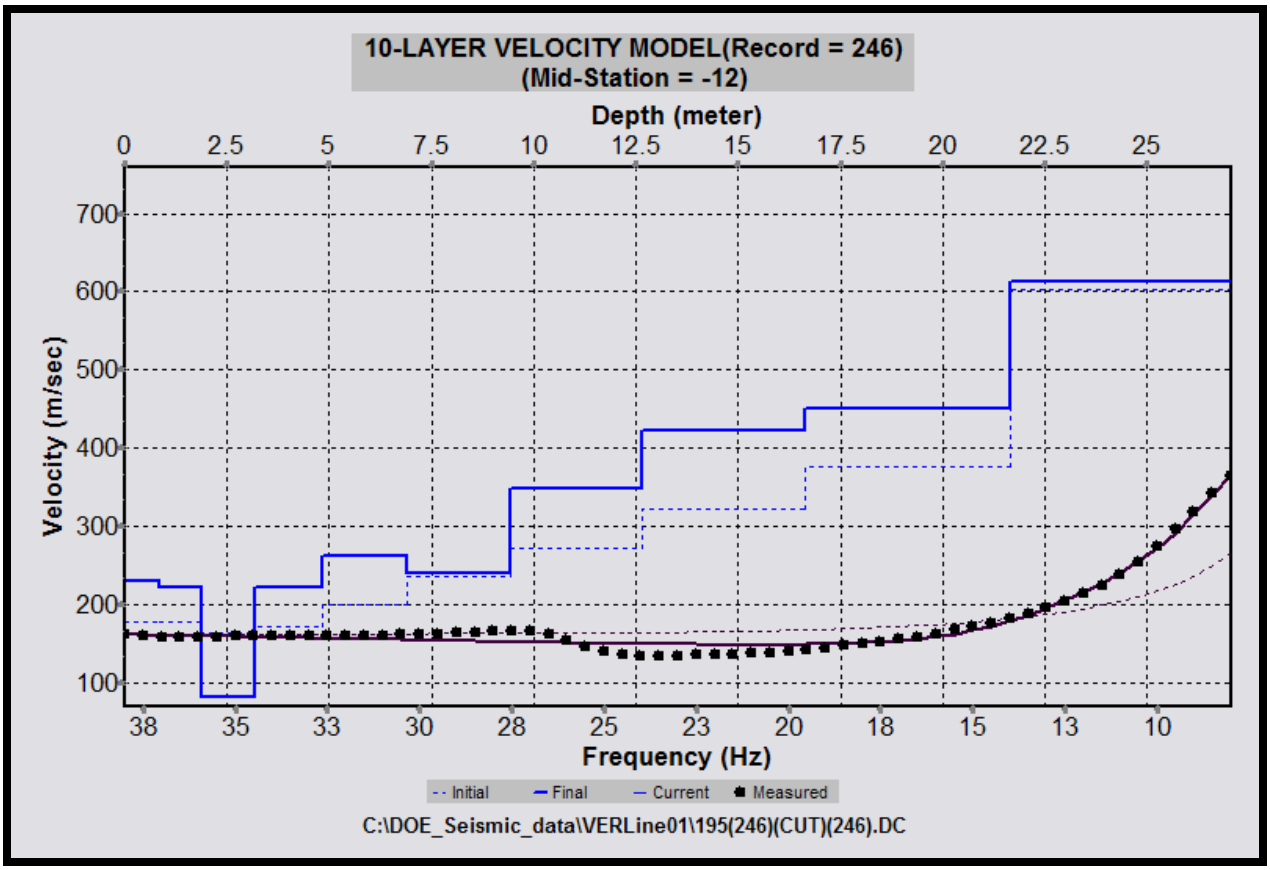

Figure 7. Active multichannel analysis of surface waves (MASW) inversion for 1D Shear velocity structure using the method of Park et al., (1999) 600 msec is equivalent to 1968.5 feet per second.

As part of this investigation, marine reflection surveys were also completed at the Versailles site. These single channel reflection seismic surveys used the EdgeTech™ full spectrum sub-bottom profiler (FS-SB) as an energy source. The FS-SB uses chirp technology to generate and transmit a wideband FM pulse that is linearly swept over a full spectrum range. The full spectrum pulse waveform is amplified by a 2 kW power amplifier, which drives the transmitting transducer. The reflected waveform is recorded by two hydrophones located in a tow vehicle. The frequency range of the 20 msec pulse is 2 - 16 kHz. Interpreted profiles are shown below, and all data is shown in an attachment to this report.

Because this was a single channel system, no processing was completed on the marine lines other than frequency filtering, reflection amplitude adjustment, or gain manipulation. In the reflection seismic profiles, sub-bottom bathymetry was clearly imaged and some sub-bottom features observed. Two of the profiles showed regions of enhanced reflectivity (Figure 8) and (Figure 9). One of the profiles showed an erosional feature in-filled with sediment (Figure 10).

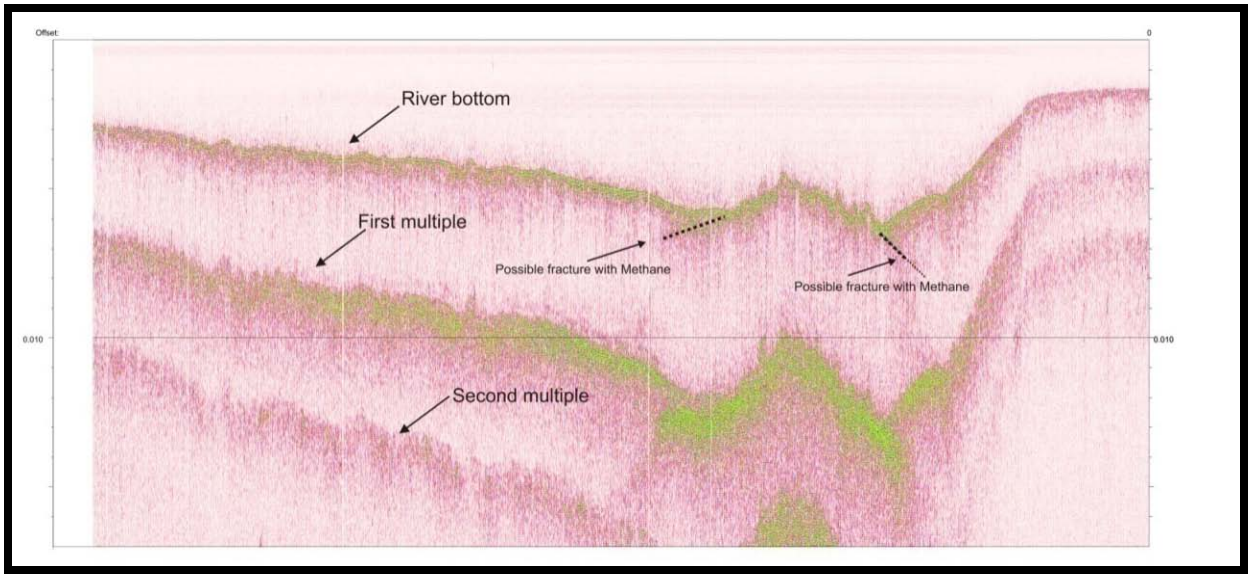

Figure 8. Profile Marine Line 02 showing possible gas filled fracture; the high reflectivity of this region may be associated with gas-filled voids or fractures.

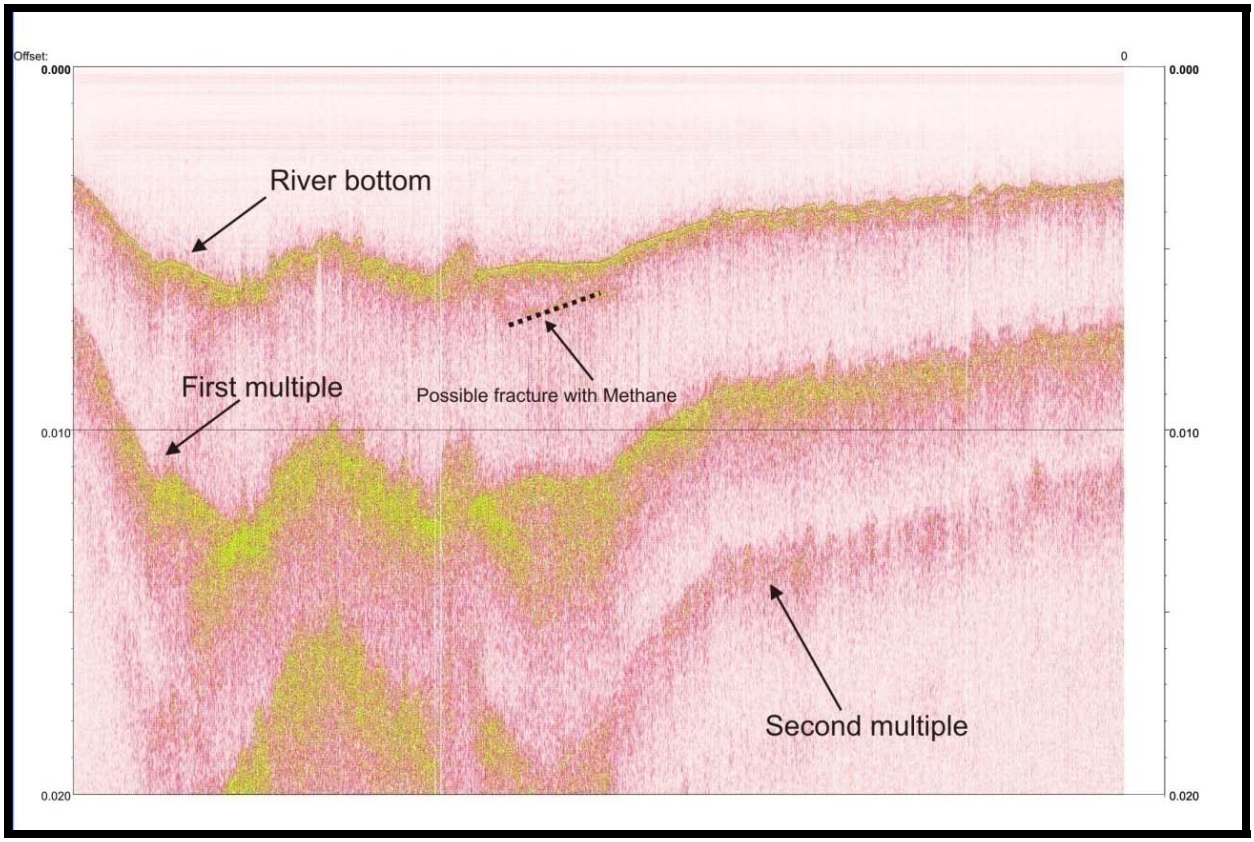

Figure 9. Profile Marine Line 05 showing a possible high reflectivity feature possibly related to a gas-filled fracture.

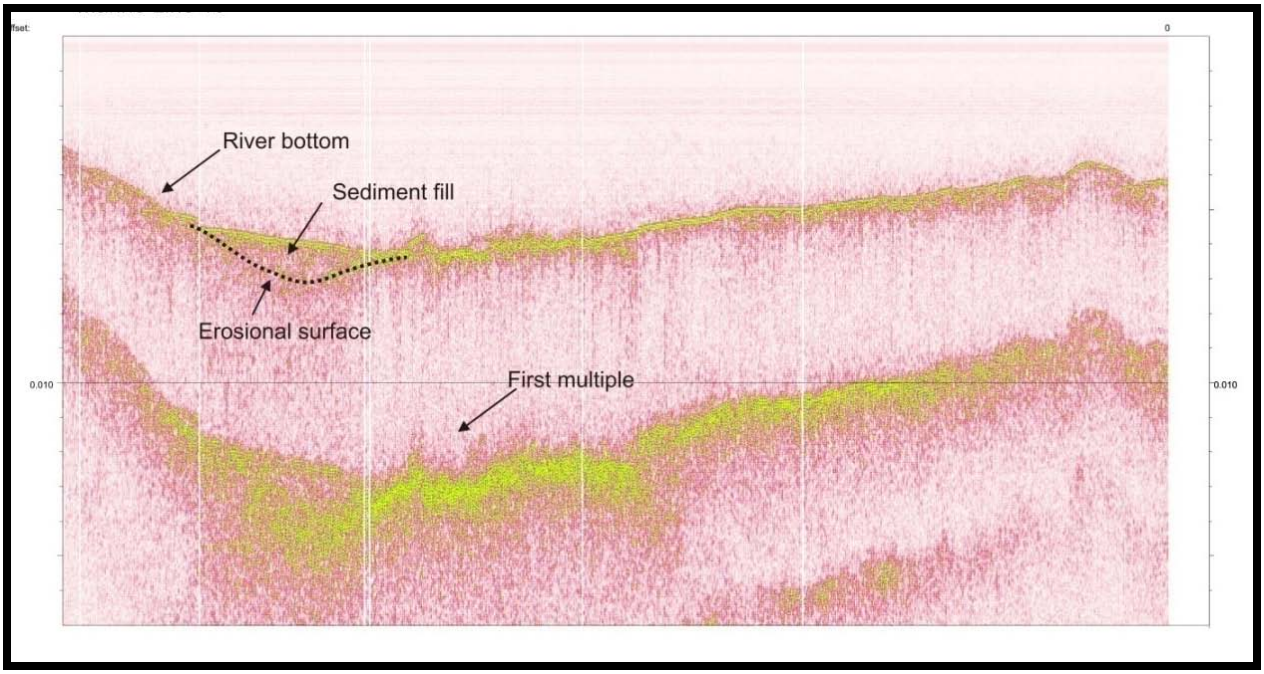

Figure 10. Marine Line 16 shows an erosional surface. This feature is distinct from the previous two figures in that the surface has been filled with sediments.

The final reflection seismic survey completed at Versailles was a three dimension (3D) reflection seismic survey using an I/O System II reflection seismic system (Figure 11). The system used OYO GS20DX geophones, I/O RSX and I/O ALX electronic boxes and an IVI EnviroVib™ vibrator truck. The EnviroVib™ used a SIB-100 seismic vibrator controller system to control the energy source. Communication between the I/O System II electronics and the SIB-100 was accomplished via a RST-100 seismic source radio trigger system. This system was interfaced with recording truck electronics by Mr. Wayne Mathis (HL Technologies), who was responsible for quality control of the recording electronics and recording the seismic data. The EnviroVib™ system was swept four times at each energy point and these signals were stacked to increase the signal to noise ratio of the final stacked trace recorded at each geophone location. The correlated geophone records were then written to tape in standard SEG-D format. Unstacked reflection seismic data was recorded at a sampling rate of 1 msec and written as a signed 24 bit value with a recorded record length of 5 seconds (Figure 12).

All reflection seismic lines and seismic attributes for these lines are shown in an attachment to this survey. A common midpoint (CMP) map showing the location of all CMP locations in the Versailles surveys is also included with the attachment to this report, which shows all reflection seismic line CMP locations associated with all reflection seismic lines completed in this 3D survey. Tables giving the global positioning satellite (GPS) determined Universal Transverse Mercator (UTM) coordinates of each geophone and shot location allow this data to be exactly reproducible with an identically configured future reflection seismic survey if needed.

Figure 11. Geophone location diagram for Versailles 3D reflection survey.

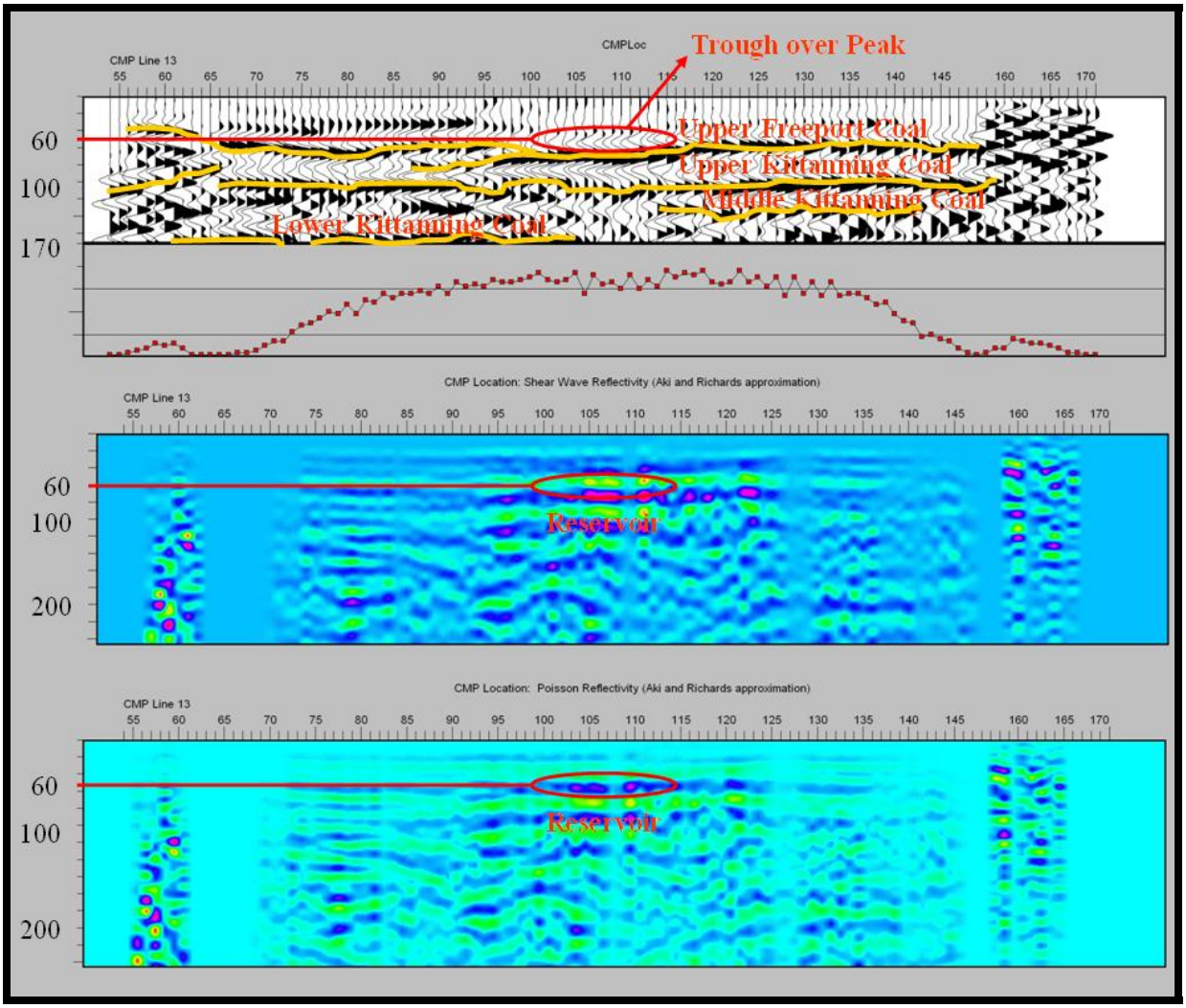

Figure 12. Shear wave reflectivity and Poisson reflectivity from CMP Line 13 of the Versailles 3D reflection seismic survey. Enhanced parameter variation is observed between CMP locations between 100 to 115. Note the uniform fold within the region of variation of this seismic attribute.

The processing of these lines included receiver and static determination and correction, Butterworth filtering, 3D crooked line processing and predictive deconvolution, as well as techniques related to data processing of reflection amplitude variation with offset before stacking to invert the data for Poisson and shear wave reflectivity (Figure 13). Specific processing parameters included the Bin size (in-line) of 10.0 feet and the Bin size cross line (x-line) of 37.5 feet. Predictive deconvolution parameters were a predictive length of 55 ms, pre-whitening (%) of 3.5, inverse filter length (ms) of 50 and a design length window of 100 ms. Butterworth filtering was calculated using a Low cut frequency of 10 Hz with a low rolloff rate (dB/oct) of 18.0 and a High cut frequency of 70 Hz with a High rolloff rate (dB/oct) of 18. A zero phase selection was used for the Butterworth filter operation. Floating datum statics were calculated and stored in separate Receiver and Source Datum databases. The data were then statically corrected to a reference datum. All of these steps were completed at the trace level in 3D

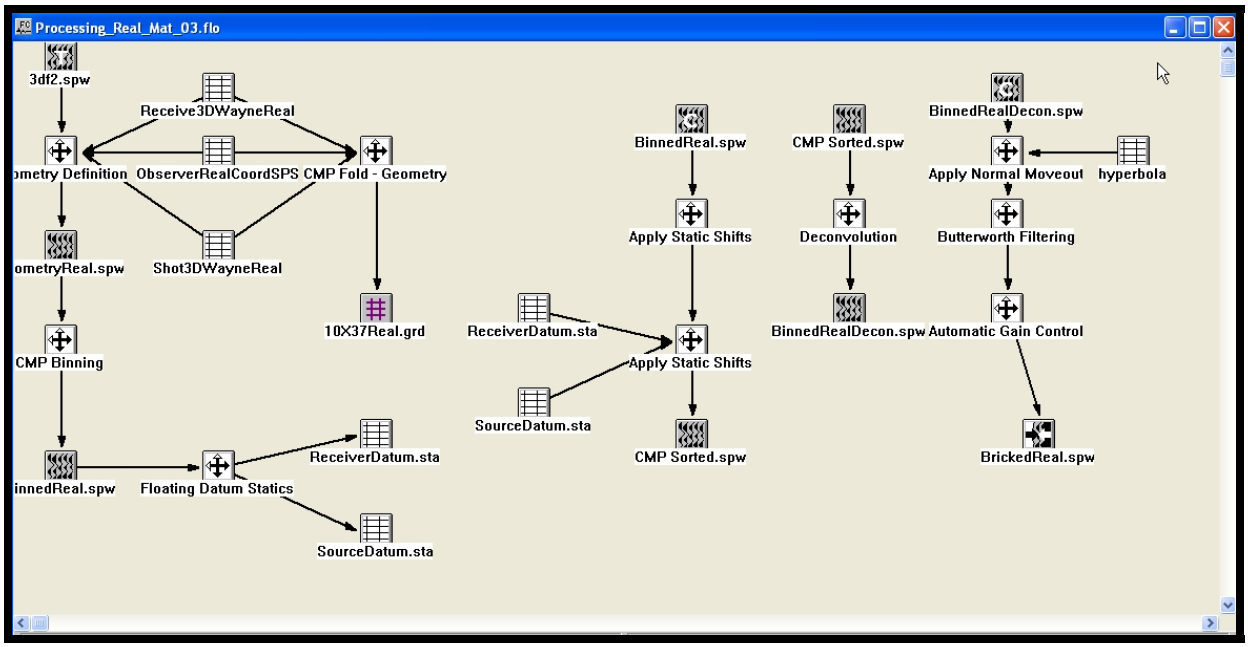

Figure 13. Processing sequence for Versailles 3D reflection seismic survey.

processing operations using software from Parallel Geoscience Corporation (Version 2.2.6). Some acquisition related geometry artifacts are present because of the variation in geometry of the energy points and geophones. This type of 3D geometry of energy points and geophones is called a swath acquisition (Cordsen et al., 2000) and can produce a variation in fold between lines.

Using these two seismic attributes, several zones of seismic attribute variation were identified. Clear reflectors were observed in the seismic lines collected within Versailles including amplitude variation along reflecting horizons. Unfortunately, in some regions, probably because of the presence of relatively unconsolidated overburden or fill, transmission of elastic waves was significantly attenuated. These regions are referred to as "wipe out" zones. Because of this and the variation in fold related to our swath acquisition with curved geophone and energy lines, we decided to focus on the highest quality lines and reflectors and apply a more advanced processing technique available in the Parallel Geosciences package, Amplitude variation with Angle (referred to as AVA or AVO processing) to extract seismic attributes at specific CMP locations. After processing, several regions of possible gas accumulation, identified by anomalous variation of these seismic attributes, were observed after amplitude variation with offset (AVO) processing.

Interpretation of these seismic data showed regions of significant negative polarity reflections interpreted to be related to the presence of highly reflective, perhaps coal unit (Figure 12). Interpretation of AVO-derived seismic attributes appeared to show regions of anomalous pore filling phases in horizontal and sub vertical geometries We interpreted the horizontal AVO anomalies to represent possible accumulations and reservoirs of natural gas in the subsurface.

Sub-vertical geometries may represent migration paths related to sequence stratigraphic boundaries or fracture systems.

Specifically, we observed the following regions of possible gas accumulations by identifying regions of anomalous seismic attribute characteristics (Table 1).

Table 1. Shallow (< 100 msec two-way travel time) possible gas accumulation zones identified by AVO derived shear wave reflectivity anomalies.

CMP Line Number	CMP Location	Two-way travel time (msec)
Line 7	85 to 98	Surface to 60 msec.
Line 9	102 to 116	50 msec
Line 10	127 to 132	50 msec
Line 11	95 to 128	Surface to 100 msec
Line 13	98 to 122	40, 50, 60 and 80 msec
Line 14	98 to 121	20, 40, 60 and 80 msec
Line 15	103 to 109	40 and 70 msec
Line 16	84 to 132	20 to 60 msec
Line 17	69 to 76	50 msec

Deeper regions of possible gas accumulation, identified by noting anomalous regions of the shear wave reflectivity AVO seismic attribute, are listed in Table 2:

Table 2. Deeper (> 100 msec two-way travel time) possible gas accumulations identified using AVO derived shear wave reflectivity anomalies.

CMP Line Number	CMP Location	Two-way travel time (msec)
Line 7	55 to 63	180 to 320 msec
Line 7	137 to 145	180 to 460 msec
Line 9	76 to 81	240 to 360 msec
Line 9	112 to 124	330 to 520 msec
Line 10	60 to 83	200 to 440 msec
Line 11	55 to 63	240 to 320 msec
Line 15	51 to 55	230 msec
Line 16	87 to 104	140 to 320 msec

Converting these two-way travel times to depths is complicated by the lack of accurate sonic velocity data for this region. Seismic velocities for rocks can vary within a specific lithology considerably, as shown in Figure 14. In the region studied, review of the regional geology suggests that shale, sandstone, and coal are the most commonly expected lithologies in the shallow subsurface. Limestone may also be present at greater depths.

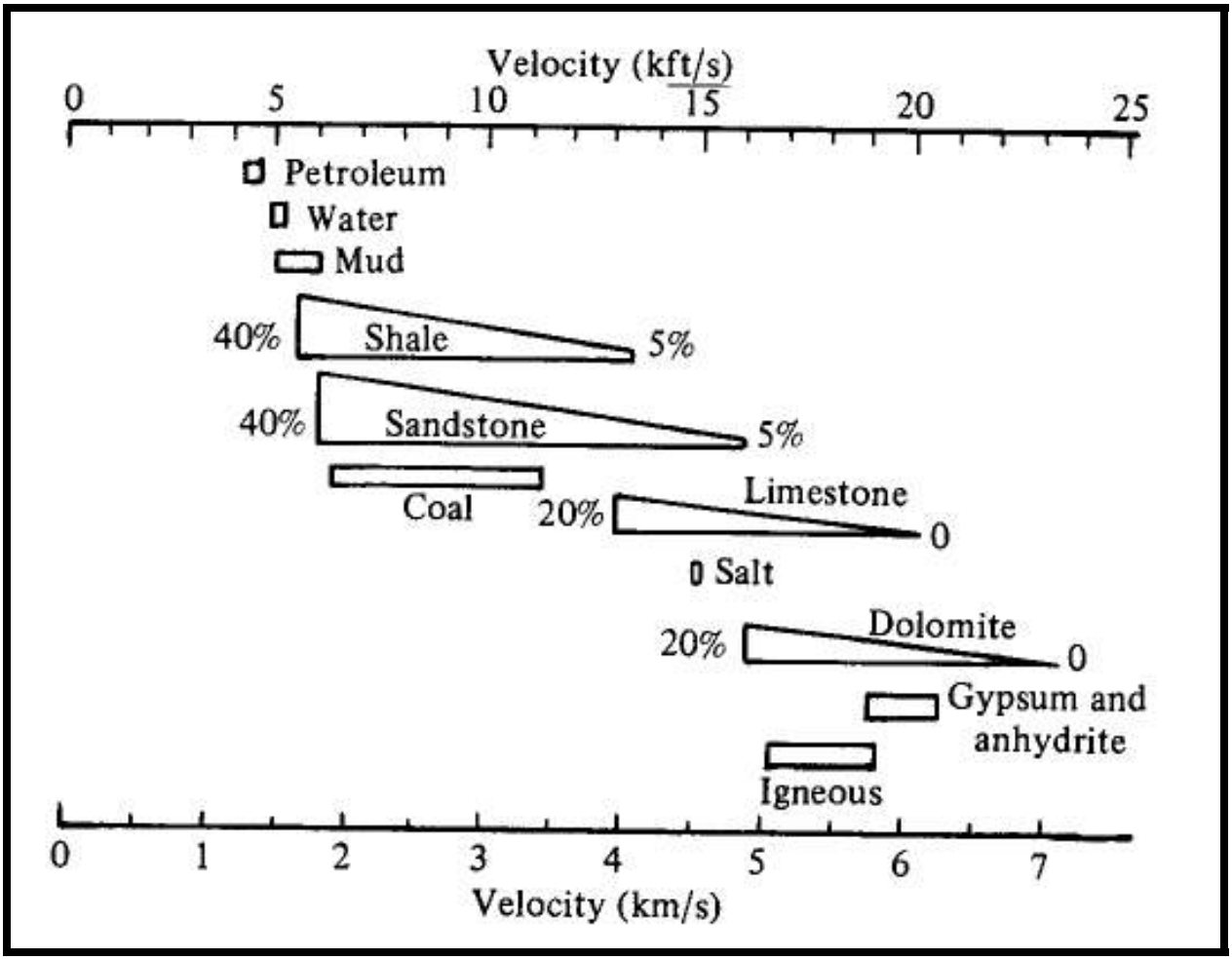

Figure 14. Seismic velocities in thousands of feet per second (kft/s) of crustal rocks from the Berkeley Course in Applied Geophysics. The readers of this report are encouraged to review the Seismic Methods portion of this excellent on-line resource (http://appliedgeophysics.berkeley.edu:7057/).

Some of the AVO seismic attribute data also appear to have identified anomalous zones at greater depths (Figure 15) that may represent the original exploration target of the McKeesport Gas field, which was the Speechley sandstone (William Schuller, communication 2007).

A field survey of the rocks and geology immediately adjacent to Versailles and well exposed along the adjacent river showed the presence of fracture systems, which along with abandoned and either open or partially open gas wells from the McKeesport Gas field, may connect source rocks of gas to shallow structures.

The porosity and permeability of several of these rock samples were measured at the Department of Civil and Environmental Engineering at the University of Pittsburgh. Generally, surface units had low porosity; however, some variation in permeability was observed. The variation in soil types within the region, as reported in Ackenheil (1968) and shown in Figure 16, is also

significant. Specifically in Figure 16, the region of soil type R-7 (Ackenheil, 1968) is highly correlated with a region of higher surface gas detected using a portable gas detector. These results and their interpretation are presented in detail in an accompanying report prepared as part of this study.

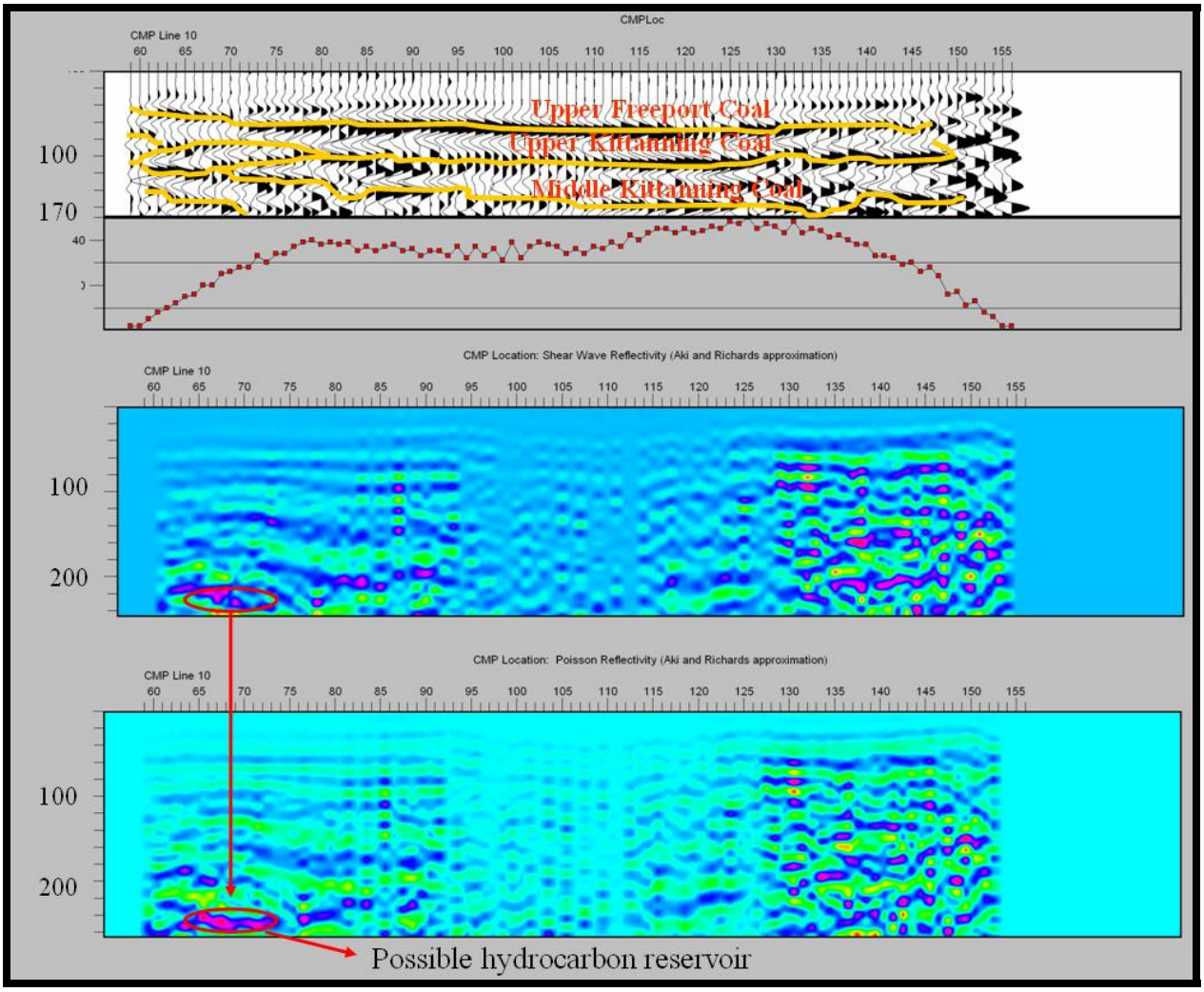

Figure 15. Parameters shown in the previous figure showing a deeper possible accumulation of natural gas between CMP locations 60 to 75, possibly the Speechley sandstone, which was the original target of the McKeesport Gasfield exploration activity (William Schuller, communication, 2007). This is the first modern reflection seismic imaging of this target in this area completed. Note the slightly anticlinal form of the reflectors at 200 msec. Note that the anomalous character of reflections is present in both the Shear Wave reflectivity and Poisson Reflectivity seismic attribute and within regions of relatively constant fold.

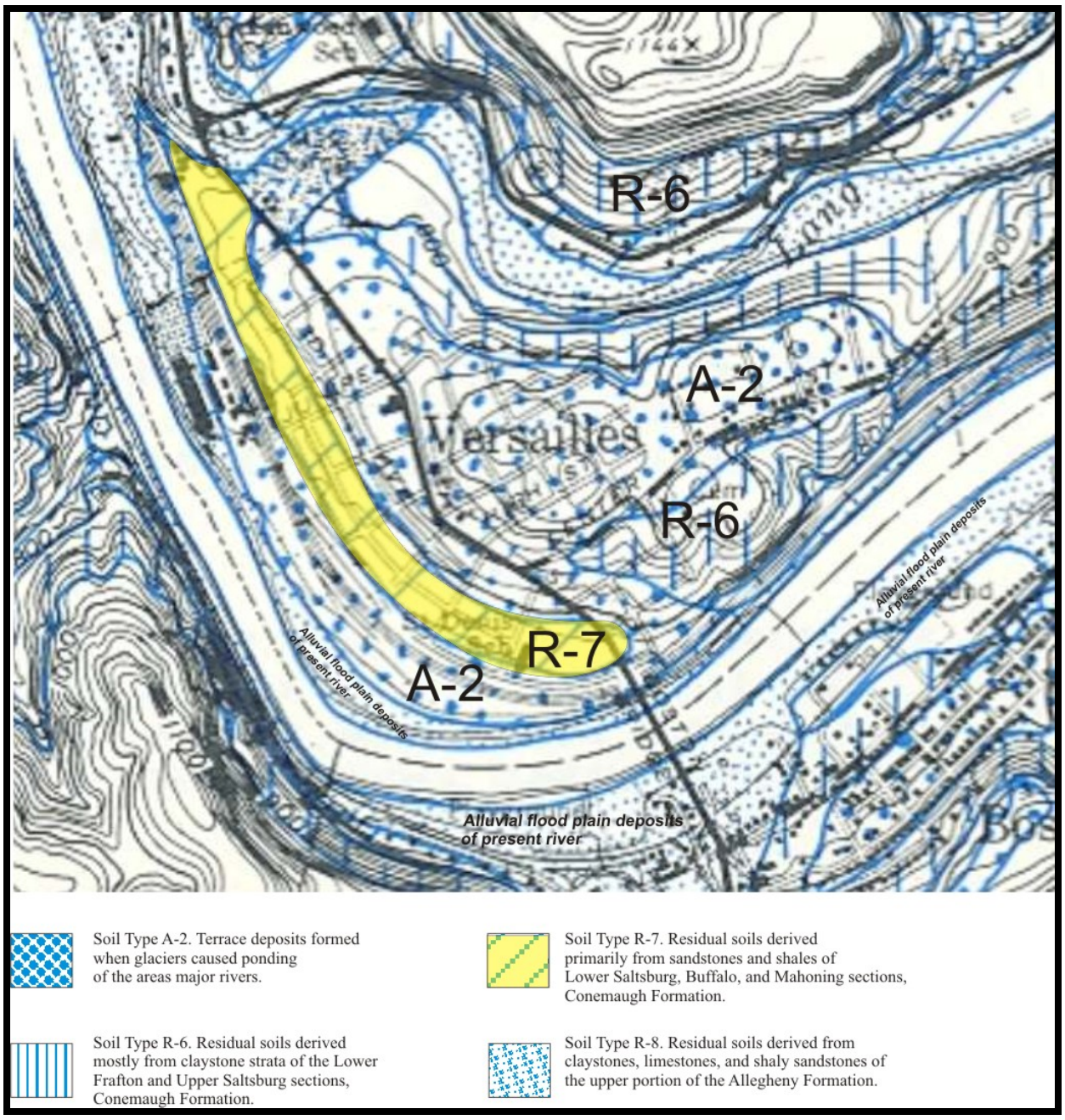

Figure 16. Soil map of Versailles region from Ackenheil (1968). Soil types R-7 and A-2 would be expected to have a lower clay content and potentially higher potential for vertical soil gas migration.

(This page intentionally left blank)

4.0 Stratigraphy of the McKeesport Area and Interpretation of Well Logs in Versailles, PA

Two wells were drilled as part of the original McKeesport Gasfield E&P (exploration and production) activities and logged by Century Geophysical Corporation, who provided Log ASCII Standard (LAS) format digital records. The wire-line tools used were natural gamma ray, sonic velocity, density, and caliper measurements. Well locations are shown in Figure 17. The logs were interpreted with respect to an expected stratigraphic sequence of sandstone, shale, perhaps some limited limestone, and coal units and after reviewing the interpretation of Mr. Mark Thomas of RDS. We completed our analysis of the wireline logs using Seismic Micro Technologies Kingdom Suite™. Coal beds were primarily identified as units of lower density; sandstone, limestone, and shale beds were identified using gamma logs annotated with reference to sandstone, shale, and limestone reference lines (Figure 18 and Figure 19).

Basic interpretation of wireline logs response in these wells required two clearly defined response lines, for sandstone and shale, to be determined. The sand reference line was determined using the gamma log and the response of the Mahoning sandstone with a 15 API response value observed between 218' to 228' depth in well number 1. The shale line was determined from shale unit number 3 (Table 3) with a gamma log response value of 135 API observed between 228' and 240' depth in well number 1. The limestone reference line was determined for the Upper Freeport Limestone observed between 256' and 278' in well number 1. Within this interval, a gamma tool response of 105 API was observed.

Other data, such as caliper variation, correlated with these responses (Figure 20 and Figure 21). Detailed description of beds and formations derived from borehole well logs is provided (Table 3).

The beds from the Upper Freeport coal to the Buffalo sandstone belong to the Conemaugh Group and the beds from the Middle Kittanning coal to the Upper Freeport coal belong to the Allegheny Group; all have been well-studied in the past. They include sandstones, shales, marine limestones, and coal beds, as shown in Figure 22.

The Conemaugh Group is dominated by siliciclastic strata, including claystone, shale, siltstone, and sandstone. It contains several named sandstone formations (or members), including the Mahoning sandstone (Milici, 2004).

The lower half of the Allegheny Group contains several marine or brackish-water units, such as the Vanport Limestone. The upper part of the Allegheny group is entirely composed of non-marine units. There are four major coal zones within the Allegheny Group, which makes it an important target for coal bed methane development. In ascending order, these include the Middle Kittanning coal, the Upper Kittanning coal, the Lower Freeport coal, and the Upper Freeport coal (Ruppert et al., 2001). Available data indicate that the average gas content for the Freeport coals is about 192 cf/ton, and about 252 cf/ton for the Kittanning coal beds (Bruner et al., 1995, 1998).

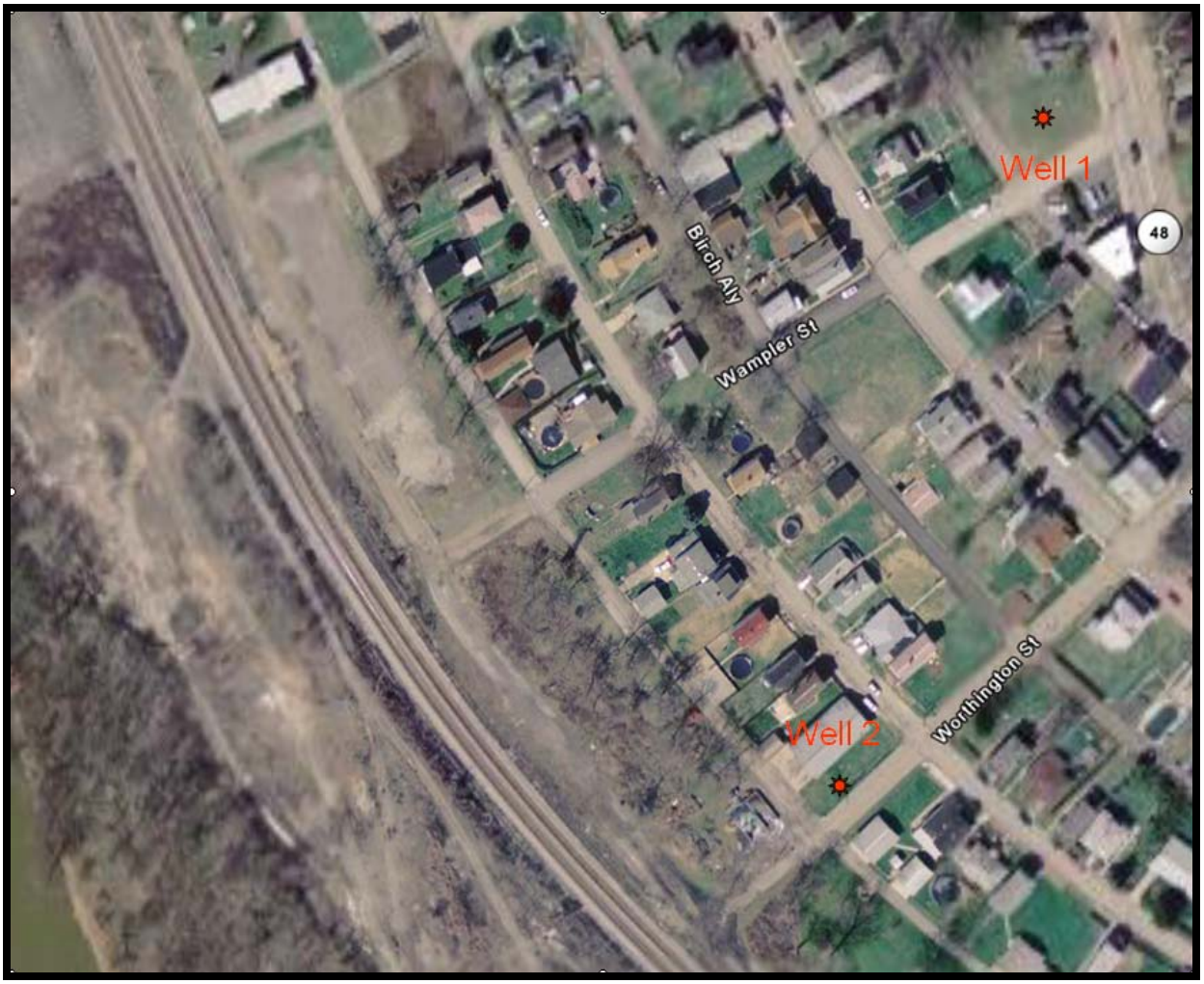

Figure 17. Well # 1 is located at 4722 Walnut Street, Versailles, PA. The total recorded depth of the well is 581.50 feet. Well #2 is located at the Borough municipal garage, Versailles, PA. This well was drilled to a depth of 575 feet and examined to a depth of 479.10 feet.

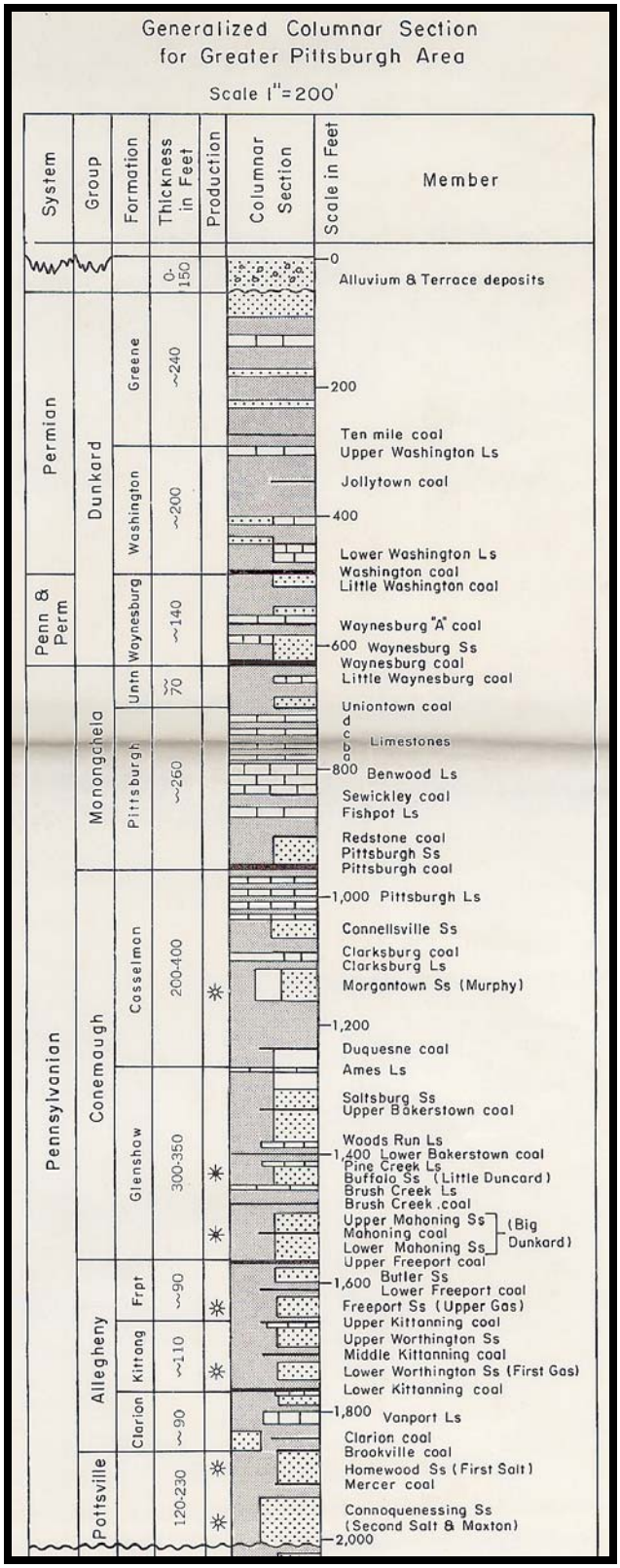

Figure 18. Detailed reference stratigraphic column for the Greater Pittsburgh region County from Lytle and Balogh (1975).

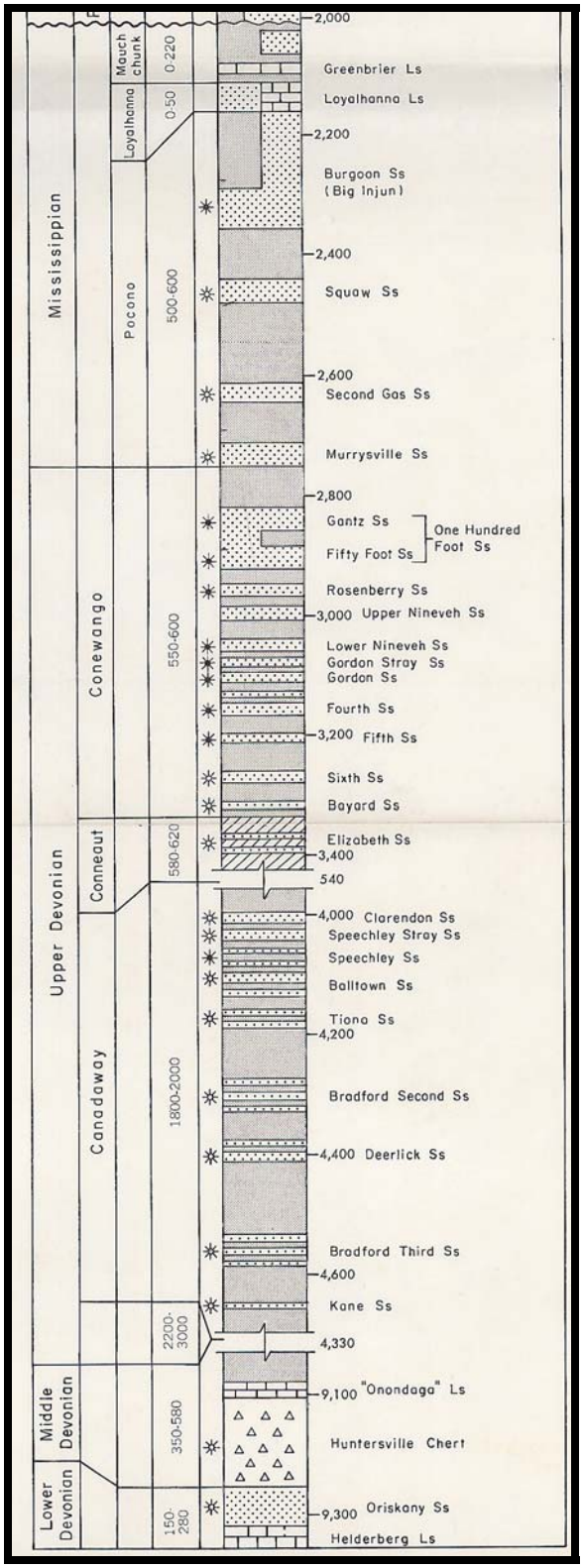

Figure 19. Detailed lower portion of the regional stratigraphic column for the Greater Pittsburgh region. The unit labeled Murrysville Ss (sandstone) and One Hundred Foot Ss (sandstone) are noted. This is taken directly from Lytle and Balogh (1975).

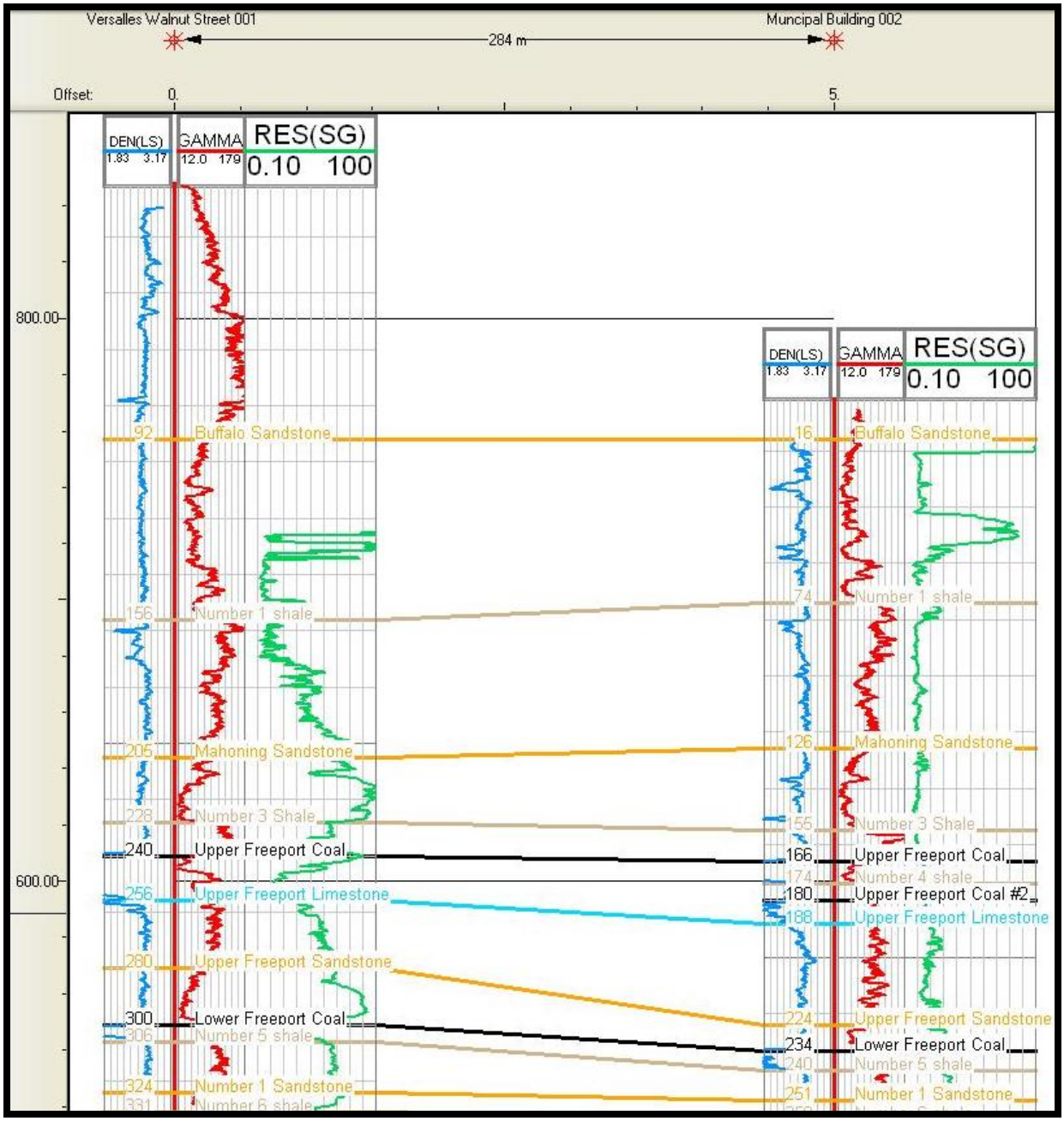

Figure 20. Correlation of Borough garage well with 4722 Walnut Street well interpreted section is between 520 and 850 ft above mean sea level. Refer to the associated table for the lithologies, simple fills are used to identify first-order correlations only.

The Buffalo sandstone is generally less than 30 feet in thickness. Where well developed, the sandstone is massive in character, coarse to pebbly in texture and gray to buff in color. It is resistant to weathering and erosion, becoming darker through exposure. The Buffalo sandstone has been an important resource, being quarried for houses, churches, schools and heavy masonry. Under deep cover, it becomes the Buell Run sand of the driller and yields petroleum, natural gas, and brine (Stout, 1943).

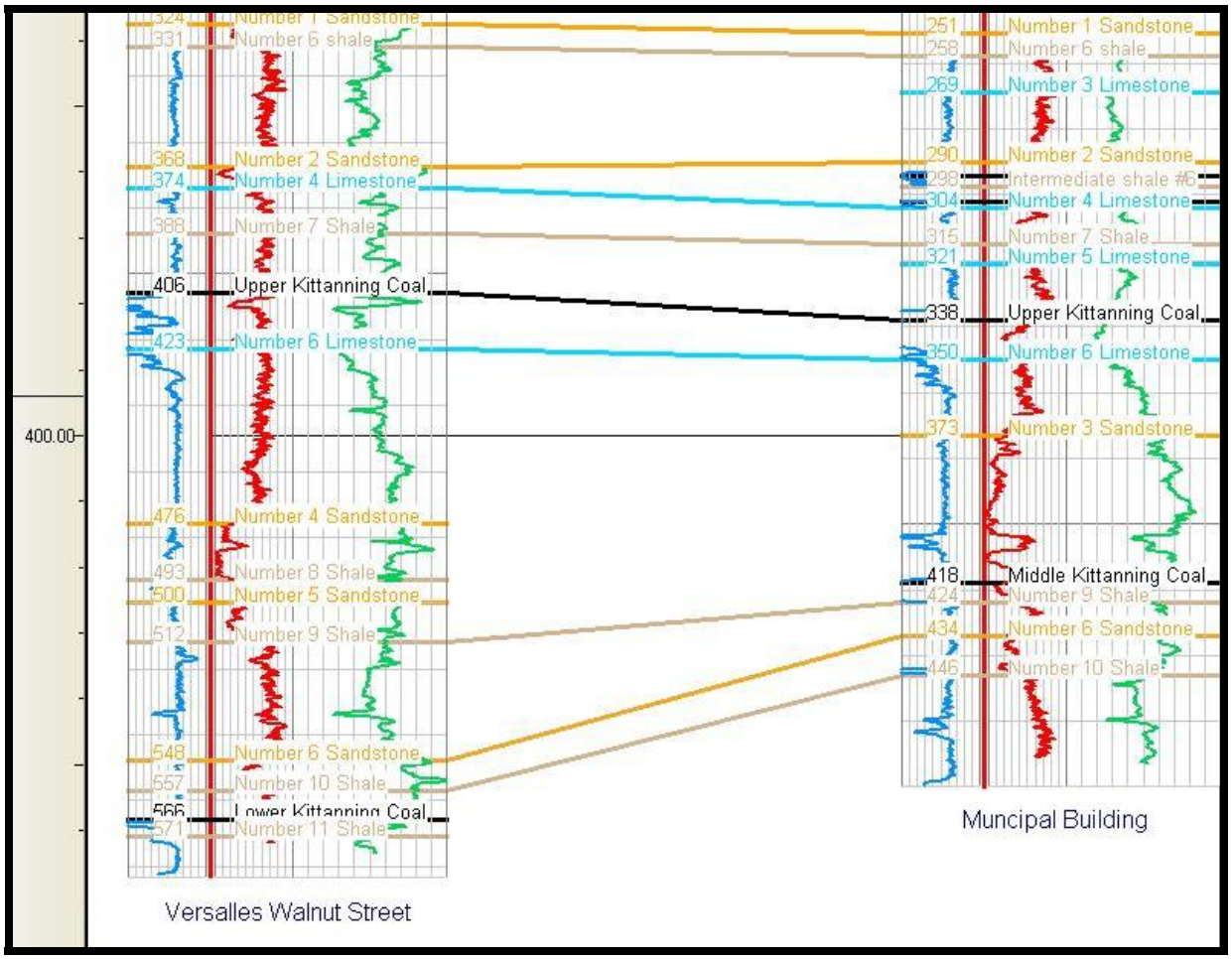

Figure 21. Correlation of Borough garage well with 4722 Walnut Street well is interpreted between 360 to 520 ft above mean sea level. Refer to the associated table for the lithologies; simple fills are used to identify first-order correlations only.

In the Versailles area, the Brush Creek coal only reaches a few feet in thickness; however, it is a known source of coal bed methane and has been commercially developed in the past.

The Mahoning sandstone varies from a fine-grained to coarse-grained or conglomeratic sandstone. The pebbles, which are milky quartz and commonly not more than one-fourth inch in diameter, are for the most part confined to the basal portion of the deposits. The Mahoning sandstone is commonly cross-bedded. In places, this physical feature is prominently developed. Within the Mahoning sandstone, significant variation is observed in the hardness and in the weather resistance of the material. In general, it is poorly cemented and crumbles readily on exposure to the elements (Stout, 1943). Figure 20 shows combined density gamma ray logs for the Mahoning sandstone and underlying Upper Freeport coal.

Table 3. Detailed interpretation of stratigraphy in Versailles area based on two borehole well logs. Units shown in italics were used as type-response units in interpreting the wire-line logs. Please note that the previous figures only show first-order correlations, units such as the predicted limestones, are actually quite thin where encountered and could represent shale responses; depths are in feet.

System	Group	Well number 1		Well Number 2	
		Depth to top	Formation Top Name	Depth to top	Formation Top Name
Upper Pennsylvanian	Conemaugh	92	Buffalo sandstone	16	Buffalo sandstone
		138	Buffalo Limestone or Shale	58	Buffalo Limestone or Shale
		147	Buffalo sandstone 2	66	Buffalo sandstone 2
		156	# 1 shale	74	# 1 shale
		160	# 1 Limestone or Shale	80	# 1 Limestone or Shale
		166	# 2 Shale	86	# 2 Shale
		173	# 2 Limestone or Shale	95	# 2 Limestone or Shale
		205	*Mahoning sandstone*	126	Mahoning sandstone
		228	*# 3 Shale*	155	# 3 Shale
		240	Upper Freeport coal	166	Upper Freeport coal
Middle Pennsylvanian	Allegheny	256	Upper Freeport Limestone or Shale	174	# 4 Shale
				180	Upper Freeport coal
		280	Upper Freeport sandstone	188	Upper Freeport Limestone or Shale
				224	Upper Freeport sandstone
		300	Lower Freeport coal	233.5	Lower Freeport coal
		306	# 5 shale	240	# 5 Shale
		324	# 1 Sandstone	251	# 1 Sandstone
		331	# 6 shale	258	# 6 Shale
		342	# 3 Limestone or Shale	269	# 3 Limestone or Shale
		367.5	# 2 Sandstone	290	# 2 Sandstone
		374	# 4 Limestone or Shale	294	# 1 Coal
		388	# 7 Shale	297.5	Intermediate shale #
		394	# 5 Limestone or Shale	302	# 2 Coal
		406	*Upper Kittanning coal*	304	# 4 Limestone or Shale
		423	# 6 Limestone or Shale	315	# 7 Shale
		476	# 4 Sandstone	321	# 5 Limestone or Shale
		493	# 8 Shale	338	Upper Kittanning coal
		500	# 5 Sandstone	350	# 6 Limestone or Shale
		512	# 9 Shale	373	# 3 Sandstone
		548	# 6 Sandstone	418	Middle Kittanning coal
		557	# 10 Shale	424	# 9 Shale
		566	Lower Kittanning coal	434	# 6 Sandstone
		571	# 11 Shale	446	# 10 Shale

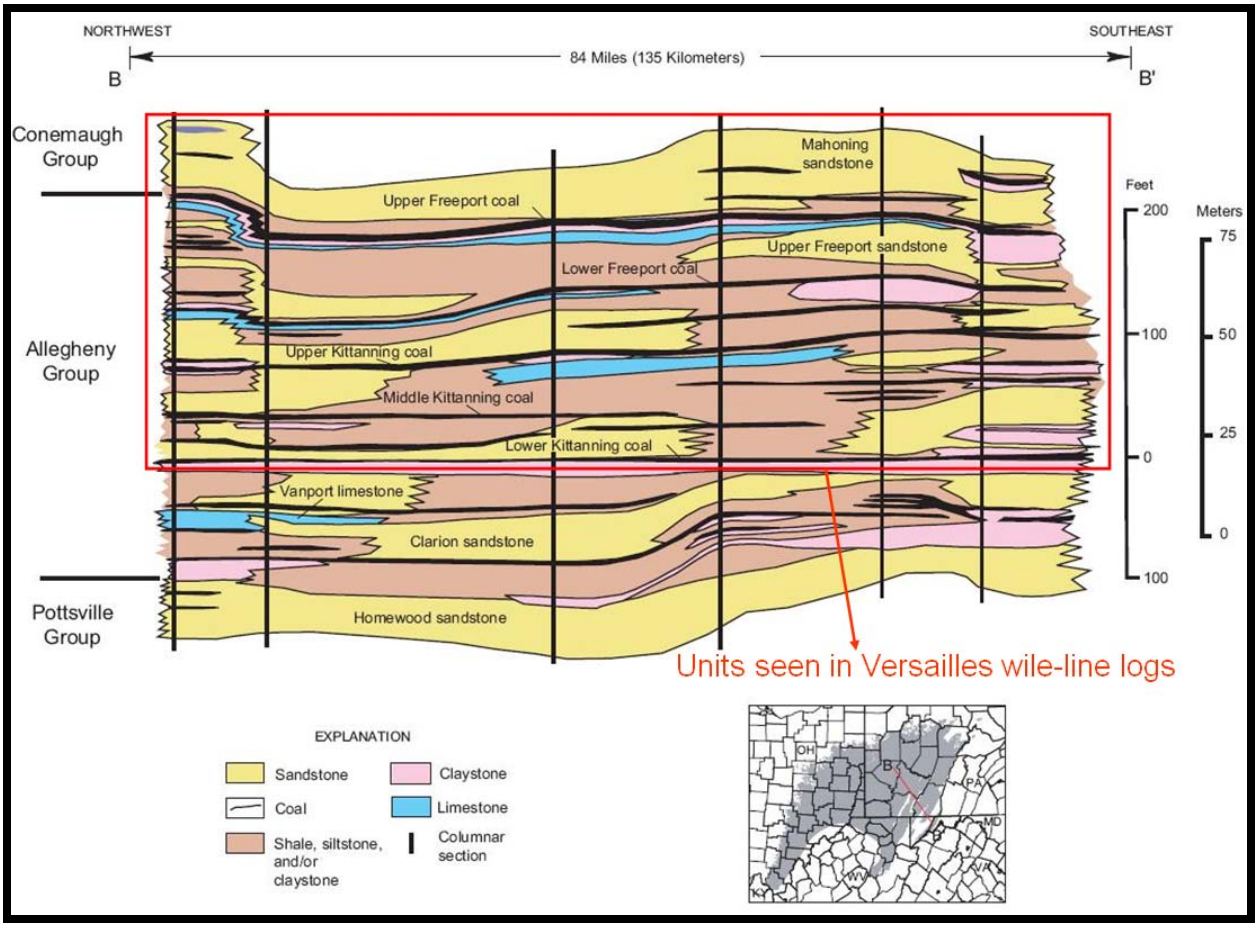

Figure 22. Interpretational cross-section showing units seen in Versailles wire-line logs (after Milici, 2004).

The Upper Freeport sandstone stratigraphically is located within the interval between the Lower Freeport coal and the Bolivar clay. It may be absent from the section, may fill only a part of the interval, may occupy this entire stratigraphic interval, or may expand so that it replaces overlying or underlying beds. It is generally loosely bonded, medium-grained sandstone, decidedly micaceous, and somewhat ferruginous in character. Clay matter also forms part of the bond. It is always cross-bedded, the planes being best marked on weathered surfaces. The color of the rock varies from light gray to brownish buff, the intensity of the shade depending on the quantity of the iron components present and on the degree of weathering. The Upper Freeport sandstone varies in thickness from 1 to 60 feet (Stout, 1943).

The Lower Freeport sandstone is stratigraphically located in the interval between the Middle Kittanning coal and the Lower Freeport limestone. The deposits vary from 5 to 75 feet or more in thickness. The Lower Freeport sandstone is generally massive in character, more or less marked by cross-bedding planes, somewhat micaceous in mineral content and medium to coarse in texture. The freshly quarried stone varies in color from very light gray, through yellowish and drab to reddish brown, the shades depending largely on the state of oxidation of the iron components. The chief bonding material is iron oxide in the limonite form. In Ohio, the Lower

Freeport sandstone was employed for building purposes. At various places along the line of outcrop across the state it has served many purposes such as construction of houses, blast furnaces, mills and mill dams, carding mills, retaining walls, culverts, bridges, abutments and foundations (Stout 1943).

The Upper Freeport, Lower Freeport, Upper Kittanning, and Middle Kittanning coals are considered thermally mature with respect to methane generation; the $\%R_o$ values exceed 0.6 to 0.8. Much of the coal bed methane gas is probably of thermogenic origin. In southwestern Pennsylvania, microbial gas in Pennsylvanian coal beds has been reported mixed with thermogenic gases (Laughrey and Baldassare, 1998). Microbial methane associated with coal beds has been generated from the formation of the first Pennsylvanian peat deposits to the present day, where surface waters interact with shallow coal beds (Laughrey and Baldassare, 1998). It is interesting to note that the lower Kittanning coal bed yielded a gas content of 352 cubic feet per ton (cf/ton) under ambient conditions, one of the highest then ever measured from a coal bed in the bituminous coal fields of Pennsylvania (Puglio and Innacchione, 1979).

In general, the stratigraphic sequence deposited during the Pennsylvanian period represents a classic thermocline sequence with alteration of transgressive and regressive cycles. In the upper part of the stratigraphic section (above the Upper Kittanning coal), most of the units can be correlated to each other, showing that changes in depositional environments are of regional scale. Geologic units below the Upper Kittanning coal have been interpreted to have been deposited in meandering river system present in the area in middle Pennsylvanian time, which could be responsible for the greater complexity of sediment load throughout the same area.

(This page intentionally left blank)

5.0 Regional Stratigraphy

In general, the logged area is underlain by Upper Devonian – Lower Mississippian strata composed of interbedded shales, sandstones and coals. Two distinctive marker beds are present throughout the southern Allegheny County: the Murrysville sandstone and the Hundred Foot sandstone formations, which used to be sources for gas production in the area in early 1900's. These sandstones are interbedded with shale markers. The overall sequence from oldest to youngest is shown in Figure 23.

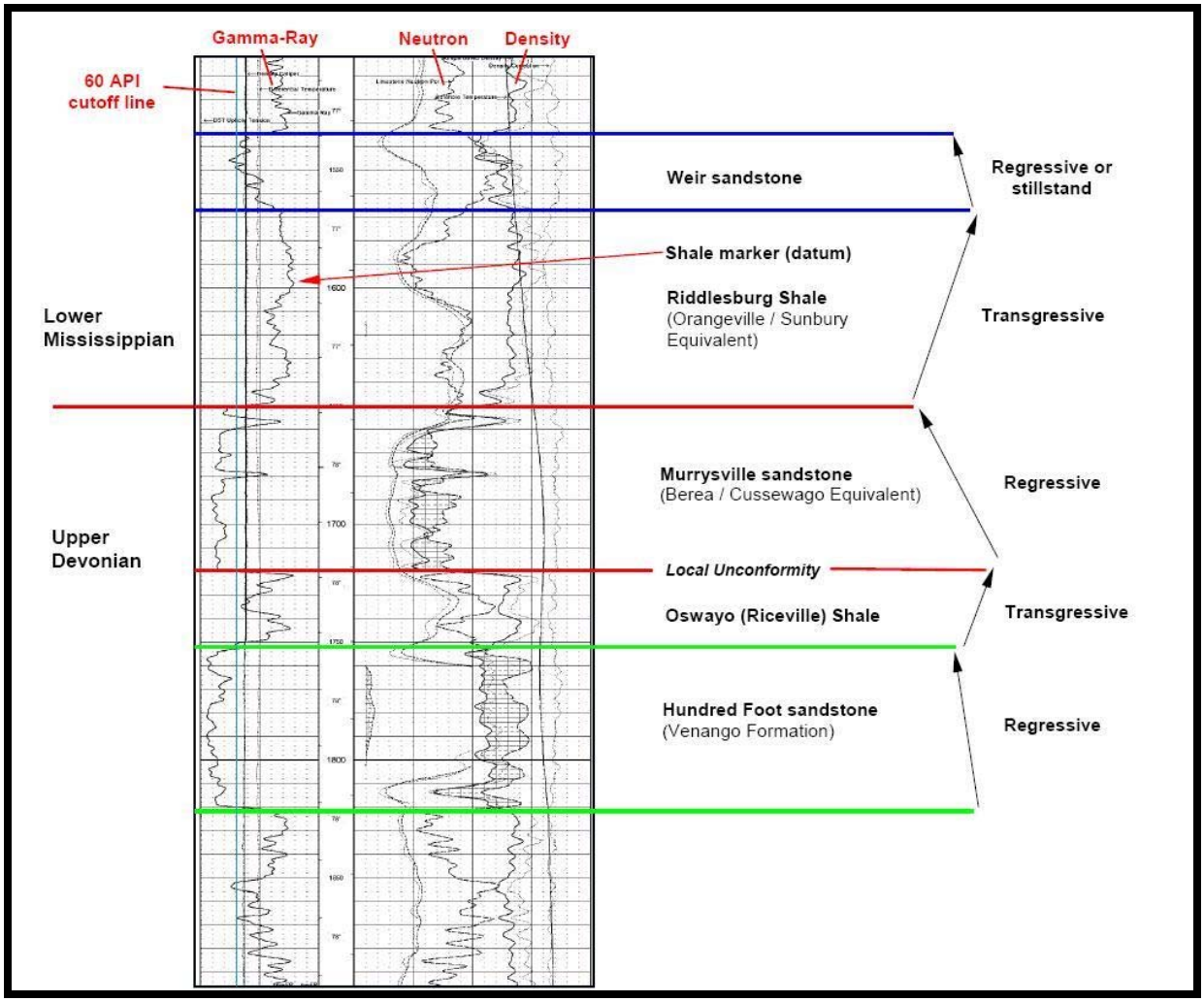

Figure 23. Type log showing formations used for the correlations in this study. The log is a Compensated Density log, API # 3712924778, taken from Westmoreland County. The transgressive and regressive sequences are those recognized in this study (McDaniel, 2006).

The Hundred Foot sandstone is the lowermost unit in this study. It is dominantly fine to coarse, angular to subangular, quartzite sandstone and conglomerate and is white to gray in color. Interbedded siltstone and shale are common throughout much of the Hundred Foot within the

study area. The Hundred Foot sandstone is thought to be migrating barrier-bar sandstone. It appears that that this formation was used to store natural gas in the Versailles area during the late 1950's,

The Riceville Shale consists mostly of white, light-gray and tan, fossiliferous siltstone and gray silty-shale and mudstone, and rests conformably above the Hundred Foot Sand. The Riceville represents deeper-marine sediments deposited just prior to the westward progradation of the Murrysville (Pashin and Ettensohn, 1995).

The Murrysville sandstone is Devonian in age and displays a distinct facies change from fluvial to deltaic. In general, the Murrysville is dull greenish-yellow to gray and may contain conglomeratic lenses with pebbles greater than 5 mm in diameter. This unit also contains interbedded siltstone and shale. The Murrysville is thought to represent a fluvial environment that transported sediments westward into a shallow restricted sea that covered much of Ohio, western Pennsylvania, and West Virginia during the late Devonian (Harper et al., 1989; Harper and Laughrey, 1987).

The Riddlesburg Shale is deposited disconformably above the Murrysville, and contains dark gray to greenish and grayish black laminated shale and siltstone with occasional sandstone and limestone beds. Harper et al., (1989) have interpreted the Riddlesburg as restricted marine because it contains burrows, brachiopods, bivalves, and occasional plant debris. It also marks and records a major transgressive event above the Murrysville (Figure 24). The Riddlesburg Shale grades upward into the Weir sandstone, a coarsening-upward succession of fine-to coarse-grained sandstone and conglomerate.

The Weir may represent shoreface and coastal deposition along a fluvial-dominated shoreline (Harper et al., 1989). The Weir has also been referred to as the 2nd Gas sandstone, another informal drillers' term. Although beyond the scope of this paper, there is a second sandstone that occurs in Allegheny, Washington, and Greene Counties above the Riddlesburg Shale called the Squaw (and occasionally the Papoose) sand that may somehow be related to the Weir sandstone further east, although the exact relationship remains undefined.

In Figure 25 (McDaniel, 2006), 15 logs are correlated from eastern Allegheny County, through northwestern Westmoreland County and into southern Armstrong County. This section displays the most striking example of the thinning of the Murrysville. The thick Murrysville sandstone section represents braided-delta deposition while the thin represent off-delta sedimentation. Sea-level fluctuations and long shore currents would have influenced these delta lobes.

The Hundred Foot sandstone is best developed along this section, with thinning from south to north, and the blocky sandstone indicates that we are within the barrier system, and away from the tidally influenced lagoon.

The Weir sandstone is almost non-existent along this section due to being offshore from the coastal sequence. Sandstone in this area is thin and discontinuous and may represent small bars of shelf sandstones west of the coastal beach system. The coarsening-upward sequence seen previously in the eastern sections is altogether absent in this area (McDaniel, 2006).

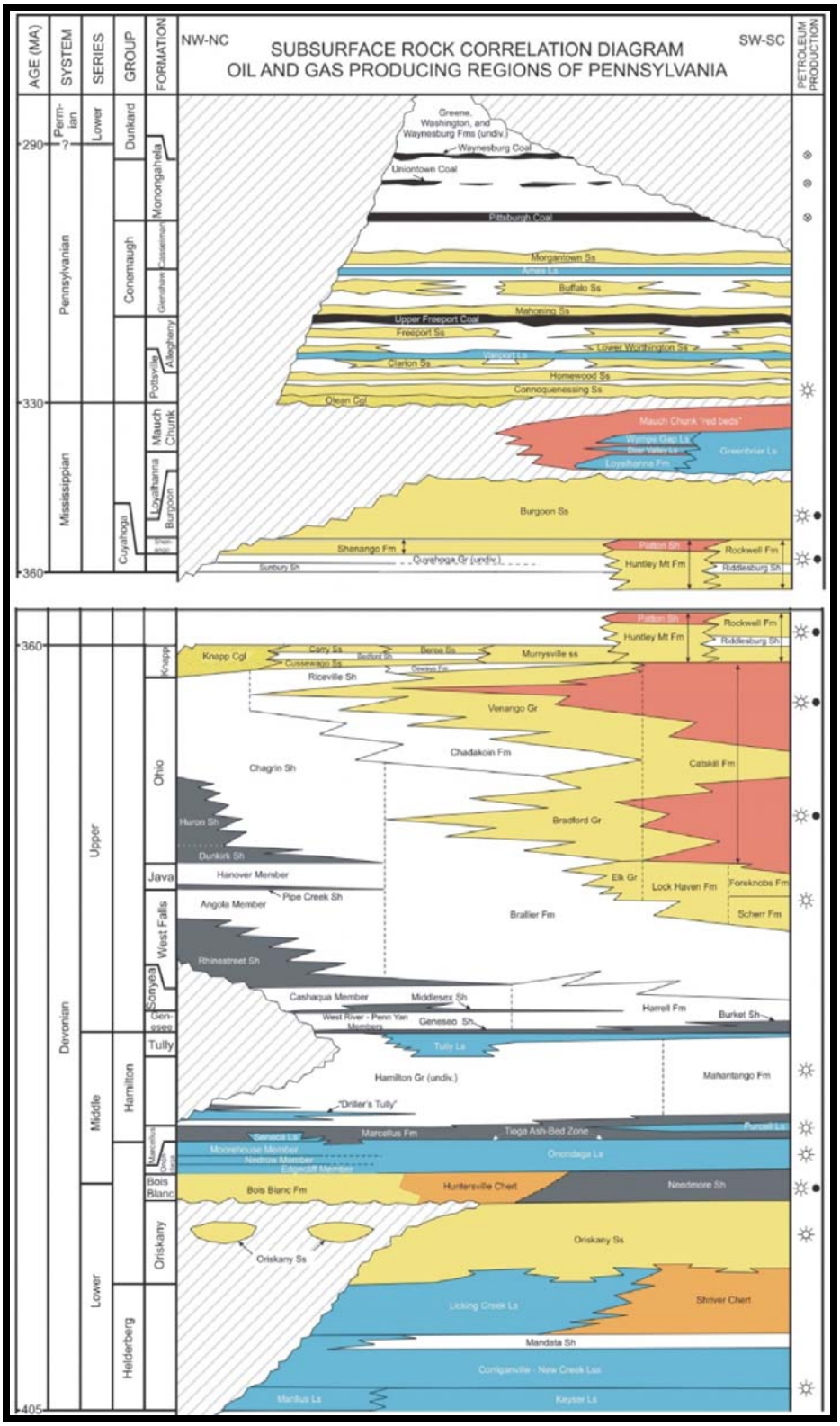

Figure 24. Statigraphic column for southwestern Pennsylvania showing oil and gas producing units. The Versailles area correlates with the left hand portion of this figure (SW) corresponding to the southwest Pennsylvania region.

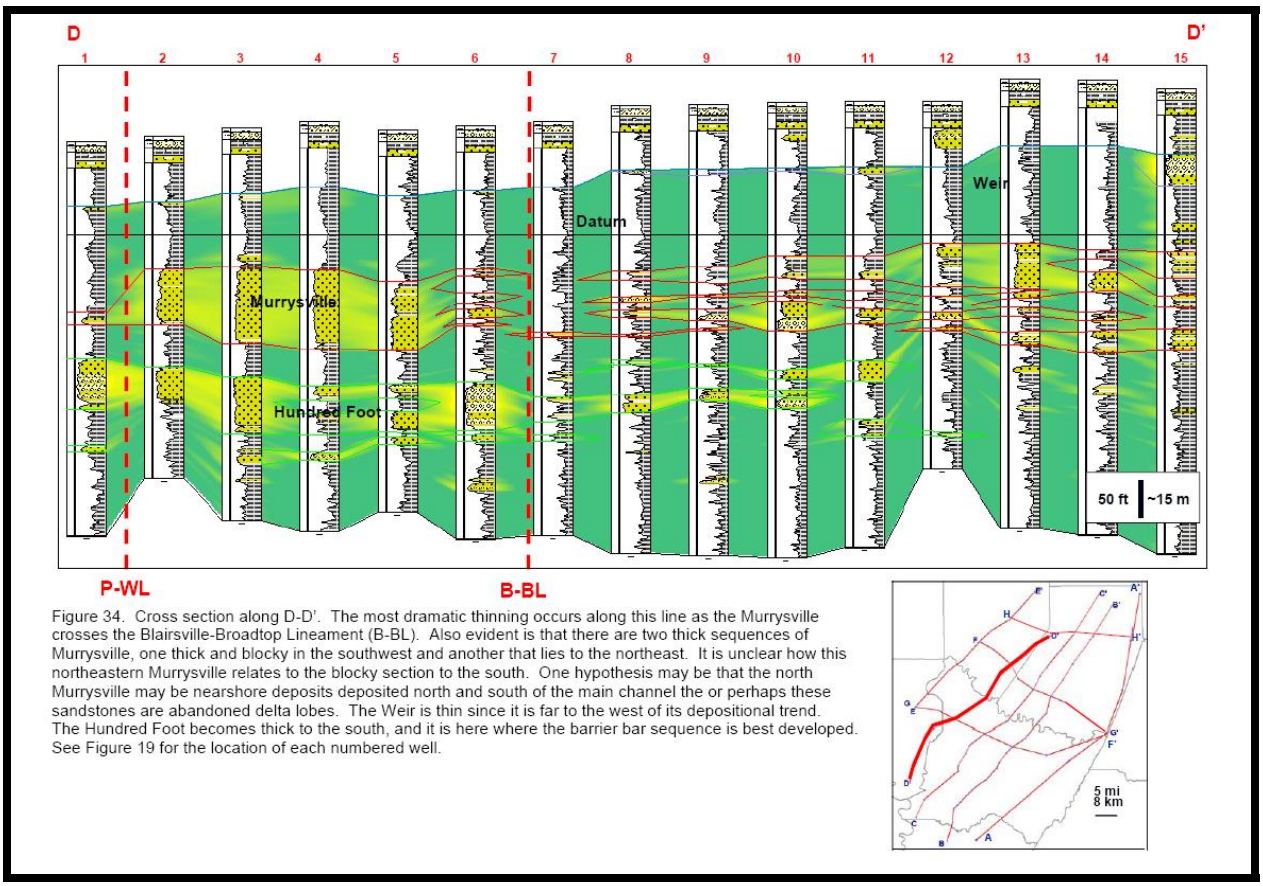

Figure 34. Cross section along D-D'. The most dramatic thinning occurs along this line as the Murrysville crosses the Blairsville-Broadtop Lineament (B-BL). Also evident is that there are two thick sequences of Murrysville, one thick and blocky in the southwest and another that lies to the northeast. It is unclear how this northeastern Murrysville relates to the blocky section to the south. One hypothesis may be that the north Murrysville may be nearshore deposits deposited north and south of the main channel the or perhaps these sandstones are abandoned delta lobes. The Weir is thin since it is far to the west of its depositional trend. The Hundred Foot becomes thick to the south, and it is here where the barrier bar sequence is best developed. See Figure 19 for the location of each numbered well.

Figure 25. Correlated cross-section (MacDaniel, 2006).

A geologic reconnaissance of the region directly across from Versailles was conducted in order to encounter and visually identify members of the stratigraphic column in the vicinity of Versailles, PA. As there were no outcrops found close to the known logged wells, geological data were collected from the opposite side of Youghiogheny River. A biking trail, following the river from the Boston Bridge Park was followed in order to get access to the best exposed outcrops in the area. A total of three stops were made on the way and a total of five outcrops were documented and sampled. Locations of observation stops are marked relative to the locations of logged wells, on Figure 26, along with a schematic summary of observations.

The first stop (40^{o} 18'45"N; 79^{o} 50'13"W) was approximately 500 meters (1640 feet) NW from the beginning of the trail. The outcrop is located on the left from the road, exposing about 5 vertical meters (16 feet) of thin-bedded grey-brownish shales (Figure 27, sample 1). The exposure is located approximately 10 meters (32 feet) above the base water level. The shales are micro-grained; bed thickness does not exceed 7-10 millimeters (0.28 inches to .39 inches). No reaction with HCl was noted. The attitude of these beds is sub-horizontal, no folding or unconformity was noticed. About 20 vertical meters (66 feet) above the outcrop (up the slope), another exposure was encountered. A thicker-bedded (also sub-horizontal) micaceous siltstone (sample 2) is micro-grained. When studied as a whole, these two outcrops represent a

stratigraphic column coarsening and thickening upward and presumably deposited in a fluvial environment.

Following the trail further in the NW direction, the same grey-brown shales can be observed on the left side (Figure 27). Stop 2 (40 °18'57.22"N; 79 °50'21"W) is located about 500 to 700 meters (1640 feet to 2297 feet) away from Stop 1. At the lowest point of this stop, the shales fully repeat those exposed at the first outcrop; therefore, no sample was taken. Approximately 20 vertical meters (66 feet) higher, another outcrop was found (sample 3). The exposed rocks are shaly, but with thicker bedding and coarser-grained matrix compared to the rocks at the base. This is presumably a transitional zone from shales to siltstones, which were encountered further up the slope (sample 4), approximately 70 vertical meters (230 feet) above the water level. Sample 4 is very similar to sample 2.

Following the trail further in the NW direction, a sign "Dead Man's Hollow," can be observed on the left side, approximately 500 meters (1640 feet) away from Stop 2. A pathway separates to the left from the original trail and Stop 3 (40°19'04"N; 79 °50'26.5"W) is located about 10-15 meters (33 feet to 49 feet) along that pathway The pathway goes into the valley of a small creek (Figure 27) and exposes an elongated outcrop on the left measured vertically 5-7 meters (16 feet to 23 feet) roughly at and extending laterally another 100-150 meters (328 feet to 492 feet) westbound along the southern boundary of the valley. At the base, the rocks are grey shales (Figure 27), which are extremely thin-bedded (1-3 mm thickness; 0.04 inch to 0.12 inch) and otherwise similar to those observed at stops 1 and 2. Moving further west, the shale grades into micaceous siltstones and sandstones (sample 5), revealing facies change within the same formation. In Figure 28 cross-bedding is depicted.

Based on the altitude, varying from 760 to 960 feet above mean sea level, the sub-horizontal attitude of the bedding and the elevations of the known wells (771 feet, Borough garage well and 847 feet, Walnut Street well), it is logical to assume that the encountered rocks must be of the same formation as at in-between the tops of two wells. In Figure 29, a correlation model with the existing two wells is shown. According to this figure, the encountered rocks should be a part of the Buffalo member of the Conemaugh group.

In our interpretation, the observed rocks were formed in a fluvial non-marine environment, as most of the material composing shale and siltstones is of terrigenic or even volcanic origin. No lime material was present in any of the samples (negative reaction with HCl). In Figure 30, a simplified model of facies change within a single formation is depicted that would explain field observations. It is speculative to interpret depositional environments of the material in more detail; however, transitions from shale to siltstones and to sandstones with notable facies changes could characterize a braided or meandering river system, and samples 4 and 5 could be described as typical channel sandstones. Deposition in a fluvial environment would also explain the presence of mica (muscovite) in some of the samples, as it presumably had to travel from distances of hundreds of miles or kilometers (no volcanic activity is known in the vicinity of the encountered outcrops).

In terms of potential for hydrocarbon accumulation further analysis is needed. However, rough field techniques (the rule of tongue) were used to identify the siltstones and sandstones as rocks

with micro-porous fabric (potential reservoirs) and the shale as impermeable rocks with extremely low effective porosity (potential seal). If siltstones and sandstones of the group are proven to allow natural gas migration, it would be fair to assume that in an environment of facial changes, there could be stratigraphic traps present in the region under study.

Table 4. Samples collected in Versailles area.

#	Color	Mineral Composition	Grain size	Roundness	Name	Fossils, Comments
1	Gray-Brown	Quartz, feldspar, mica	Very fine-grained	Well-rounded	Shale	Thin-bedded in the outcrop
2	Gray	Quartz, feldspar, mica	Fine grained	Well-Rounded	Siltstone	Dirty siltstone, some cross-bedding in the outcrop
3	Gray-Brown	Quartz, feldspar, mica	Very fine grained	Well-rounded	Shale	No fossils
4	Gray	Quartz, feldspar, mica	Fine grained	Well-rounded	Sandstone	Plant fossils
5	Gray	Quartz, feldspar, mica	Fine grained	Well-rounded	Sandstone	Slightly higher mica content, slightly coarser-grained than sample 4

Figure 26. Location of outcrops in relation to known wells in Versailles.

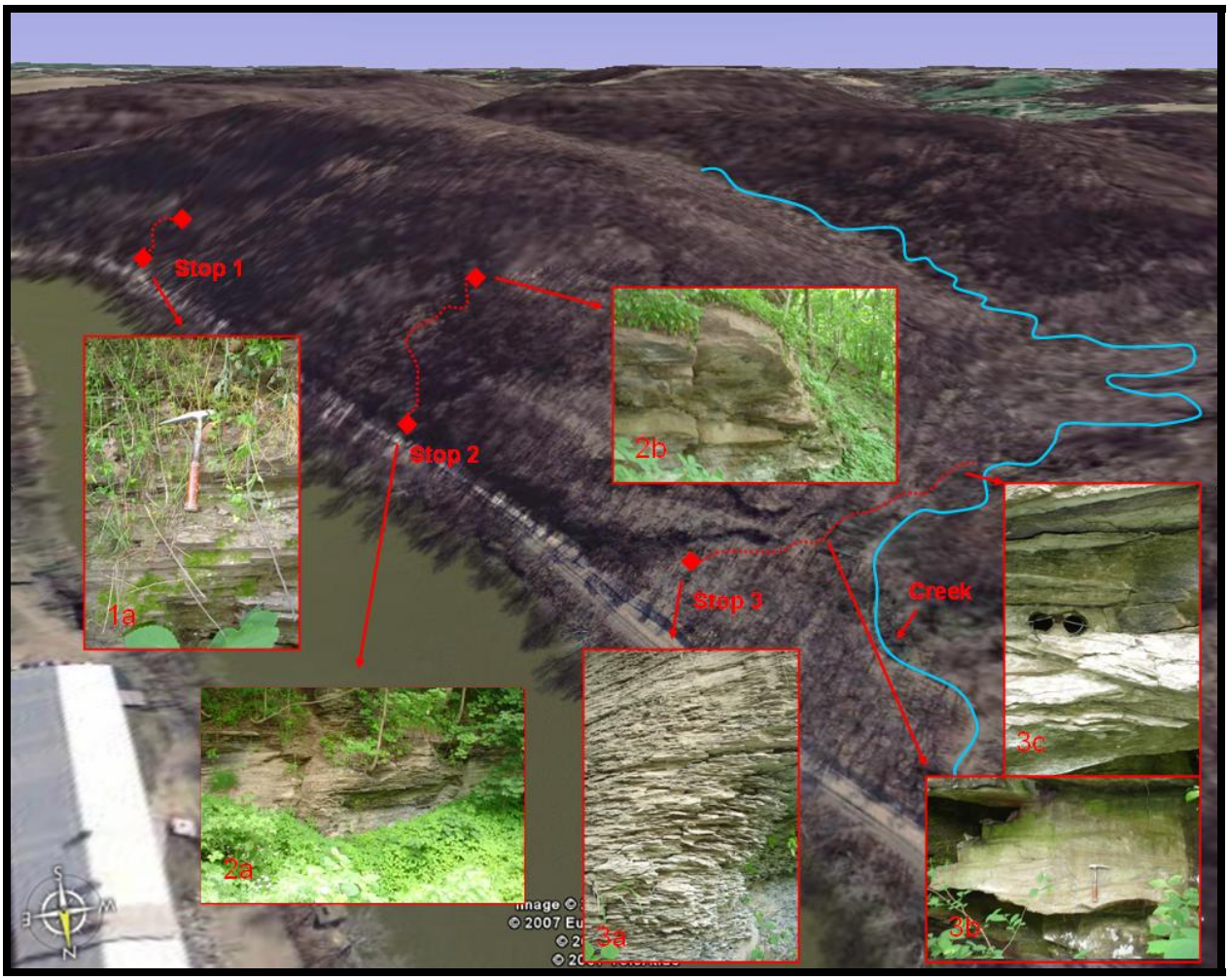

Figure 27. 3D view of the region under study with local photographs: 1a – Shale, stop 1, 2a – Shale, stop 2, 2b – Sandstone, stop 2, 3a – Shale, stop 3, 3b – Siltstone stop 3, 3c – Cross-bedding in sandstone, stop 3.

Figure 28. Various types of cross-bedding encountered at stop 3. 3a – Trough cross-bedding, 3b – Hummocky cross-bedding, 3c – Planar cross-bedding.

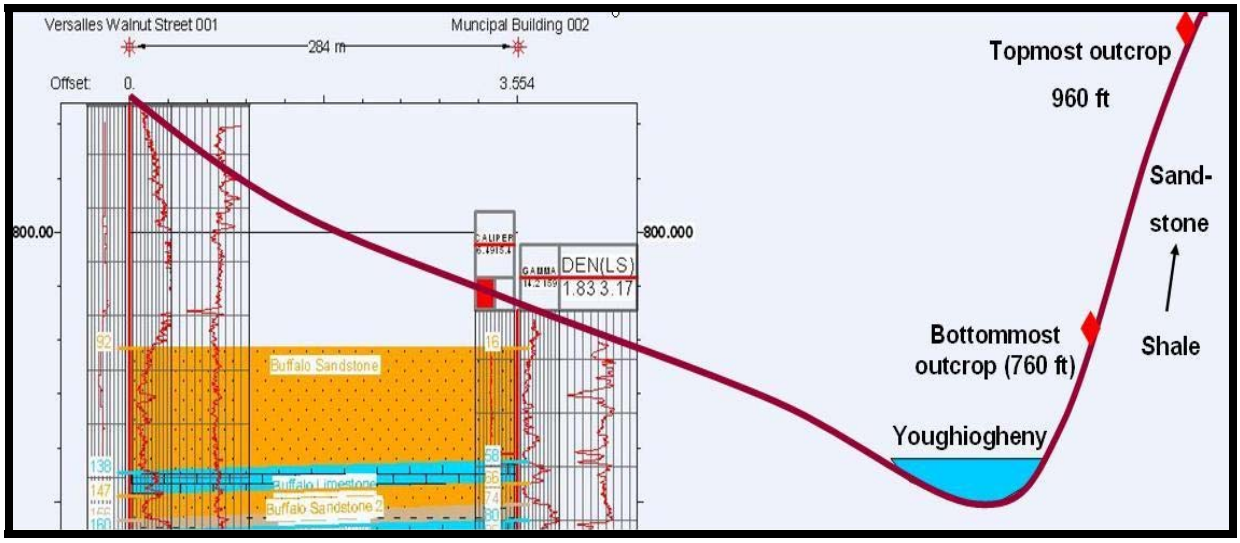

Figure 29. Vertical correlation of observed outcrops and logged wells.

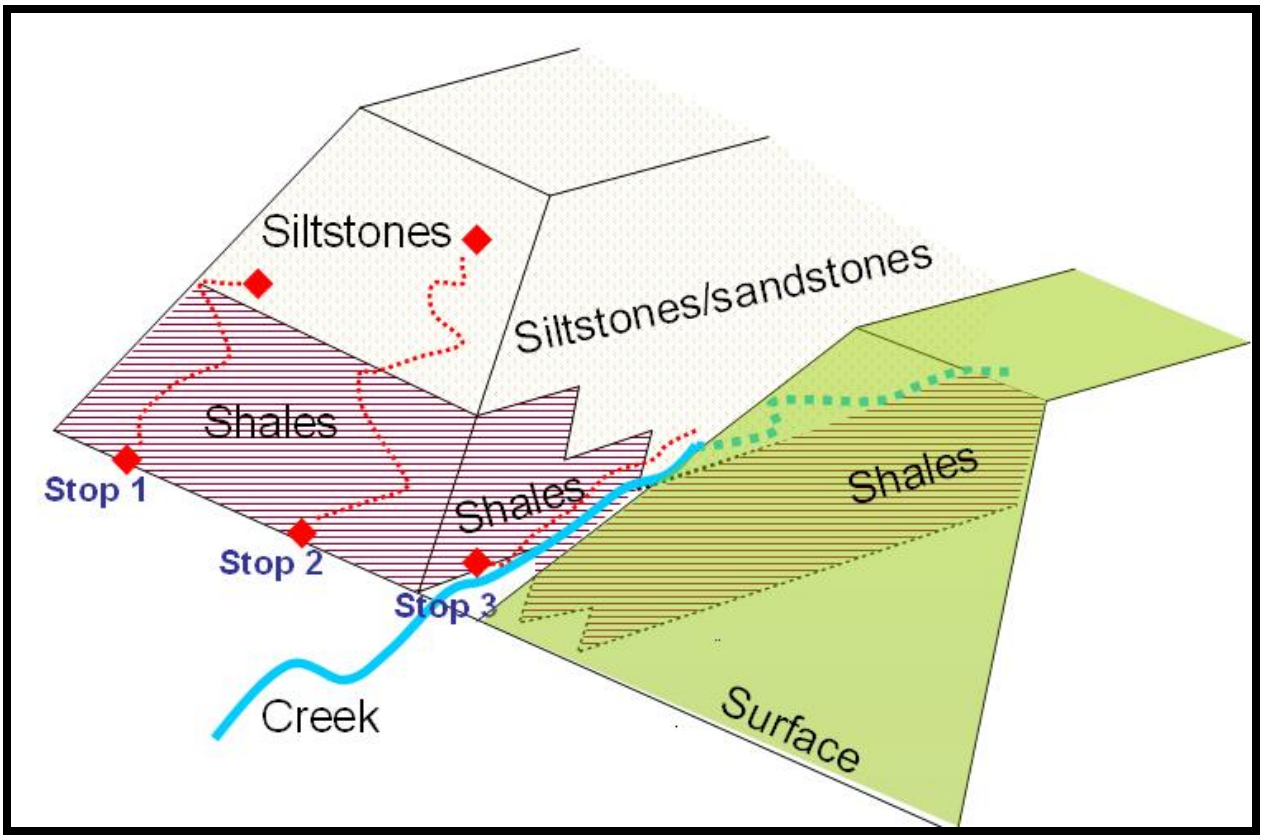

Figure 30. Schematic description of a possible facies variation in the surveyed area.

The samples were tested for effective porosity as well as for hydraulic conductivity. In order to prepare the samples for tests, they were cut into cubes, measured, accurately weighed (some of them repeatedly) in a dry state and their densities were calculated.

A porosity test was implemented using a 1 liter glass tube, sealed from one end and scaled at 10 ml intervals. The tube had an opening wide enough to accommodate samples in raw or partially cut state and to allow 800 milliliters of tap water in addition to each sample. All of the equipment necessary for these tests was available at the soils laboratory at the Department of Civil Engineering, University of Pittsburgh, with the help of Dr. J. S. Lin and Dr. R. Quimpo.

For each sample, the tube was filled with 800 ml of H_2O and then the dry sample was dropped into the tube, raising the water level in the tube by its volumetric content. Then, its specific gravity was calculated, as its total mass normalized by its volume. For each sample, 5 to 10 hours were allowed in order for the water to saturate the rock; then samples were removed from water, wiped externally and weighed again. The specific gravity at 21°C was determined to be 0.961 kg/m^3. Based on the change in sample masses, porosity was calculated as:

Equation 1: Calculation of effective porosity

$p = (\Delta m/0.961)/V*100\%$

where p is the effective porosity and Δm is the mass of the water contained in sample, in grams (representative of the volume of interconnected pore space in milliliters).

In Table 5, the measurements are provided along with the calculated density and effective porosity values.

Table 5. Effective Porosity $V(H_2O)$ – volume of water used for the experiment in milliliters, V sample – measured volume of sample in pre-cut or partially-cut state, m_{dry} – electronically measured mass of dry sample, $m_{dry(2)}$ – mass of dry sample electronically measured, m_{sat} – electronically measured mass of a water-saturated sample, **Δ**m – difference between the dry mass and the saturated mass, **ρ**(dry rock) – calculated density (specific gravity) of dry sample, Effective porosity (%) – percentage of interconnected pore-space filled with water upon the completion of the experiment. * – two out of 5 samples (1 and 4) had to be pre-cut in order to be accommodated into the experimental tube. All of the samples were further cut into accurate geometrical shapes for the second experiment described below.

Samples	**$V(H_2O)$**	**V sample (ml)**	**m_{dry}**	**$m_{dry(2)}$**	**m_{sat}**	**Δm**	**ρ(dry rock)**	**Effective porosity (%)**
1	800	50	124.5		125.7	1.2	2.49	2.50
2	800	56	145.1		146.9	1.8	2.59	3.34
3	800	25	59.3	59.4	60.1	0.8	2.37	3.33
4	800	68	170.7		176.1	5.4	2.51	8.26
5	800	69	173	173	177.6	4.6	2.51	6.94

Hydraulic conductivity was determined using a slightly modified version of the falling head test in soil mechanics. According to Darcy's law, during gradual discharge, the equation for the coefficient of permeability is:

Equation 2: Equation used to estimate hydraulic conductivity

$-a*dh/dt = k*(h/L)*A$ (from Cernica, 1995)

Where a is the area of a standpipe, dh/dt is the time derivative of hydraulic drawdown, k hydraulic conductivity (meters per second), h water level in the standpipe, and A is the cross-sectional area of the sample.

Solving this differential equation using the method of separating variables and then integrating, we can derive Equation 3 for k:

Equation 3: Derived equation to calculate hydraulic conductivity

$$k = \frac{aL}{At_f} \ln \frac{h_0}{h_f}$$ (from Cernica, 1995)

In order to complete the experiment, rock samples were cut into cubic shapes at the Rock Laboratory of the Department of Geology and Planetary Science (University of Pittsburgh). In Table 6, linear dimensions (x,y,z) of the samples are shown in millimeters and meters; in addition, the cross-sectional area A is calculated as well as the total volume of each sample cube (both in cubic meters and in milliliters).

Table 6. Linear dimensions of the samples after they were cut in the laboratory.

Samples	x (mm)	y (mm)	z (mm) (L)	X (m)	Y (m)	Z (m) (L)	A (m^2)	Vol (ml)	Vol (m^3)
1	90.00	32.00	13.00	0.090	0.032	0.013	0.002880	37.440	0.000037
2	40.00	37.00	21.00	0.040	0.037	0.021	0.001480	31.080	0.000031
3	39.00	30.00	12.00	0.039	0.030	0.012	0.001170	14.040	0.000014
4	60.00	42.00	13.00	0.060	0.042	0.013	0.002520	32.760	0.000033
5	59.00	26.00	23.00	0.059	0.026	0.023	0.001534	35.282	0.000035

No equipment was available for this test at the University of Pittsburgh so an apparatus was designed and built in order to complete the experiment. A standpipe with a radius of 0.5 cm was used. The standpipe was equipped with a 10 ml scale bar (total of ten scale markings at 1 ml per scale). The beginning elevation of water table above the relative surface (floor) was 1.07 m.

For each sample, flow was allowed until the drawdown in the standpipe reached 100 mm. Then the time was measured for such drawdown to occur and the desired coefficient was calculated according to Equation 3 of this section. Finally, the following values were calculated for the experimental hydraulic coefficients (Table 7).

These results are significant because they show the low porosities of the sampled units and the extent of variation in hydraulic conductivity. These results suggest that gas leakage to the near surface probably occurs through abandoned well bores or fractures rather than through the solid bed rock.

Table 7. Results of hydraulic conductivity experiment.

Sample	A (m2)	L (m)	a (m3)	h0 (m)	hf (m)	t, sec	k (m/sec)
1	0.002880	0.013	7.854E-05	1.07	0.97	7020	4.95495E-09
2	0.001480	0.021	7.854E-05	1.07	0.97	2800	3.90503E-08
3	0.001170	0.012	7.854E-05	1.07	0.97	10020	7.88774E-09
4	0.002520	0.013	7.854E-05	1.07	0.97	900	4.41698E-08
5	0.001534	0.023	7.854E-05	1.07	0.97	180	6.41882E-07

(This page intentionally left blank)

6.0 Interpretation of Seismic Data

Velocity analysis was performed based on the sonic velocity data acquired by Century Geophysics in 2006 as a result of the down hole survey of two wells located in Versailles, PA. There were a total of four velocity zones identified for Borough garage well and five for the Walnut Street Well.

Sonic velocity readings were only provided for the Walnut Street Well and only for a limited and shallow portion of the stratigraphic column. Therefore, in many cases, either the averaged or interpolated values were used or in the case of Walnut Street well, the values were extrapolated from the Borough garage well, based on the stratigraphic correlation discussed earlier.

Zone one is a near-surface low velocity zone (further LVZ). It was present in both well logs with thickness varying from 3.2 m (10.5 feet) at Walnut street well location to 5 m (16.4 feet) at the Borough garage well. The velocity through LVZ was estimated at 0.91 km/sec (2986 feet/sec) based on 1D modeling performed using SurfSeis™ 1.80 software.

Zone two is only present at the Walnut Street well and is represented by strata located at depths from 3.2 to 28.5 m (10.5 feet to 93.5 feet). A weighted average value (2.81 km/sec or 9219 feet/sec) was assigned to this zone based on averaging of 3387 sonic velocity readings taken from the Walnut Street well wire log.

Zone three is part of the cross-section from LVZ to the Upper Freeport coal, where the Borough garage well is missing reliable sonic velocity readings. Therefore, known sonic velocity values from similar units were used to calculate arithmetically averaged velocities for sandstone, shale, limestone and coal (Table 8).

Table 8. Averaged sonic log P wave velocities of sedimentary units present in Versailles area in units of km/sec and feet/sec.

Sandstone	**Shale**	**Limestone (or shale)**	**Coal**
1.54	2.01	2.4	1.54
4.2	3.98	3.9	1.42
2.18	3.99	3.25	1.49
2.07	4.2	3.88	1.616
3.8		1.4	
4.76		2.99	
Average (km/sec)			
3.09	3.545	2.97	1.5165
Average (feet/sec)			
10134	11630	9744	4975

The thickness of zone three is 45 m (148 feet; between depths of 5 to 50 m) in the vicinity of Well 1, and 55 m (180 feet; between depths of 28.5 to 73.5 m) in the vicinity of Well 2. This

zone includes the Buffalo and Mahoning sandstones as well as the Brush Creek coal and is bound by the Upper Freeport coal at the bottom, but does not include the latter.

Zone 4 includes all the strata from the Upper Freeport coal to the Lower Kittanning coal and is characterized by interpretable and accurate sonic velocity data available from Well 2. This data was further extrapolated onto Well 1 using stratigraphic correlation and an assumption of a sub-horizontal dip of the layers. In the vicinity of Well 1, zone 4 includes all the strata in the depth range between 50 (164 feet) and 180 m (591 feet). Although the Lower Kittanning coal is located below the deepest horizon of Well 1, 180 m (590 feet) is a fairly accurate estimate for the depth to this horizon based on seismic reflection data. In the vicinity of Well 2, zone 4 comprises all the strata between 73.5 (241 feet) and 174 m (571 feet).

Zone five was defined as all strata beneath the interpretable extent of well log sonic velocity data. Since no detailed data on sonic velocity measurements were available beneath the 175 m depth (574 feet), the zones were assigned an average generalized velocity of 2.81 km/sec (9219 feet /sec; similar to zone 2). The estimated depths to regional coal units are shown in Table 9.

Table 9. Correlation of seismic data with the stratigraphic column.

Name	Estimated TravelTime (ms)	Estimated depth (m)	Estimated depth (ft)	Reflector
R1	27	26	85	Brush Creek coal 2
R2	44	51	167	Upper Freeport coal
R3	91	104	341	Upper Kittanning coal
R4	110	128	420	Middle Kittanning coal
R5	150	180	591	Lower Kittanning coal
R6	175	219	719	Clarion #1 (Brooksville) coal

Coal seams are generally weaker than the enclosing strata. When subjected to structural deformation (faulting and folding), fracture systems are formed within the coal beds, allowing space for the coal bed methane (CBM) or methane from lower strata to be stored and migrate. .

Natural fracture systems usually form as closely spaced orthogonal cleat systems early during the coalification process (Burner et al., 1998). In the Appalachian basin, it is common for secondary fracture system to occur as a result of tectonic activity and to be superimposed upon previously existing cleats. These secondary fracture systems significantly increase the fracture porosity. However, according to Pashin and Hinkle (1997), wherever the dip of the folded coal seams exceeds 10°, the secondary porosity tends to destroy the initial cleat and then replace it with closely spaced inclined fractures and normal faults. The occurrence of bedding parallel faults and associated structures within coal beds may significantly increase fracture porosity, both within the coal beds and in the enclosing strata (Milici et al., 1986).

Long distance migration of methane through coal beds is unlikely, especially if the coal beds are wet, because formation waters would inhibit desorption of methane into a fracture network. In contrast, relatively porous sandstone beds adjacent to coal source rocks may provide a network

of fractures and pore spaces sufficient to support long-distance migration of desorbed gases (Milici, 2004). Seals preventing methane migration from the coal bed can be either impermeable rocks overlaying the coal beds (shales, limy shales) or groundwater contained in the pore space of coal seams, which would increase the pressure, trapping the methane within the coal bed.

Processed reflection seismic data were carefully examined and plotted tied to common mid-point (CMP) locations. Figure 31 is a map showing CMP locations aligned to form 12 lines.

Stacked reflection seismic data amplitudes were plotted versus calculated Poisson Ratio coefficients and Shear wave reflectivity charts. There could be three types of natural gas deposits in the area under study: CBM trapped within a coal seam, CBM which escaped from a coal seam and trapped in a reservoir adjacent to the coal seam, and methane in either location that has migrated upwards from lower strata. Peng et al., (2006) emphasized six main concepts applicable to interpretation of such gas deposits.

1. Gas always lowers Poisson's ratio in sandstone
2. Cleats and fractures in coal seam result in higher Poisson's ratio
3. Top of gas sands can be recognized by negative AVO gradient
4. Top of the CBM reservoir has a positive AVO gradient
5. Coal seams have strikingly high reflection amplitude
6. Gas sands have low impedance

The fact that reflectors on the seismic data align within reasonable error allowance with the known coal seams revealed the accuracy of analytical velocity analysis performed for the Borough garage well. Furthermore, the correlated marker beds can be continued and traced in other CMP lines, allowing further interpretations to be performed. The R6 reflector lies beyond the extent of both wells surveyed in the area under study; however, according to various sources (Johnson, 1929; Milici et al., 2004), this might be the Clarion #1 or Brooksville coal bed, which is the lowermost member of the Allegheny group and according to the geologic data should be approximately 40 to 50 m (131 feet to 164 feet) below the Lower Kittanning coal.

A total of three potential reservoir locations were delineated and targeted for further analysis. The interpretational cross-section of CMP line 10 is shown as Figure 32. Bright spots are regions of anomalous S wave reflection coefficient distribution, which might indicate gas accumulation. In terms of reflection amplitudes, they are represented by sets of “trough over peak” anomalies, which also indicate possible gas accumulation. In Figure 32, the deepest reservoir location is depicted at 240 milliseconds, which corresponds to 308 m (1011 feet) of depth for this particular location. This depth would be coincident with the Pottsville Group (possibly the Homewood sandstone, Milici et al., 2004)

A shallower reservoir was detected on combined cross-sections for CMP lines 13 and 14 (Figure 33, Figure 34, Figure 35, Figure 36, and Figure 37). Here, two-way travel time to the reservoir can be averaged at 50 milliseconds, which for this particular location would correspond with a depth at 67 m (220 feet) and can be correlated with the Mahoning sandstone unit adjacent to the Upper Freeport coal and sealed by a shale unit from above.

Figure 31. Common mid-point locations, Versailles, PA.

Finally, the shallowest reservoir anomaly was detected on the CMP line 11 (Figure 38). On this line, some near-surface disturbance is notable. The data is noisy, but a signature is present, similar to the one describing reservoirs in previous interpretations. This anomaly is adjacent to a different coal zone than the Upper Freeport (possibly Brush Creek) coal, and could be the Buffalo sandstone. Estimated depth to this reservoir could reach 50 m (164 feet).

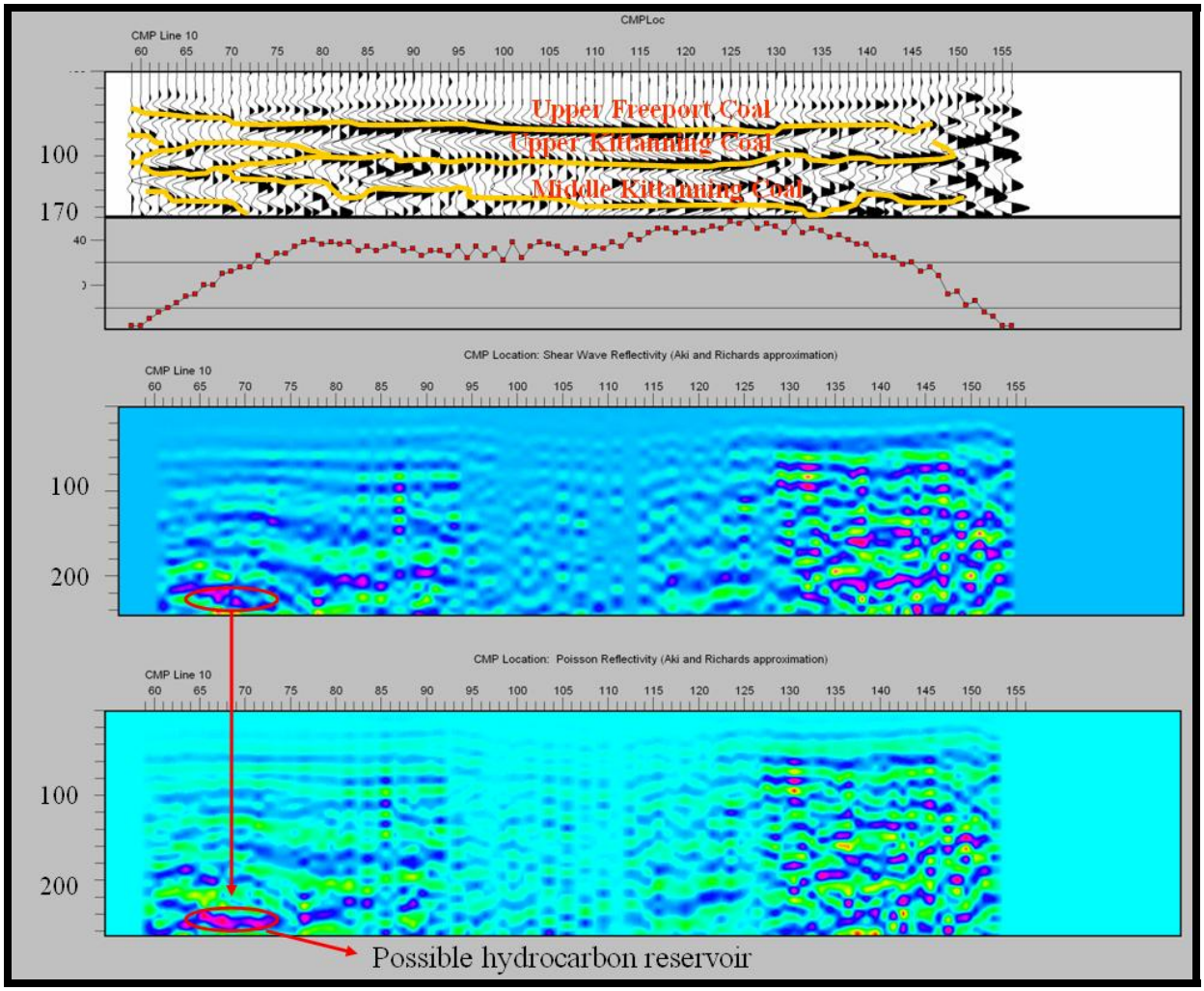

Figure 32. Seismic interpretation of line 10 (Deep reservoir).

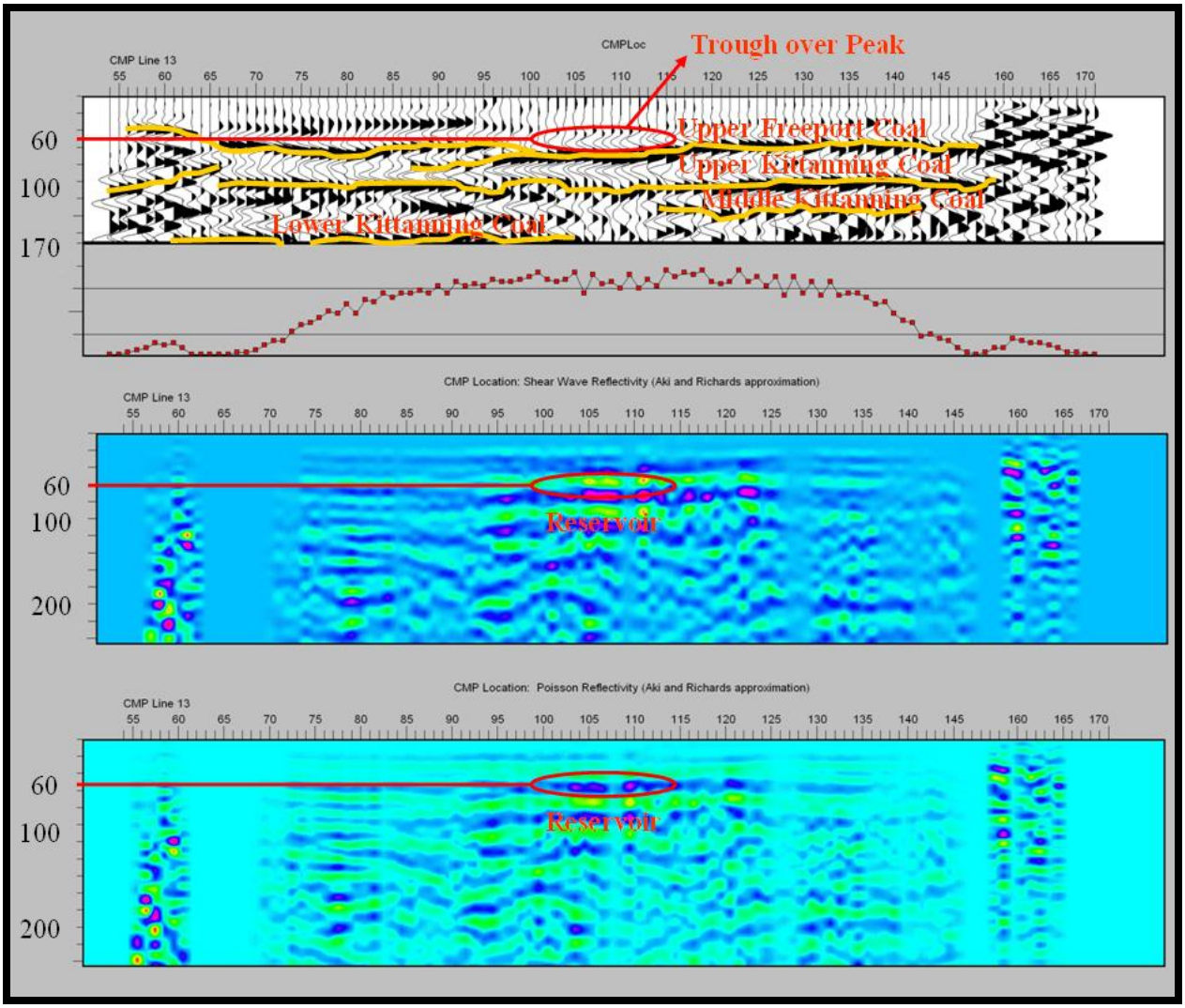

Figure 33. Seismic interpretation of line 13 (Shallow reservoir).

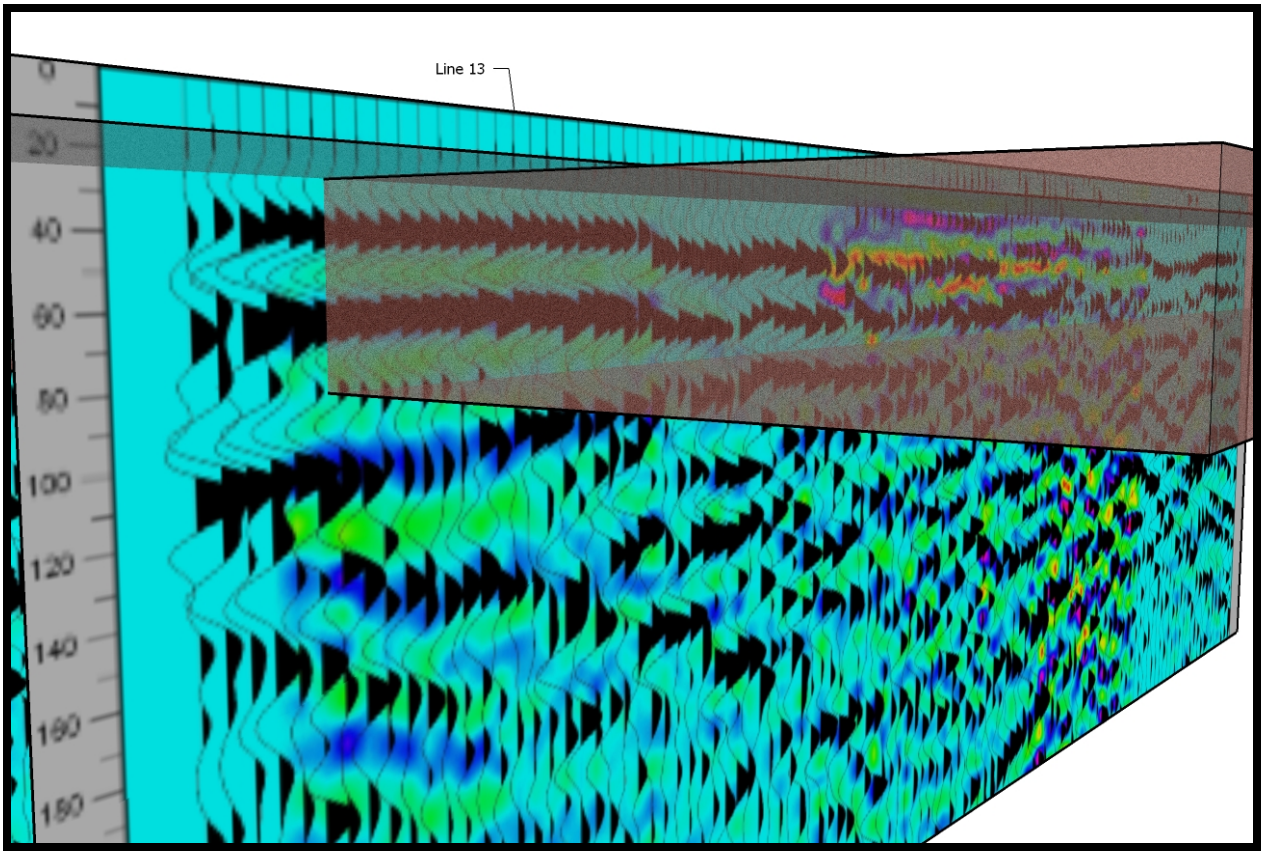

Figure 34. Line 13 showing seismic attributes interpreted to be potential gas accumulations. The sources of the gas is not known and could represent multiple or single sources. The vertical migration of gas, in our model, is stopped by low permeability or porosity layers, such as clay rich shales, or near the surface clay rich soils. The box in this figure between 20 ms and 80 ms, which shows CMP line 13 and two way travel time in ms, is a region of reflectors that are identified as potential manifold sources for gas.

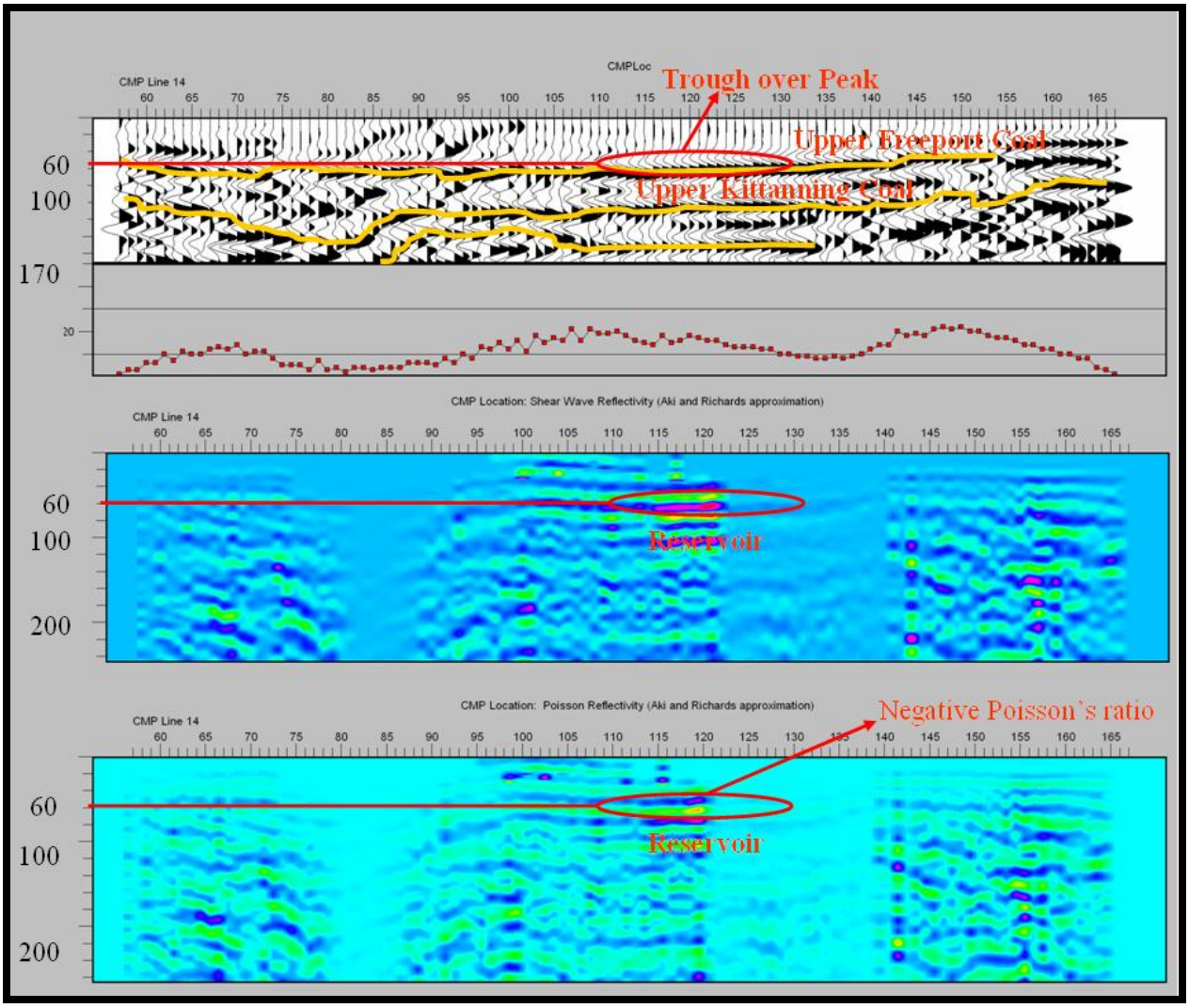

Figure 35. Seismic Interpretation of line 14 (Shallow Reservoir). The Upper Freeport coal is indicated by the red line at approximately 60 msec.

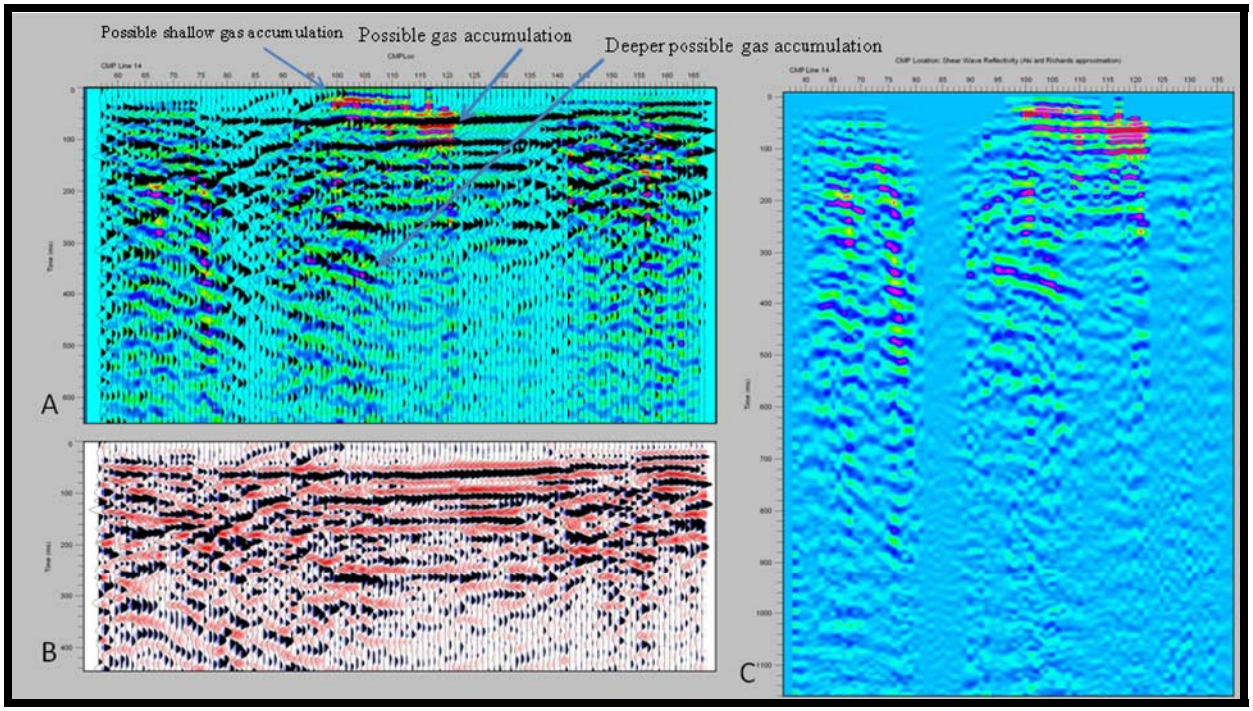

Figure 36. CMP Line 14 showing (A) superimposed reflectivity and shear wave reflectivity attribute, (B) reflectivity and (C) shear wave reflectivity. This CMP line shows multiple regions of possible gas accumulation. Where abandoned wells are present each of these possible gas accumulation, regions could leak gas to the surface.

Figure 37. CMP Location map for Line 14.

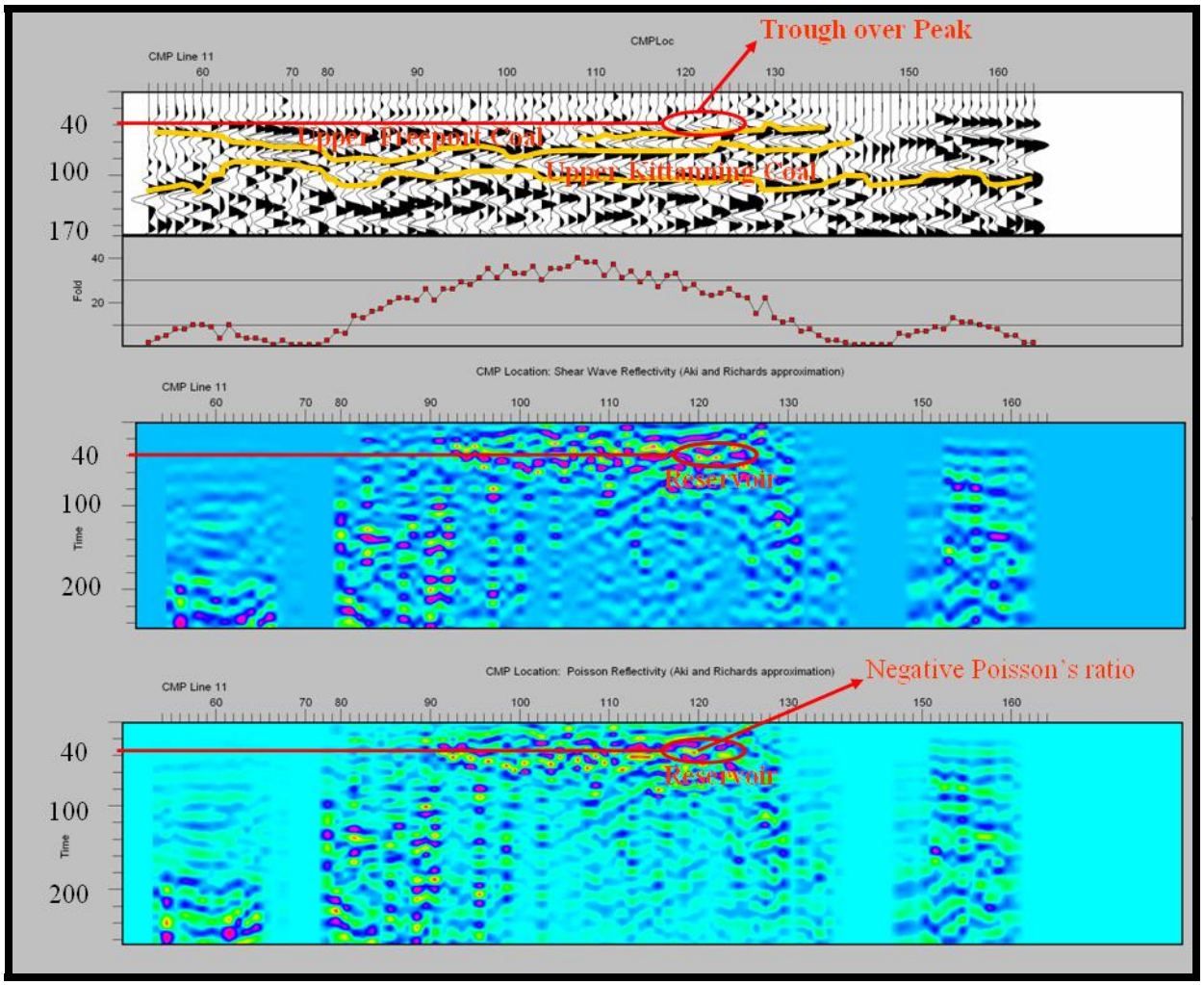

Figure 38. Seismic interpretation of line 11 (Near surface reservoir). Upper Freeport coal is identified with red line at 40 msec.

(This page intentionally left blank)

7.0 References

Ackenheil A. C., 1968, Mining and Physiographic study of Allegheny County, PA, prepared for the board of County commissioners, Nov 1968.

Aki, K.; Richards, P. G. 1979, Quantities Seismology Theory and Methods, volume 1; San Francisco.

Allison, M. Lee, 2001, Hutchinson, Kansas: A Geologic Detective Story, Geotimes.

Bruce, B. and Bowers, G., 2002, Pore pressure terminology, The Leading Edge.

Bruner, K. R., Oldham, A. V., Repine, T. E., Markowski, A. K., and Harper, J. A., 1995, Geological aspects of coalbed methane in the northern Appalachian coal basin, southwestern Pennsylvania and north-central West Virginia: Gas Research Institute Topical Report GRI-95/0221.

Bruner, K. R., Oldham, A. V., Repine, T. E., Markowski, A. K., and Harper, J. A., 1998, Geological aspects of coalbed methane in the northern Appalachian coal basin, southwestern Pennsylvania and north-central West Virginia: Pennsylvania Geological Survey Open File Report 98-13, 72 p.

Cernica, J. N., 1995, Soil Mechanics. Department of Civil Engineering Youngstown State University, New York, 125-126.

Cordsen, A., Galbraith, M., and Pierce, J., 2000, Planning Land 3-D Seismic Surveys, Geophysical Developments Series No. 9, Society of Exploration Geophysicists, 204 pp.

Dobrin, M. B. 1976, Introduction to Geophysical Prospecting, 3-d ed. McGraw-Hill, New York.

Exploration Technologies, Inc., 2000, Subsurface geochemical assessment of Methane gas occurrences. Assessed at http://www.eti-geochemistry.com/Report-04-2000/index.html.

Fetter C.W., 1994, Applied Hydrogeology, third edition, Englewood Cliffs, NJ.

Gassmann, F., 1951, Elastic waves through a packing of spheres: Geophysics, 16, 673-685.

GeoQuest International. 1981, Applied Seismic Stratigraphic Interpretation manual, Houston, p.416-417.

Harper, J. A. and C. D. Laughrey, 1987, Geology of the oil and gas fields of southwestern Pennsylvania, Pennsylvania Bureau of Topographic and Geologic Survey, Mineral Resources Rep. M87, 166 p.

Harper, J. A. 1989, Upper Devonian and Lower Mississippian stratigraphy and depositional systems, *in* Geology in the Laurel Highlands of Southwestern Pennsylvania, J. A. Harper ed., 54th Annual Field Conference of Pennsylvania Geologists Guidebook, Oct. 5,6, and 7, p. 191-202.

Kant, S. 2004, Seismic Signal Processing with special reference to anisotropy. Springer, 2004.

Laughrey, C. D., and Baldassare, F.J., 1998, Geochemistry and origin of some natural gases in the Plateau Province, central Appalachian basin, Pennsylvania and Ohio: American Association of Petroleum Geologists Bulletin, v. 82, no. 2, p. 317-335.

McDaniel, B. A. 2006. Subsurface Stratigraphy and Depositional Controls on Late Devonian-Early Mississippian Sediments in Southwestern Pennsylvania (M.Sc. Thesis). Department of Geology and Geography Morgantown, West Virginia.

Lide, David R., (Editor), 1991, CRC Handbook of Chemistry and Physics, 72nd edition; CRC Press; Boca Raton, Florida.

Lytle, W. S. and Balogh, L., 1975, Greater Pittsburgh Region Oil and Gas Fields Map, Map #44, Commonweath of Pennsylvania Department of Environmental Resources.

Milici, R. C., 2004, Assessment of Appalachian Basin Oil and Gas Resources: Carboniferous Coal-bed Gas Total Petroleum System: U.S. Geological Survey Open-File Report 2004-1272.

Milici, R. C., Gathright, T. M. II, Miller, B. W., Gwin, M. R., and Stanley, C. B., 1986, Subtle bedding plane faults - a major factor contributing to coal mine roof falls in southwestern Virginia: Virginia Tech. Dept. of Geological Sciences Memoir.

Nissen, S., Xia, J., and Watney, W. L., 2002, Seismic detection of shallow natural gas beneath Hutchinson, Kansas, KGS Open-file Report 2002-44.

Ostrander, W. J., 1984, Plane-wave reflection coefficients for gas sands at non-normal angles of incidence: Geophysics, v. 49, p. 1637-1648.

Park, C.B., Miller, R. D., and Xia, J., 1999, Multichannel analysis of surface waves (MASW); Geophysics, v. 64, p. 800-808.

Pashin, J. C. and F. R. Ettensohn, 1995, Reevaluation of the Bedford-Berea sequence in Ohio and adjacent states: forced regression in a foreland basin. GSA Special Paper 298. 68 p.

Pashin, J. C., and Hinkle, Frank, 1997, Coalbed methane in Alabama: Geological Survey of Alabama Circular.

Peng S., Chen H., Yang R., Gao Y., Chen X., 2006, Factors facilitating or limiting the use of AVO for coal-bed methane, 2006.

Puckette, J., and Al-Shaieb, Z., 2003, Naturally underpressured reservoirs: Applying the compartment concept to the safe disposal of liquid waste, AAPG Southwest Section Meeting.

Puglio, D. G., and Innacchione, A. T., 1979, Geology, mining, and methane content of the Freeport and Kittanning coal beds in Indiana and surrounding counties, Pennsylvania: U.S. Bureau of Mines Report of Investigations 8406, 35 p.

Reeves, T. K., Sharma, Bijon, Banerjee, Sanjay, Guo, Geneliang, Volk, Len, Djikine, David, George, Steven, 1999, An exploration3D seismic field test program in Osage county, Oklahoma, Bartlesville, OK.

Rutherford, S. R., and Williams, R.H., 1989, Amplitude-versus-offset variations in gas sands: Geophysics, v. 54, p. 680-688.

Ruppert, L. F., Tewalt, S. L., Wallack, R. N., Bragg, L. J., Brezinski, D. K., Carlton, R. W., Butler, D. T., and Calef, F. J. III, 2001, Chapter D, A digital resource model of the Middle Pennsylvanian Upper Freeport coal bed, Allegheny Group, northern Appalachian basin coal region, *in* Northern and Central Appalachian basin Coal Regions Assessment Team, 2000 Resource Assessment of selected coal beds and zones in the northern and central Appalachian basin coal regions: U.S. Geological Survey Professional Paper 1625-C, Discs 1 and 2, Version 1.0, p. D1 – D97.

Schneider. W. A., 1984, The Common Depth Point Stack, Proceedings of the IEEE, Vol. *72***,** No. 10.

Siegel, L., 2006, Playa Vista, Center for Public Environmental Oversight. Accessed 2007 at http://www.cpeo.org/pubs/

Sheriff, R. E. and Geldart, L. P. 1995, Exploration Seismology, 2-d edition. Cambridge University Press.

Snepp, F. and Moyer, P., 2006, Burning Questions, KNBC four part news segment. Assessed 2007 at http://www.knbc.com/station/8506056/detail.html. *Note: This four-part investigative series won a Peabody Award.*

Stephenson D. E., Agnew A. P., Anderson M. P., Baker W. H., Brimhall R. M., Caruccio F. T. Cherry J. A., Dreezen V. H., Groat C. G., Leavitt B. R., Lord W. B., McDonald J. B., Pettyjohn W. A., Sendelin L.V.A., Sommers D. A., Thompson D. R., Van Voast V., Woessner W. W., Yare B.S., 1981, Coal Mining and groundwater resources in the United States, National Academy Press, Washington, DC.

Stark, A., 2007, Passing Judgement (sic), passing gas, Los Angeles City Beat, Access 2007 at http://www.lacitybeat.com/article.php?id=2276&IssueNum=108.

Stout, W., 1943, Sandstones and conglomerates in Ohio: Geological survey of Ohio, Columbus, OH.

Tatham, R. H., 1982, V_p/V_s and lithology: Geophysics, 47, 336-344.

Telford, W. M., Geldart, L. P., Sheriff, R. E. 1989, Applied Geophysics, 2-d edition. Cambridge University Press.

Thomas, Mark, 2006, (NETL, RDS) Personal communication.

Vesilind, P. A., Peirce, J. J., and Weiner, R. F., 1994, Environmental Engineering 3rd Edition, Butterworth Heinemann.

Ward, Porter, and Wilmoth, B.M., 1968, Ground-water hydrology of the Monongahela River Basin in West Virginia: West Virginia Geological and Economic Survey River Basin Bulletin 1

Waters, K. H., 1978, Reflection Seismology - a tool for energy resource exploration. New York.

Yilmaz, O., 1987, Seismic Data Processing, Investigations in Geophysics Volumes 1 and 2, Society of Exploration Geophysicists.

Young, R., 2004, A Lab Manual of Seismic Reflection Processing, EAGE Publications.

Xia, J., 2002, Using the high-resolution magnetic method to locate abandoned brine wells in Hutchinson, Kansas, KGS Open-file Report 2002-43.

Xiuchen, Wei, Xiang-Yang, Li, Ou Yang, Shi Songqun, 2003. Case study of using converted PS-waves to image gas reservoirs in the Ordos Basin, China. Petro-China Langfang Research Institute.

Table 10. This table gives the energy point line number, energy point number, and energy point coordinate (in UTM Zone 17N coordinates) for the 3D reflection seismic survey, first referred to on page 10.

1	1	1965238.6	14643575.7
1	2	1965204.6	14643610.4
1	4	1965186.1	14643637.1
1	5	1965156.0	14643667.8
1	6	1965126.4	14643699.1
1	7	1965099.7	14643728.5
1	8	1965071.3	14643759.0
1	9	1965050.0	14643786.5
1	10	1965020.4	14643819.6
1	11	1964995.0	14643850.7
1	12	1964966.7	14643884.0
1	13	1964945.2	14643912.8
1	14	1964923.8	14643946.4
1	15	1964904.3	14643985.5
1	16	1964888.1	14644019.7
1	17	1964867.5	14644052.5
1	18	1964845.7	14644084.2
1	19	1964824.5	14644118.7
1	20	1964804.0	14644154.3
1	21	1964785.1	14644192.4
1	22	1964766.5	14644228.0
1	23	1964745.0	14644266.5
1	24	1964731.1	14644298.9
1	25	1964713.1	14644335.9
1	26	1964695.7	14644377.2
1	27	1964679.7	14644408.6
1	28	1964667.3	14644444.3
1	29	1964652.7	14644479.4
1	30	1964639.0	14644515.5
1	31	1964621.9	14644554.7
2	32	1965346.6	14643682.6
2	33	1965314.8	14643708.2
2	34	1965286.0	14643734.4
2	35	1965255.9	14643759.0
2	36	1965227.1	14643790.2
2	37	1965200.5	14643817.7
2	38	1965176.0	14643848.3
2	39	1965149.2	14643877.0
2	40	1965125.0	14643908.2
2	41	1965097.4	14643937.6
2	42	1965074.2	14643968.0
2	43	1965048.3	14644000.9
2	44	1965025.9	14644032.1
2	45	1965004.0	14644064.7
2	46	1964981.3	14644099.3
2	47	1964960.2	14644132.3
2	48	1964936.6	14644167.2
2	49	1964912.8	14644203.1

2	50	1964892.1	14644239.7
2	51	1964877.3	14644275.5
2	52	1964858.9	14644304.0
2	53	1964842.5	14644339.8
2	54	1964824.5	14644375.0
2	55	1964809.7	14644404.2
2	56	1964789.0	14644450.6
2	57	1964771.0	14644486.4
2	58	1964739.7	14644564.4
2	59	1964723.0	14644602.9
3	60	1965455.7	14643755.4
3	61	1965424.8	14643776.8
3	62	1965395.6	14643808.4
3	63	1965364.4	14643837.3
3	64	1965340.0	14643860.9
3	65	1965308.8	14643893.2
3	66	1965285.8	14643924.9
3	67	1965256.4	14643952.8
3	68	1965229.3	14643981.6
3	69	1965202.9	14644011.9
3	70	1965174.9	14644045.9
3	71	1965153.0	14644073.6
3	72	1965130.3	14644106.7
3	73	1965107.3	14644140.3
3	74	1965082.7	14644171.8
3	75	1965059.4	14644211.9
3	76	1965042.3	14644243.8
3	77	1965021.2	14644280.6
3	78	1965004.0	14644313.0
3	79	1964984.2	14644350.3
3	80	1964968.2	14644388.7
3	81	1964951.0	14644420.4
3	82	1964929.1	14644463.3
3	83	1964915.7	14644501.2
3	84	1964900.6	14644536.4
3	85	1964882.4	14644574.3
3	86	1964864.6	14644607.4
3	87	1964848.4	14644644.8
3	88	1964833.1	14644679.5
3	89	1964812.7	14644714.0
3	90	1964795.2	14644755.1
3	91	1964785.1	14644794.4
3	92	1964771.5	14644826.4
4	93	1965640.1	14643945.8
4	94	1965610.9	14643972.6
4	95	1965578.8	14643997.5
4	96	1965549.9	14644016.9
4	97	1965524.5	14644049.4
4	98	1965489.5	14644070.2
4	99	1965462.4	14644100.3
4	100	1965434.7	14644129.4
4	101	1965409.1	14644160.2
4	102	1965384.5	14644189.2

4	103	1965358.8	14644221.5
4	104	1965335.6	14644253.9
4	105	1965316.5	14644291.3
4	106	1965296.5	14644320.9
4	107	1965274.4	14644360.0
4	108	1965258.0	14644394.3
4	109	1965234.8	14644426.0
4	110	1965208.8	14644455.8
4	111	1965190.8	14644490.2
4	112	1965174.6	14644528.2
4	113	1965158.0	14644563.7
4	114	1965146.3	14644594.7
4	115	1965127.4	14644636.2
4	116	1965114.1	14644672.9
4	117	1965096.0	14644709.5
4	118	1965078.7	14644745.0
4	119	1965064.2	14644781.8
4	120	1965054.9	14644820.5
4	121	1965041.0	14644855.7
4	122	1965023.1	14644893.1
4	123	1965005.5	14644932.0
4	124	1964983.6	14644969.5
4	125	1964964.1	14645005.0

Table 11. 3D geophone locations. Columns show geophone line number, geophone station number, geophone location in UTM 17N coordinates and geophone elevation.

1	1	1965243.7	14643752.4
1	2	1965231.1	14643767.6
1	3	1965216.1	14643783.4
1	4	1965202.2	14643798.9
1	5	1965194.3	14643814.5
1	6	1965181.9	14643827.9
1	7	1965167.5	14643841.5
1	8	1965156.0	14643857.3
1	9	1965144.0	14643872.7
1	10	1965128.9	14643886.5
1	11	1965115.3	14643905.4
1	12	1965101.8	14643917.2
1	13	1965087.1	14643930.6
1	14	1965075.5	14643947.1
1	15	1965063.9	14643962.1
1	16	1965053.2	14643979.3
1	17	1965040.7	14643994.8
1	18	1965028.4	14644011.0
1	19	1965016.0	14644025.1
1	20	1965007.4	14644033.0
1	21	1964991.2	14644057.8
1	22	1964978.4	14644074.7
1	23	1964965.9	14644093.6
1	24	1964958.0	14644107.1
1	25	1964946.1	14644123.7
1	26	1964934.0	14644142.5
1	27	1964923.3	14644161.8
1	28	1964911.6	14644175.6
1	29	1964903.0	14644192.1
1	30	1964891.8	14644211.2
1	31	1964882.3	14644225.7
1	32	1964873.5	14644244.6
1	33	1964867.3	14644263.1
1	34	1964859.2	14644279.9
1	35	1964851.4	14644300.4
1	36	1964839.4	14644318.3
1	37	1964830.3	14644336.3
1	38	1964821.9	14644354.7
1	39	1964812.8	14644372.7
1	40	1964805.2	14644390.6
1	41	1964822.0	14644414.2
1	42	1964807.9	14644441.2
1	43	1964799.7	14644458.7
1	44	1964791.5	14644476.8
1	45	1964783.6	14644494.8
1	46	1964775.4	14644513.7
1	47	1964769.6	14644533.3
1	48	1964759.8	14644551.6
2	1	1965377.2	14643847.6

2	2	1965363.2	14643861.6
2	3	1965349.0	14643874.5
2	4	1965336.7	14643888.5
2	5	1965321.6	14643903.2
2	6	1965298.5	14643920.0
2	7	1965295.4	14643932.0
2	8	1965283.0	14643947.6
2	9	1965267.0	14643959.0
2	10	1965256.4	14643977.3
2	11	1965244.4	14643992.1
2	12	1965230.4	14644007.5
2	13	1965216.4	14644023.2
2	14	1965203.0	14644038.9
2	15	1965189.5	14644056.2
2	16	1965181.1	14644070.6
2	17	1965164.3	14644083.2
2	18	1965150.9	14644097.6
2	19	1965138.9	14644113.3
2	20	1965125.8	14644128.4
2	21	1965117.0	14644144.9
2	22	1965106.6	14644165.4
2	23	1965095.1	14644179.5
2	24	1965080.8	14644197.9
2	25	1965068.3	14644216.0
2	26	1965061.0	14644227.7
2	27	1965054.8	14644243.7
2	28	1965041.6	14644263.2
2	29	1965032.3	14644280.9
2	30	1965020.7	14644297.0
2	31	1965012.9	14644316.0
2	32	1965004.3	14644334.9
2	33	1964993.0	14644352.2
2	34	1964986.0	14644366.8
2	35	1964977.7	14644389.4
2	36	1964970.0	14644406.6
2	37	1964960.3	14644424.0
2	38	1964948.5	14644446.3
2	39	1964939.4	14644464.5
2	40	1964929.6	14644494.0
2	41	1964924.3	14644500.9
2	42	1964915.2	14644520.3
2	43	1964908.5	14644537.7
2	44	1964900.3	14644556.6
2	45	1964892.4	14644575.8
2	46	1964883.4	14644595.5
2	47	1964878.8	14644614.5
2	48	1964871.2	14644632.3
2	49	1964863.1	14644649.4
2	50	1964850.6	14644669.2
2	51	1964844.6	14644684.4
2	52	1964834.8	14644701.3
2	53	1964821.5	14644714.1
2	54	1964815.2	14644732.9

3	1	1965442.3	14643953.6
3	2	1965426.9	14643968.8
3	3	1965413.9	14643980.7
3	4	1965400.1	14643996.2
3	5	1965386.1	14644011.0
3	6	1965372.5	14644025.0
3	7	1965370.0	14644034.8
3	8	1965347.9	14644055.8
3	9	1965333.8	14644068.7
3	10	1965320.3	14644084.5
3	11	1965308.6	14644099.9
3	12	1965293.4	14644112.9
3	13	1965281.1	14644130.2
3	14	1965270.6	14644147.2
3	15	1965258.8	14644163.3
3	16	1965248.8	14644179.9
3	17	1965231.7	14644204.2
3	18	1965210.9	14644227.6
3	19	1965198.5	14644246.6
3	20	1965187.2	14644268.2
3	21	1965178.7	14644278.7
3	22	1965167.1	14644292.5
3	23	1965161.8	14644314.5
3	24	1965134.1	14644320.4
3	25	1965120.6	14644342.3
3	26	1965129.3	14644368.0
3	27	1965121.5	14644384.9
3	28	1965111.8	14644400.0
3	29	1965101.9	14644416.0
3	30	1965095.3	14644435.5
3	31	1965085.7	14644452.5
3	32	1965076.8	14644470.7
3	33	1965065.9	14644487.5
3	34	1965056.6	14644504.8
3	35	1965051.4	14644519.9
3	36	1965036.8	14644552.7
3	37	1965033.2	14644560.9
3	38	1965025.0	14644580.8
3	39	1965018.2	14644599.7
3	40	1965008.9	14644616.3
3	41	1965002.9	14644636.7
3	42	1964992.5	14644650.9
3	43	1964980.8	14644671.5
3	44	1964963.0	14644680.3
3	45	1964954.6	14644703.2
3	46	1964961.5	14644732.3
3	47	1964956.0	14644747.7
3	48	1964950.2	14644763.5
3	49	1964941.9	14644783.1
3	50	1964930.1	14644803.5
3	51	1964921.8	14644821.8
3	52	1964914.8	14644840.1

8.0 Appendix I: Fundamental Concepts Related to Reflection Seismic Techniques.

This portion of the report is written to aid the motivated reader in the understanding of the methodology of reflection seismology. It is written at a level that, when combined with the references, allowed a detailed understanding of the strengths of this advanced technique. As part of the program to investigate the abandoned McKeesport Gas field region geophysics was used to investigate the subsurface. Geophysics is defined by the Environmental and Engineering Geophysical Society as: "*The non-invasive investigation of subsurface conditions in the Earth through measuring, analyzing and interpreting physical fields at the surface*". In this section, fundamental concepts related to reflection seismic surveys and our studies will be summarized. Please refer to the references for additional details regarding seismic processing or more general references such as Yilmaz (1988) or Young (2004).

Reflection Seismology has been a central and standard method for oil and gas exploration since 1927 when the Geophysical Research Corporation working in the Maud oil field of Oklahoma commercially implemented the technique. There is a monument to this important geophysical event at this site (http://www.seg.org). Reflection seismology is a non-invasive geophysical system that consists of an energy source, an energy transfer medium and an energy receiving unit (Figure 39). In the Versailles studies, elastic P waves were used with either vertical component geophones, or a hydrophone to record elastic waves which traveled from the energy source, through the earth via the processes of transmission and reflection. In one of the techniques applied to these data, seismic surface waves, which move along the surface of the earth, were used to determine earth structure.

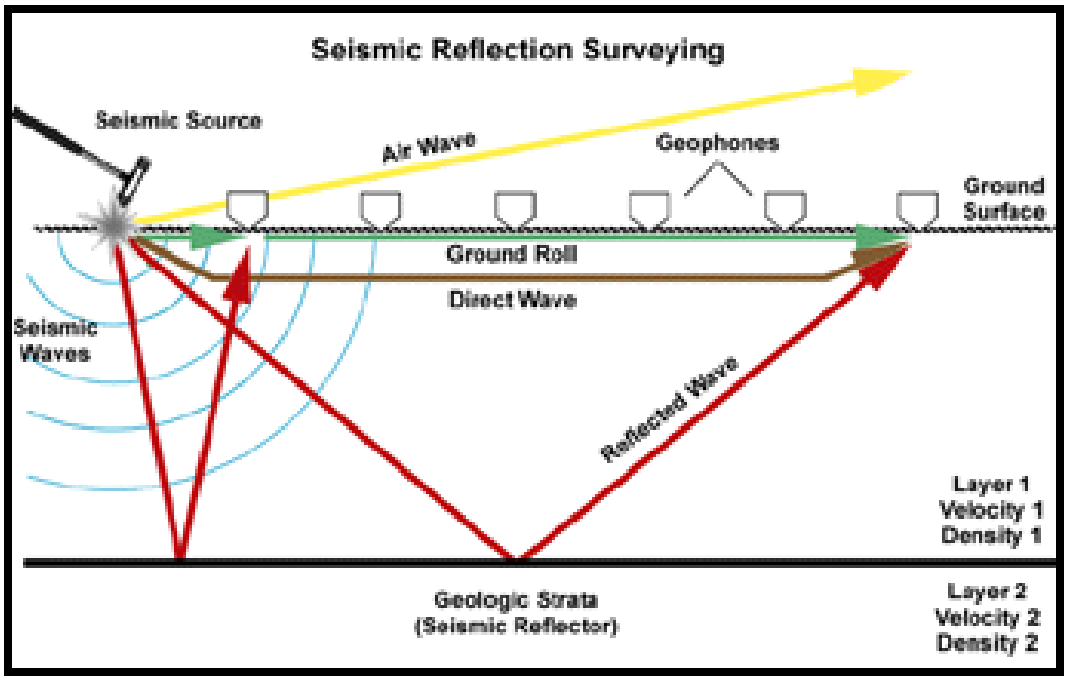

Figure 39. Reflection seismology outline from: www.isgs.uiuc.edu/appgeophy/images/-seismic_reflection/reflection_surveying.gif.

In reflection seismic studies, the energy source can be anything producing an elastic disturbance in the earth medium, ranging from natural sources such as automobile traffic, trains or even earthquakes to controlled artificial energy sources of known force, waveform and amplitude, positioned at a precise location either on the surface or below it. These can include hammer-strikes, dynamite explosions, special weight-drop machinery, and for marine reflection surveys, marine transmitting transducers or air guns.

The spatial location of energy source in seismic exploration is called source point (SP) or energy point (EP) and the distance between source points is called the source point interval. Energy released at the source point produces an elastic wave field which is both transmitted and reflected at impedance boundaries. Each reflection is delayed by the amount of time required to travel from the source to the reflected interface and back and decreases in amplitude with travel time due to spherical divergence of the elastic wave field and attenuation.

We completed three seismic surveys in the Versailles area. For the initial reflection survey, we used a 60 channel geotechnical system called a Stratavisor and collected three short lines to determine shallow velocity structure. These lines were useful in estimating expected P and S wave velocities and showed significant fill in the region of the Brownfield site along the river (Figure 40).

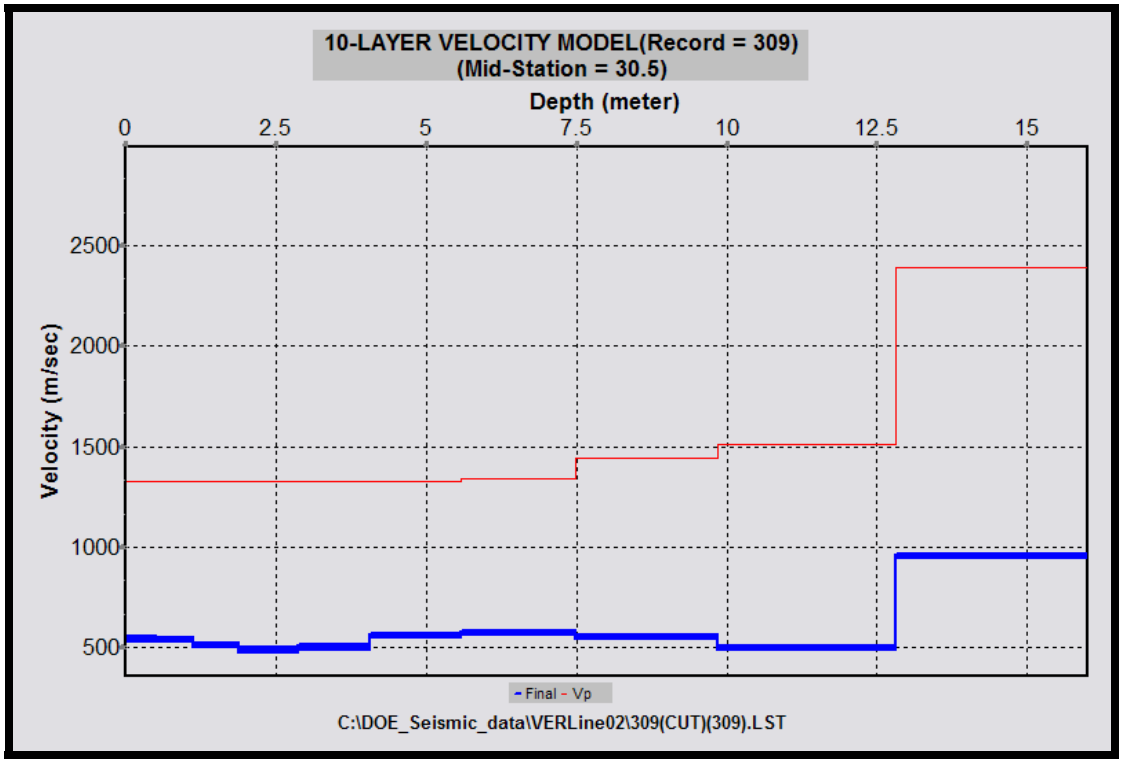

Figure 40. P and S velocities derived from MASW techniques described later in the report. S wave velocities with respect to depth are shown in blue along with their uncertainty; P wave velocities are shown in red. In this figure 12.5 meters is equivalent to a depth of 41 feet.

We then completed a marine reflection seismic survey and then, using an I/O System II, a 3D survey reflection seismic survey. For the Stratavisor reflection lines, a sledge hammer strike on a thick steel plate was used as the energy source. In the marine seismic, a full-spectrum transmitting transducer was used as the energy source. In our large 3D survey, we used an Industrial Vehicles Incorporated (IVI) EnviroVib™ source. The Vibroseis™ method (Figure 41) uses a long source signal of preciously known characteristics that is reflected and recorded. This source signal is then correlated with the geophone records to yield a highly precise reflection record for each geophone.

Another portion of any seismic data acquisition system is sensitive to the physical displacement of the ground on the surface caused by elastic deformation. In our reflection studies, vertical component geophones (Figure 11) were placed at intervals along profiles. Distance between linear arrays of geophones is referred to as cross line spacing, while distance between groups of geophones is referred to as receiver spacing. The distance between a source point and a geophone is called the offset and appears on the x-axis of some later figures. In our marine survey we recorded elastic waves in water using a hydrophone, which recorded variation in water pressure related to the arrival of elastic wave fronts at the sensor.

The overall earth response recorded at the geophones. These geophones record the superimposed reflections from each of the subsurface reflecting horizons. In our surveys immediately after being recorded this record was then cross-correlated with the EnviroVib™ source sweep (Dobrin, 1976).

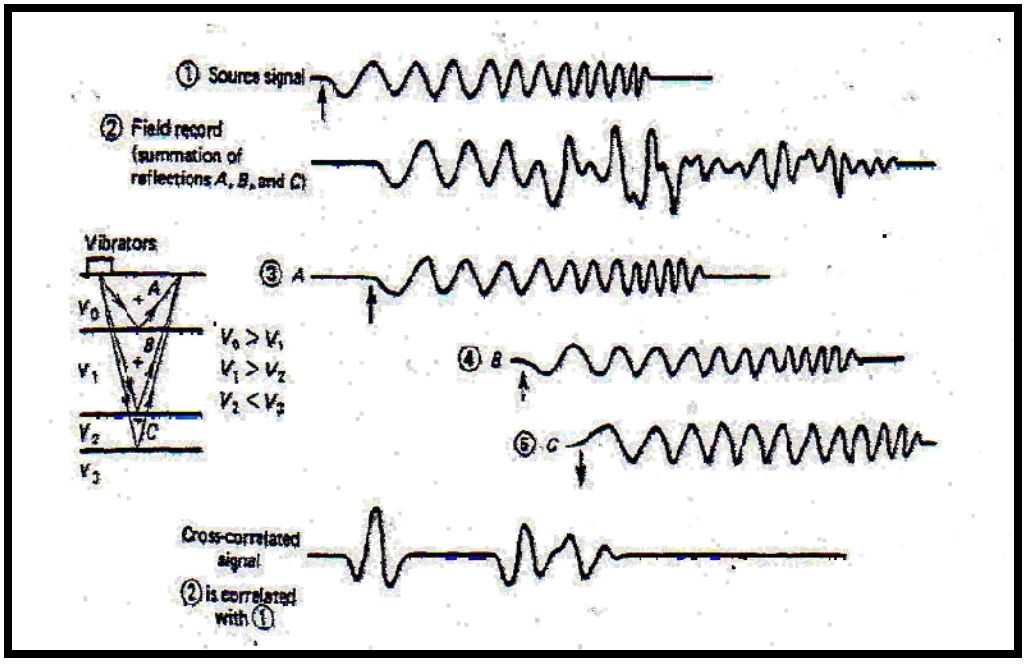

Figure 41. Schematic description of Vibroseis™ data processing (Reeves et al., 1999), (1) Source signal (a single sweep with gradually increasing oscillation frequency), (2) Field record (a trace with combined reflections from different boundaries), (3) Reflection from boundary A, (4) Reflection from boundary B, and (5) Reflection at boundary C.

The entire length of the sweep was used in the cross-correlation process (Figure 41). The cross-correlated record accurately records the location of the reflecting horizons.

In general, elastic wave propagation can take place through solids, liquids, and gases. The transfer medium is the substance through which the elastic seismic waves propagate, which is the earth. In our study, this was earth material, or in the marine profiles, earth material, pore-filling phases, and water.

In addition to surface waves, which travel along the surfaces of material, elastic waves can travel through solids in two different styles of elastic deformation, each corresponding to a distinct elastic seismic wave. These are, elastic compression parallel to the direction of elastic wave field motion (this type of elastic wave is a P wave) or elastic deformation perpendicular to the direction of elastic wave propagation (this type of elastic wave is an S wave). Both are shown in Figure 42.

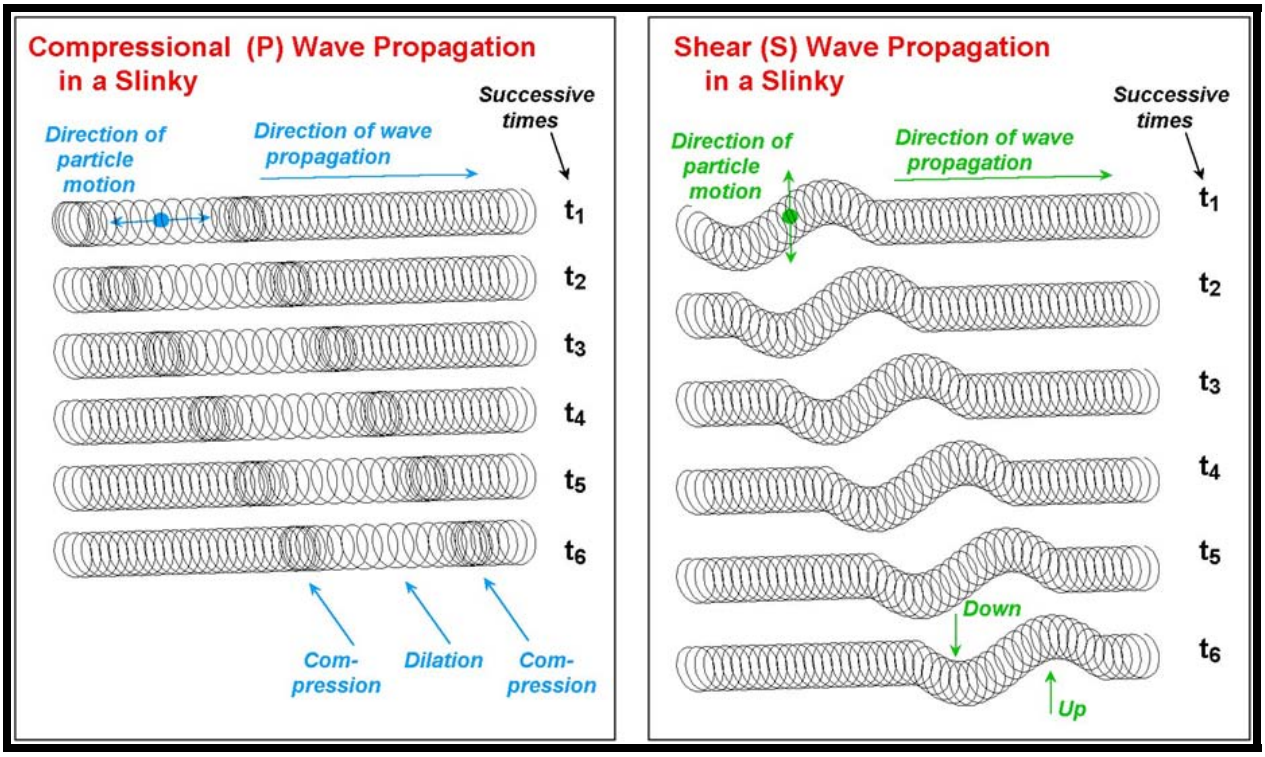

Figure 42. Propagation of P and S elastic waves, taken slinky as an example (Provided by Larry Braile, Purdue University, http://web.ics.purdue.edu/~braile/new/-SeismicWaves.ppt).

In a defining material characteristic, fluids do not have shear strength; therefore, they do not allow S wave propagation. In our studies, P waves were observed and analyzed. However, in AVO (amplitude variation with offset) processing of the 3D data set, parameters related to S wave propagation were derived and will be discussed in more detail in a later section of this report. We will focus on the propagation of elastic waves through solid materials for those

unfamiliar with seismic techniques. However, please note that in the Stativisor seismic study, the active multichannel analysis of surface waves (MASW) inversion for 1D shear velocity structure using the method of Park et al., (1999) was used and this methodology should be reviewed either in the publication of Park et al., (1999) or at the excellent Kansas Geological Survey web site.

There are two easily understood physical laws involved in the process of elastic wave propagation:

Equation 4: Newton's second law of motion

$F = ma$

This is one (the second) of Sir Issac Newton's laws of motion, in which F is the force, applied to a body of mass m in order to produce motion with acceleration a, and

Equation 5: Hooke's law of elastic deformation

$E * (\Delta L / L) = F / A$

This is Hooke's law of elastic deformation for a perfectly elastic rod of initial length L and cross-sectional area A, where force F, normalized over area A represents stress, and deformation ΔL normalized over initial length L represents strain. In this equation, E – is the coefficient, called the Young's modulus, which describes the material response to elastic strain.

Poisson's ratio is the ratio of lateral strain (the change in diameter divided by the original diameter) to the longitudinal strain (the change in length divided by original length) for elastic deformation and defined by the equation:

Equation 6: Poisson's ratio

$$\nu_{yx} = -\frac{\varepsilon_x}{\varepsilon_y}$$

Where: ν_{yx} is the resulting Poisson's ratio, ε_x is transverse strain with respect to the direction of elastic wave field propagation, and ε_y is axial strain with respect to the direction of elastic wave field propagation.

These parameters and the shear modulus (μ), which is the ration of shear stress to the shear strain for an elastic material, are used to define velocities of elastic wave propagation through media. P wave velocity (V_p) is defined with respect to these parameters by the equation;

Equation 7: P wave velocity

$$v_p = \sqrt{\frac{k + \frac{4}{3}\mu}{\rho}} v_p = \sqrt{\frac{k + \frac{4}{3}\mu}{\rho}}$$

Where: *k* is the bulk modulus, μ is the shear modulus, and ρ the density of the material through which the wave is propagating

S wave velocity (V_s) equation is defined by the equation in the form of:

Equation 8: S wave velocity

$$v_s = \sqrt{\frac{\mu}{\rho}}$$

As mentioned earlier, the shear modulus of any fluid is 0; therefore, S waves experience attenuation related to rock porosity, void-filling phases, and fluid or gas filled fractures to a larger degree than P waves.

In the large reflection I/O System II seismic system, groups of geophones were controlled by electrically powered RSX boxes, which provided necessary amplification for the recorded signal, digitized the analog input signal to 24-bit digital packets and communicated with other portions of the receiver array. The RSX boxes also monitored the functionality of recording lines, geophones and electronic components. The reflection seismic geophone lines were connected with ALX boxes, which were then connected to the seismic recording truck. The entire receiver array or chain of detectors was controlled from a data recording vehicle, synchronized with the energy-source in order to accurately acquire data. The amplification of the I/O System II from the vertical component geophone to the initial recording of the signal was approximately a factor of 4,000,000. The specifics of each system will be discussed in more detail when these individual results are presented later.

The basis of seismic methodology is accurately measuring elastic wave reflections, which can be quantified by the concept of a reflection coefficient, related to the boundaries of geological elements. Acoustic impedance is a key concept in understanding what a reflection coefficient is the acoustic impedance and is defined as Z=V*ρ, where V is the seismic velocity (of elastic solid body P wave propagation) and ρ is the rock density. When an elastic wave propagates through the media and faces a boundary, separating the mediums with different impedances – some of the energy will be reflected off the boundary, while some will continue through the boundary forming a propagating elastic wave. For an elastic wave striking the boundary between two rock layers, the reflection coefficient is defined in:

Equation 9: Reflection coefficient

$$R = \frac{Z_1 - Z_0}{Z_1 + Z_0}$$

Here Z_0 and Z_1 are impedances of the second and the first mediums respectively. The transmission coefficient is defined by:

Equation 10: Transmission coefficient

$$T = \frac{2Z_0}{Z_1 + Z_0}$$

The most popular method of reflection seismic data acquisition is the Common Depth Point (CDP), which was invented by the geophysicist Harry W. Mayne in 1956, originally referred to by him as the CRP (central reflecting point) processing. The method involves recording data from varied source and geophone locations and then combining the data during processing using a common depth point (CDP) or common midpoint (CMP) as a sorting and grouping key. The CDP or CMP position is shared between all sources receive pairs in this method. Summing these various pairs, after geometry-dependent corrections have been made, significantly increases the signal to noise ratio for each reflecting horizon.

In reflection seismic processing, this process of summing receiver-source pairs, or stacking, consists of sorting out all the individual shot records, that is the records of the geophones which record a single energy point (or shot gather), and reorganizing these around a central midpoint (or common depth point) which reflect elastic energy back to the surface with respect to each pair of shot and geophone. This can be a difficult concept to grasp initially, but is critical to all seismic reflection surveys. In our reflection seismic survey, all energy points and geophone locations were determined with GPS and recorded in UTM Zone 17N NAD83 coordinates.

In Figure 43, the offset axis ΔX = (g - s) measures the source to receiver distance, and the mid-point axis X = (s + g)/2 measures the average source and receiver distance along the seismic profile. A collection of traces parallel to the mid-point axis at a fixed ΔX is called a common offset. These traces are always a fixed distance from the source and are sometimes used to determine the character of reflecting horizons during a reflection seismic survey. Finally, the collection paralleling the offset axis at a fixed mid-point X is called a common depth point (CDP) gather or a common mid-point gather (Schneider, 1984).

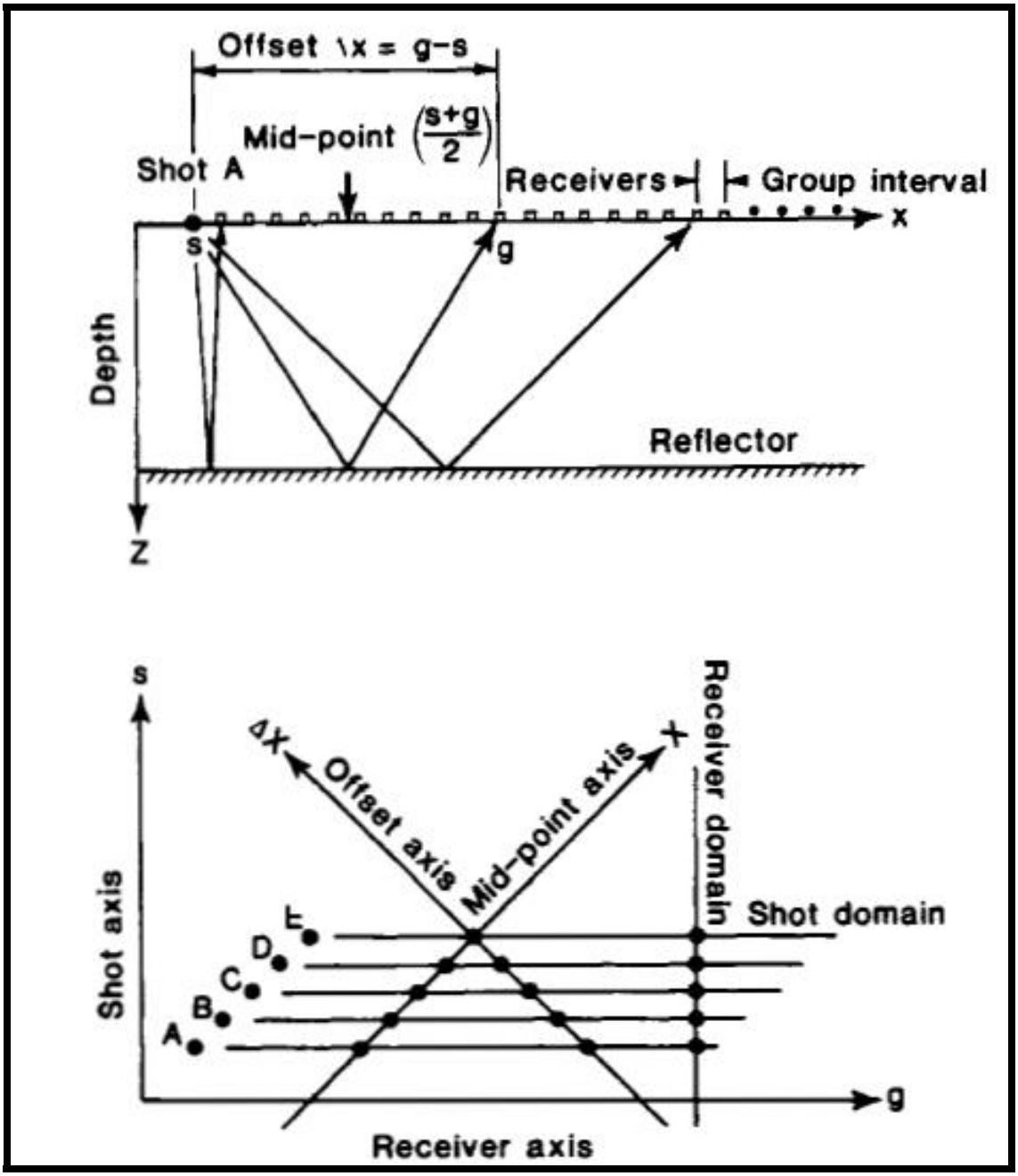

Figure 43. Seismic recording geometry, taken from Schneider (1984).

The CDP method requires multiple energy or shot points and receiving these shots in a receiver or geophone array. In some reflection seismic studies using a static receiver array of limited extent, the shot point and receiver array are advanced a small increment after each recording so as to obtain a high degree of overlapping subsurface coverage. In this way, redundancy in field data is obtained which is generally necessary to achieve significant signal-to-noise ratio gains in subsequent signal processing. The lower portion of Figure 43 illustrates a useful technique for visualizing the interrelationships among overlapping recordings in a conventional 2D seismic

survey. By plotting the energy point (or shot point) coordinate against the receiver or (geophone coordinate) in an orthogonal coordinate system, the overlapping recording geometries can be visualized.

Our survey was somewhat more complex in that we completed a 3D reflection seismic survey. In this methodology, all geophones record each energy point. These records are then sorted with respect to common bins, or spatial regions, in a 3D volume. In addition, our geophone and energy source lines were not straight and had to conform to streets. This introduces considerable complexity with respect to the simple geometry shown in Figure 43.

The foundation of seismic interpretation assumes that seismic reflections can be related to geologic boundaries in the subsurface. Since our observations are in the offset and two-way reflection time domain, we can invert the observed travel times to depth or distance to obtain the desired subsurface geologic model (Schneider, 1984), when this is well constrained by sonic velocity well logs.

In general, the first step in data processing is to analyze the noise level in the data. Each seismic system has its own dynamic range, energy source, receiver characteristics and geologic environment in which the data is collected. A dynamic range is an indicator of system quality and is measured in decibels (dB). It describes signal to noise ratio and the maximum possible value of this ratio is referred to as high dynamic range. In the frequency spectrum signal recorded by our geophone array, there was a high-frequency component; therefore, by applying a low-pass or bandpass frequency filter to seismic traces, it was possible to significantly improve the signal to noise ratio.

An additional processing step related to seismic reflection processing is that the processed reflection data is deconvolved. The ultimate objective of deconvolution is to extract the reflectivity function from the seismic trace and thus improve the vertical resolution and recognition of events (Sheriff, 1995).

An additional consideration to reflection seismic data processing is the static corrections of both the energy points and geophones. Before stacking, in order to adjust the two-way travel time data so that reflections accurately follow a well defined function of change in two-way travel time with respect to increasing offset, the differences in geophone and energy source elevations and the presence of a low P wave velocity zone in the subsurface due to either cultural or soil layer must be accounted for. This processes results in static corrections for both energy points and geophones that must be accurately determined and then applied to each seismic trace.

Static corrections transfer all of the two-way travel time data collected on the irregular earth surface to a flat horizontal datum, usually close to the average elevation surface in the study region. Static corrections most simply just involve time-shifting of every seismic trace independently by an amount defined by difference in elevation and a known or estimated velocity model between the Earth’s surface and the horizontal datum (Kant, 2004). Our static corrections were determined for all geophone and energy source locations and carefully checked with respect to reflecting horizons.

When reflection data are sorted using the concepts presented into CDP (or CMP) gathers, a Normal Moveout (or NMO) mathematical relationship between offset (x) and two-way travel time (t) can be derived for a reflecting horizon at depth (h). On a single seismic gather, reflections from a single horizontal reflector at depth (h) form a hyperbola in these CMP offset-two-way travel time coordinates. The expected two-way travel time with respect to this horizontal reflector is:

Equation 11: Normal Moveout

$$t = \sqrt{\frac{x^2 + 4h^2}{V^2}}$$

Where x is the offset, h is the depth to the reflector and V is the velocity from the surface to the reflective surface.

The average velocity to a reflector is a function of increase in reflection time, dependant on the offset distance. This velocity analysis can be obtained from the CDP data. The following are suggested steps in order to perform accurate velocity analysis, as suggested by Waters, (1978).

1. Selection of seismic traces, corrected for near-surface time differences, applied to a single subsurface point (common depth point).
2. Application to each traces a geometrical correction factor based on an assumed velocity.
3. Assessment of correctness of this velocity, with an output of correction quality factor for each time window of the record, sometimes for each window centered on known reflections.
4. A change in a selected velocity over a pre-determined range.
5. A subjective picking technique, which selects the appropriate stacking velocity for each depth, record time or reflection time.

The accuracy and resolution of stacking velocities depends on acquisition factors such as offset, multiplicity, recorded bandwidth, the signal to noise ratio and lack of near or far offset traces or irregular spacing in the field (Sheriff, 1995). Velocity analysis is usually plotted on the same scale as the seismic trace so it would be easier to identify stacking velocity picks. The same picks should be used in the successive analyses.

One further operation is common before traces are being stacked. It is called muting and consists of bringing each trace to zero in order to remove high-energy near-surface arrivals (Waters, 1978). The zeroing is done before a time given by the offset divided by the muting velocity, although the processor may add a constant. In the final processing steps, the processed CDP gathers are stacked into single traces. CDP stacking involves stacking of records from the common depth point. Different source-receiver separations (offsets) (Kant, 2004) are combined to produce a single stack.

Amplitude Variation with Offset (AVO) has been used very successfully in hydrocarbon exploration to determine variation in pore-filling phases, such as gas content in gas sands (Rutherford and Williams, 1989). The theory is based on the fact that reflection coefficients may vary with increasing offset (Ostrander, 1984). Traditional AVO analysis involves calculations of AVO intercept and gradient from a linear fit of P wave reflection amplitude to the sine squared of the incidence angle.

At a boundary between two ideally elastic, isotopic and homogeneous media – an incident wave will be partitioned into reflected P wave, reflected S wave, transmitted P wave and transmitted S wave, and the reflection coefficients will be a function on V_p, V_s, ρ_1, ρ_2, and α, where V_p – P wave velocity: V_s – S wave velocity: ρ_1 – density of the first medium: ρ_2 – density of the second medium: α – incidence angle.

The parameters V_p, V_s, ρ_1, and ρ_2 are dependent on such parameters as lithology, porosity, pore fluid, and confining pressure (Tatham, 1982). The P wave reflection amplitude is a non-linear function of the angle of incidence derived from the Zoeppritz equations. Reflection at non-normal incidence leads to wave conversion and amplitude changes, especially near the critical angle (Sheriff et al., 1995).

Equation 12: Zoeppritz equations

$$R(\theta) = \frac{1}{2\cos^2(\theta)} Ip - 4\gamma 2\sin^2(\theta) Is + (2\gamma 2\sin^2(\theta) - 0.5\tan^2(\theta)) D$$

Where: $I_p = (\Delta V_p/V_p + \Delta\rho/\rho)$ (Relative contrast in P-impedance), $I_s = (\Delta V_s/V_s + \Delta\rho/\rho)$ (Relative contrast in S-impedance), $D = \Delta\rho/\rho$ (Relative contrast in density), γ - Estimate of background shear to compressional velocity ratio (V_p/V_s), θ – angle of incidence, $\Delta V_p = V_{p2} - V_{p1}$, $V_p = (V_{p1} + V_{p2}) / 2$, $\rho = (\rho_1 + \rho_2) / 2$, and $\Delta\rho = \rho_2 - \rho_1$.

The Zoeppritz equations have been simplified by Aki and Richards (Aki and Richards, 1980). The most commonly used approximation is presented in Equation 13.

Equation 13: Aki and Richards modification

$$R_{pp}(\theta) \approx R_0 + \{A_0 R_0 + \Delta V_s / (1 - \sigma)2\} sin2\theta + \Delta V_p/2V_p(tan2\theta - sin2\theta)$$

Where: $R_{pp}(\theta)$ – P-P reflection coefficient, R_0 – Normal incidence reflection, σ – Poisson's ratio $A_0 = B_0 - 2(1 + B_0)[(1 - 2\sigma)/(1 - \sigma)]$, and $B_0 = (\Delta V_p / V_p) /[\Delta Vp/Vp + \Delta\rho/\rho]$.

Subscripts 1 and 2 refer to top and bottom layers respectively. The equation consists of three terms, with the first being representative of normal incidence, the second being most substantial for representation of intermediate angle reflections (0 to 30^o), and the third being representative of greater angles (>30^o). Frequently, when the incidence angle is between 0^o to 30^o, it is convenient to use Equation 14;

Equation 14: Incident angle between 0 and 30 degrees

$R_{pp} = R_0 + B \sin 2\theta$

where $B = A_0 R_0 + \Delta\sigma/(1-\sigma)2$, or $R_{pp} = R_0 + B\theta^2$

In AVO analysis, R_0 is often referred to as the intercept and the parameter B as the AVO gradient. As can be seen from these equations, the Poisson's ratio is extremely dependant on the V_p/V_s ratio. This relationship is graphically depicted in Figure 44, based on Equation 15;

Equation 15: Poisson's ratio expressed with respect to P and S wave velocities

$\sigma = \{Vp/Vs)^2 - 2\} / \{2Vp/Vs)^2 - 2\}$

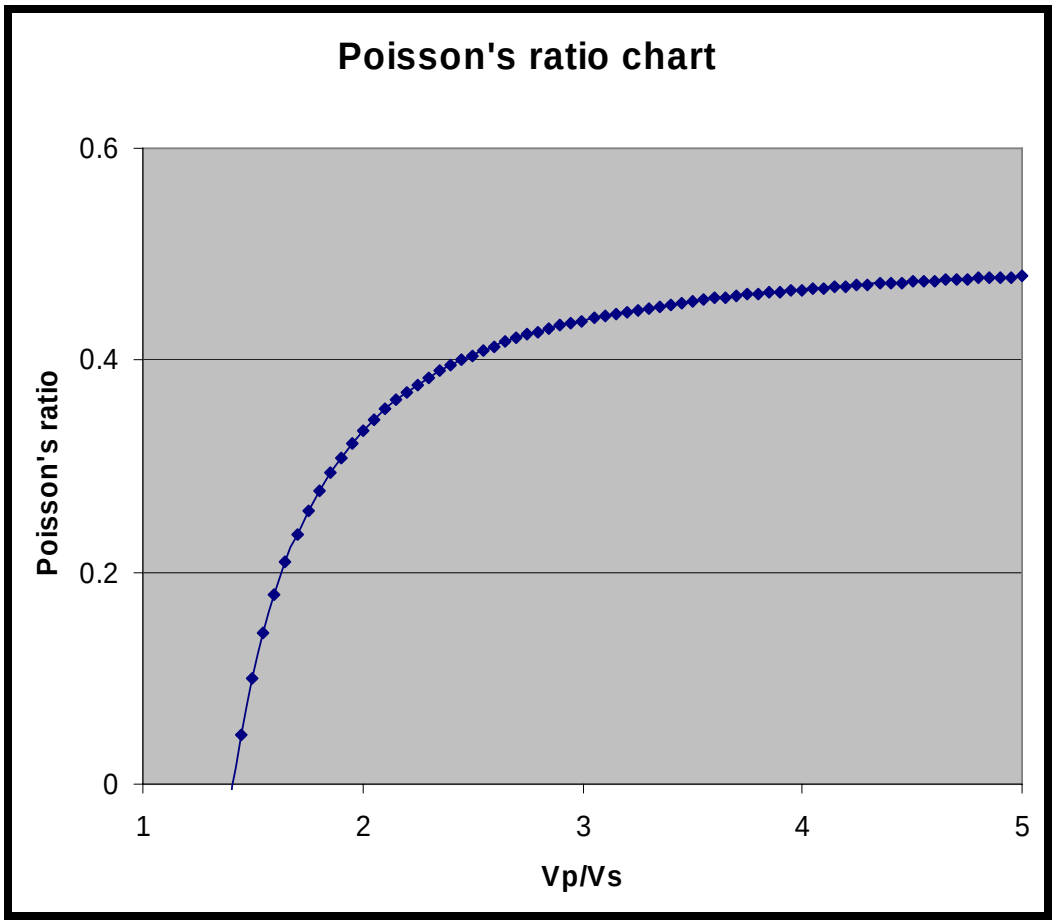

Figure 44. Dependence of Poisson's ratio with respect to V_p/V_s variation.

This becomes extremely important when V_p and V_s are being altered by introduction of natural gas to sandstone. A large drop in P wave velocity and a small increase of S wave velocity occurs when less than 5% of natural gas is introduced to a pore space of water-saturated sandstone

(Gassmann, 1951). Figure 45 demonstrates how gas saturation within a rock unit alters the V_p/V_s ratio.

Reflection coefficients can be affected by changes in physical parameters of rocks. Ostrander (1984) showed theoretical behavior of P-P reflections as a function of increasing offsets. Ostrander did this analysis for multiple cases, however, when gas-saturated sandstone is emplaced beneath a sealing shale unit of higher P wave velocity, this would result in a lower Poisson's ratio and therefore, the absolute reflection coefficient would increase with the angle of incidence (Figure 46).

Rutherford and Williams (1989) defined three classes of AVO anomalies for sandstone sealed by shale:

1. High impedance sands (characterized by positive intercept and high negative AVO gradient)
2. Near-zero impedance sands and (characterized by small positive or negative intercept and high negative AVO gradient)
3. Low impedance sands (characterized by high negative intercept and negative AVO gradient)

In our particular case, a potential seal-reservoir transition can be classified as class 3 (low impedance sands); therefore, the reflection coefficient should be negative. However, its absolute value of amplitude should be increasing with the angle of incidence.

For seismic data collected in Versailles, the following equations were used (Aki and Richards, 1979):

Equation 16: Parallel Geosciences derived ratio seismic attribute

$$\frac{A}{B} = \frac{4Vs^4 p^2 \frac{\cos i}{Vp}\frac{\cos j}{Vs} - (1-2Vs^2 p^2)^2}{4Vs^4 p^2 \frac{\cos i}{Vp}\frac{\cos i}{Vs} + (1-2Vs^2 p^2)^2}$$

Equation 17: Parallel Geosciences derived ratio seismic attribute

$$\frac{B}{C} = \frac{-4Vs^4 p \frac{\cos i}{Vp} + (1-2Vs^2 p^2)}{4Vs^4 p^2 \frac{\cos i}{Vp}\frac{\cos j}{Vs} + (1-2Vs^2 p^2)^2}$$

In the equations A, B, and C are amplitudes of incident wave, reflected wave and converted wave; where i – Angle of incidence, j – Angle equal to (90^o - i), and p – Ray parameter (equal to $\sin(i)/V_p = \sin(j)/V_s$).

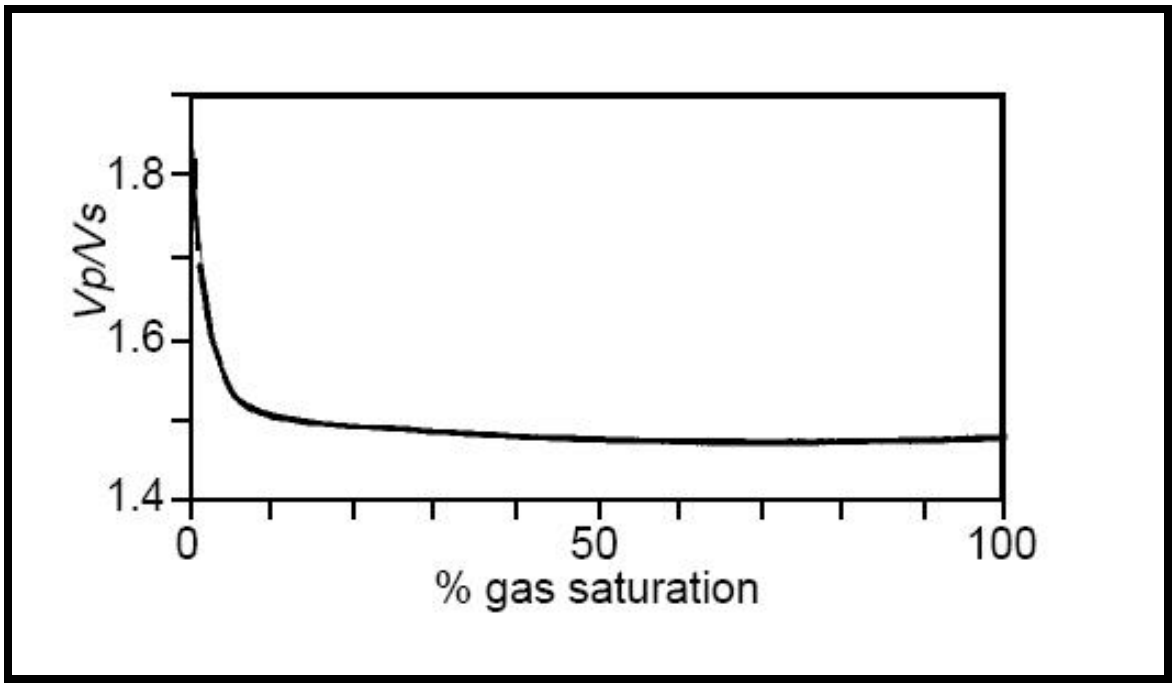

Figure 45. Dependence of V_p/V_s ratio with respect to the percentage of gas content in groundwater saturated sandstone (Ostrander, 1984).

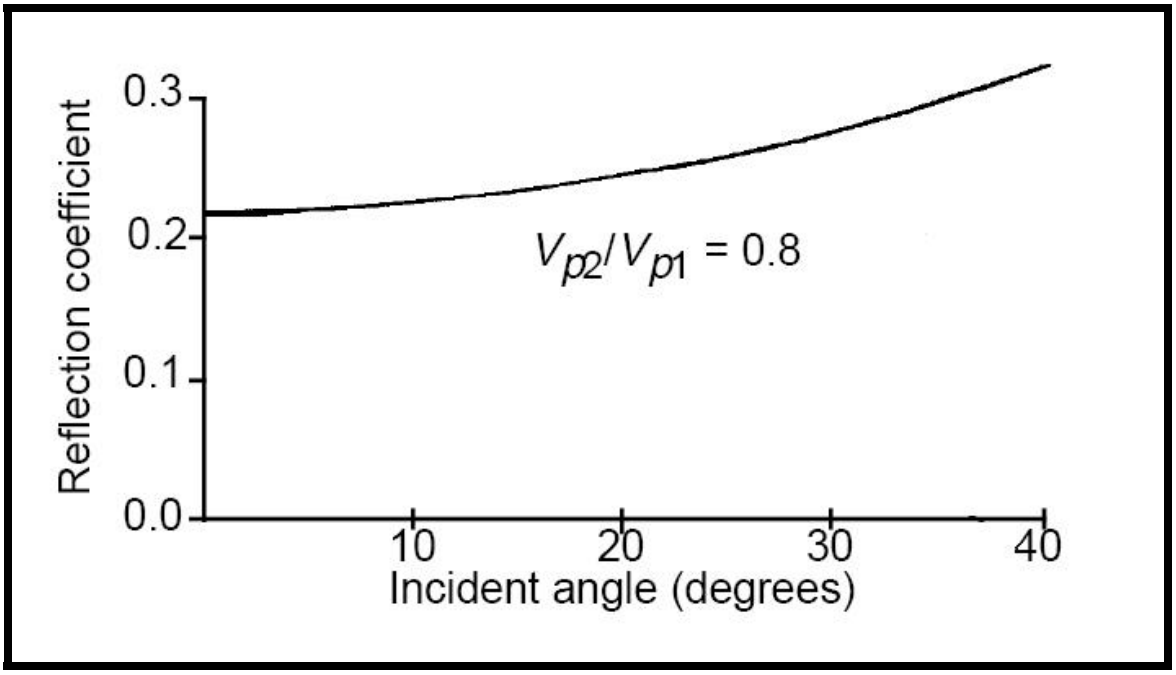

Figure 46. Dependence of the absolute value of the reflection coefficient from the angle of incidence. This relationship was shown in Ostrander (1984) for a specific case (V_{p2}/V_{p1} = 0.8), where V_{p2} is the velocity of P wave in a sandstone and V_{p1} – is velocity of P wave in the sealing shale unit.

One example is the case study by GeoQuest International (1981), which involved an Upper Tertiary gas sand about 40 feet thick. The sand was encased in shale. The enclosing shales had high sonic velocities relative to the gas sand. While the top and the bottom reflection events for the Upper Tertiary gas sand could not be seen on a seismic section because the frequencies were not sufficiently high, a sharp increase in negative seismic amplitudes could be seen at the top of the gas sand. This increase was due to low acoustic impedance of the gas-saturated sand (GeoQuest, 1981). It was concluded that amplitude analyses could be one of the best tools for delineation of gas-saturated media. However, the contact will be reflected as a trough, as predicted below:

Equation 18: Reflection coefficient

$$R = A_r/A_i = (\rho_2 V_2 - \rho_1 V_1)/(\rho_2 V_2 + \rho_1 V_1),$$

Where: A_r and A_i are the amplitudes of the reflected and the incident seismic waves, respectively, ρ_1 and V_1 are density and the velocity in the shale, and ρ_2 and V_2 are density and velocity in the gas-filled sandstone. Assuming typical values for gas-producing areas, the reflection coefficient R can be estimated at –0.5616. Therefore, an incident wave with peak amplitude in such a medium will generate a reflected trough with negative amplitude. The negative sign in the reflection coefficient indicates a phase shift. Similarly, negative amplitude would indicate a decrease in the velocity proportional to the degree of gas-saturation. Increased porosity of the reservoir may also contribute to increased negative amplitude (Reeves et al., 1999).

National Energy Technology Laboratory

1450 Queen Avenue SW
Albany, OR 97321-2198
541-967-5892

2175 University Avenue South, Suite 201
Fairbanks, AK 99709
907-452-2559

3610 Collins Ferry Road
P.O. Box 880
Morgantown, WV 26507-0880
304-285-4764

626 Cochrans Mill Road
P.O. Box 10940
Pittsburgh, PA 15236-0940
412-386-4687

One West Third Street, Suite 1400
Tulsa, OK 74103-3519
918-699-2000

Visit the NETL website at:
www.netl.doe.gov

Customer Service:
1-800-553-7681

U.S. Department of Energy
Office of Fossil Energy

Printed in the United States on recycled paper

October 2007